

Preparation Study

Thesis topic research

S.D. Petrovic

Faculty Aerospace, Section Spaceflight



PREFACE

Back in December 2013 Warren Gebbett gave a presentation on his work at the Jet Propulsion Laboratory ([JPL](#)) in Pasadena, California, USA and the opportunity for a new student to go and do research at [JPL](#). At this point I sent in my application together with eight other students. Then at the end of December I was invited for an interview in the first week of January 2014. In this interview it was concluded that I met all the requirements and that I was the perfect candidate to follow Warren up as the next student at [JPL](#) with financial backing of Dutch Space (now Airbus Defence and Space, the Netherlands). Communication with [JPL](#) was thus started and in March 2015 it was clear that I would be working for the Mars Program Formulation Office under the supervision of Roby Wilson (inner solar system group, NASA [JPL](#)). He told me to focus on the subjects, that I had already proposed, that dealt with Mars missions. At that point I was doing my internship at DLR Bremen, which lasted till June 2015. When I came back to Delft me and my supervisors Erwin Mooij (rockets, trajectories, entry and descent, TU Delft) and Ron Noomen (mission design and orbit analysis, TU Delft) agreed that it would be best to perform a study on these Mars subjects in order to prepare for my visit to [JPL](#) and to formulate final proposition thesis topics. This document is the result of that two month study.

*S.D. Petrovic
Delft, September 2015*

CONTENTS

List of Figures	vii
List of Tables	ix
1 Introduction	1
2 Overview of the subjects	3
2.1 Searching for subjects	3
2.2 Initial concepts	3
3 Mission heritage	5
3.1 Sample Return reference missions	5
3.1.1 Apollo	6
3.1.2 Luna	6
3.1.3 Particle Return Missions	7
3.1.4 Planned Missions	10
3.2 Mars Entry and Descent reference missions	11
3.2.1 Mars 3	11
3.2.2 Viking	12
3.2.3 Pathfinder	12
3.2.4 Beagle 2	13
3.2.5 Mars Exploration Rovers	13
3.2.6 Phoenix	14
3.2.7 Mars Science Laboratory	14
3.3 Hazard avoidance reference missions	15
4 Optimization	17
4.1 Different local optimization methods	17
4.2 Different global optimization methods	17
4.2.1 Sampling methods	18
4.2.2 Metaheuristics	18
4.2.3 Special techniques	18
4.3 Advanced and hybrid techniques	18
4.4 Technique comparison	18
4.5 Chosen methods	20
4.5.1 Frequently used methods	20
4.5.2 TU Delft optimization heritage	21
4.5.3 Chosen candidate methods	21
5 Integrators	23
5.1 Different integrators	23
5.1.1 Single-step	24
5.1.2 Multi-step	24
5.2 Technique comparison	24
5.3 Chosen methods	26
5.3.1 Frequently used methods in related space problems	26
5.3.2 TU Delft integration heritage	27
5.3.3 Chosen candidate methods	27

6 Reference systems and transformation	29
6.1 Different reference frames	29
6.1.1 ECI RF	29
6.1.2 SCI RF	30
6.1.3 ECEF RF	31
6.1.4 VCNE RF	31
6.1.5 BF RF	31
6.1.6 FPB RF	32
6.2 Transformation between reference frames	32
6.2.1 Static reference frame transformations	33
6.2.2 Dynamic reference frame transformations	36
6.3 Transformation between different coordinate systems	37
6.3.1 Spherical and Cartesian	37
6.3.2 Keplerian and Cartesian	39
6.3.3 Non-singular Kepler elements	42
7 Mars entry and descent	43
7.1 Entry phase	44
7.2 Atmospheric descent phase	46
7.2.1 Aero-shell and heat-shield	46
7.2.2 Parachutes	49
7.2.3 Special aerodynamic decelerators	50
7.3 Landing phase	52
7.3.1 Retro rockets	53
7.3.2 Lowering cable	53
7.3.3 Air-bags	53
8 Martian launcher methods	55
8.1 Previous investigations	55
8.2 Futuristic ideas	56
9 Transfer orbits	59
9.1 High-thrust	59
9.2 Low-thrust	60
9.3 Reference research	62
10 Research opportunities	63
10.1 Mars Sample Return research	63
10.2 Mars Entry and Descent research	63
10.3 Hazard avoidance research	64
11 Final subject definition	65
11.1 MSR final research topics	65
11.2 Mars EDL final research topics	65
11.3 Hazard avoidance final research topics	66
12 Recommended proceedings	67
Bibliography	69

LIST OF FIGURES

3.1	Lunar Module [1]	7
3.2	Lunar Ascent Module [2]	7
3.3	Apollo Command and Service Module [3]	8
3.4	Apollo re-entry capsule [3]	8
3.5	Luna SRM sequence [4]	8
3.6	Artists impression of the collection of coma samples by Stardust [5]	9
3.7	SRM after return to Earth [6]	9
3.8	Artists impression of Genesis during its collection period [7]	10
3.9	Genesis Sample Return Capsule (SRC) after crash landing [8]	10
3.10	Artists impression of Hayabusa during its 'landing' on the asteroid [9]	10
3.11	Hayabusa re-entry capsule and schematic [10]	11
3.12	Mars 3 lander [11]	12
3.13	Viking lander [12]	12
3.14	Sojourner rover on the Martian surface [13]	13
3.15	A model of the deployed Beagle 2 lander, how it should have happened [14]	14
3.16	A computer model of the deployed Spirit/Opportunity rover on Mars [15]	14
3.17	A computer model of the deployed Phoenix lander on Mars [16]	15
3.18	A 'selfie' of the deployed Curiosity rover on Mars [17]	15
3.19	Two Hazcams with corresponding electronics used on Curiosity [18]	16
5.1	Comparison of single-step methods for an eccentricity of 0.1 [19]	26
5.2	Comparison of multi-step methods for an eccentricity of 0.1 [19]	26
6.1	Graphical definition of the Earth-centred inertial reference frame [20]	30
6.2	Graphical definition of the Sun-centred inertial reference frame [21]	30
6.3	Graphical definition of the Earth-centred Earth-fixed reference frame [20]	31
6.4	Graphical definition of the Vehicle-carried normal Earth reference frame compared to the Earth-centred inertial frame [20]	32
6.5	Graphical example of a Body-fixed reference frame for a 3U-cubesat adapted from [22]	32
6.6	Graphical example of a Body-fixed reference frame used on the Apollo Command and Service module [23]	33
6.7	Graphical definition of the Flight-path body reference frame for a circular orbit [24]	33
6.8	General rotation around the x-axis [25]	34
6.9	Rotation from the ECI to the VCNE frame [25]	35
6.10	Motion and rotation of point P described in an inertial and moving frame adapted from [20]	36
6.11	Relation between spherical position coordinates and Cartesian position coordinates [26]	38
6.12	atan2 function evaluation conditions adapted from [27]	39
6.13	Definition of the Kepler elements in 2D (left) and 3D (right) [26, 28]	39
7.1	Illustration of the Viking 1 [29]; a) the complete Spacecraft (s/c), b) the entry vehicle, c) exploded view and d) EDL sequence	44
7.2	Illustration of the Mars Pathfinder (MPF) EDL sequence [30]	45
7.3	Illustration of the Beagle 2 EDL sequence [31]	45
7.4	Illustration of the Mars Science Laboratory (MSL) EDL sequence [32]	46
7.5	Graphic representation of the MER aero-shell [33]	47
7.6	Graphic representation of a Martian entry [34]	47
7.7	Typical entry characteristic graphs [34]	48
7.8	Aero-shell comparison of the different NASA Mars entry vehicles [35]	48
7.9	Disk-Gap Band parachute [36]	49

7.10 Ringsail parachute [36]	49
7.11 Hyperflo parachute [37]	51
7.12 Supersonic-x parachute [36]	51
7.13 The original ballute by Goodyear [38]	52
7.14 Selection of trailing IADs under investigation [38, 39]	52
7.15 Earliest design of an attached IAD [40]	52
7.16 Different attached IADs[38]	52
 8.1 Image of comparison table for different stages with different propellants[41]	56
8.2 Some rocket concepts visualized. a) Two stage solid rocket by Lockheed Martin /citestephenson2002, b) Single stage mono-liquid rocket by Firestar Technologies [42], c) Two stage gel rocket by Thompson Ramo Wooldridge inc. (TRW) [43] and d) Two stage bi-liquid rocket by Boeing [41]	56
 9.1 Graphical representation for Earth-Mars Hohmann transfer propellants[44]	59
9.2 Graphical representation of the four different high energy transfer orbit possibilities based on an arbitrary ellipse crossing both orbits[45]	60
9.3 Example manifold in the Jupiter-Sun system[46]	60
9.4 Example low thrust transfer trajectory using Hohmann segments[47]	61
9.5 Example of continuous low thrust trajectory[47]	61
9.6 Example of a segmented low thrust interplanetary trajectory: the Dawn spacecraft[45]	61

LIST OF TABLES

3.1 Previous Missions	6
3.2 Particle Return Missions	6
3.3 Other planned SRMs	11
3.4 Previous Mars Entry and Descent Missions	11
4.1 Optimization method comparison	18
4.2 Previous methods used for trajectory and orbit transfer optimization problems	21
5.1 Integration method comparison	24
5.2 Previous integration methods used for trajectory and orbit (transfer) problems	27
7.1 Previous Mars Entry and Descent Missions	43
7.2 Previous entry, descent and landing methods	43
7.3 Previous Mars mission heat shield characteristics	48
7.4 Previous Mars Mission parachute and entry vehicle characteristics	50
7.5 Landing methods used by previous Mars missions	53
8.1 Previous Mars Ascent Vehicle (MAV) studies	55
8.2 Futuristic non-rocket launch methods for Earth	57
9.1 Reference Mars-Earth transfer studies	62

NOMENCLATURE

β	Balistic coefficient	kg/m^2
ΔV	Velocity increment	m/s
\dot{Q}_{max}	Maximum heat flux	W/m^2
η	Numerical approximation	—
T	General transformation matrix	—
T_x	x-axis transformation matrix	—
r	State vector containing coordinate values	—
\mathbf{x}_{i+1}	Next data point	—
\mathbf{x}_i	Current data point	—
μ	Standard gravitational parameter	m^3/s^2
Ω	Right ascension of the ascending node	rad or deg
ω	Argument of perigee	rad or deg
Ω_t	Rotational velocity of the Earth	rad/s or deg/s
Φ	Increment function	—
ϕ	General rotation angle	rad or deg
ρ	Density	kg/m^3
ρ_0	Air density at the Martian surface	kg/m^3
θ	True anomaly	rad or deg
λ	Mean longitude	rad or deg
ϖ	Longitude of pericentre	rad or deg
a	Semi-major axis	m
C_{DEV}	Drag coefficient of the entry vehicle	—
C_{Dp}	Parachute drag coefficient	—
d_p	Parachute diameter	m
E	Eccentric anomaly	rad or deg
e	Eccentricity	—
$g_{0,mars}$	Gravitational acceleration at the Martian surface	m/s^2
$g_{load,max}$	Maximum deceleration	m/s^2
h	Specific relative angular momentum	m^2/s
h	Step-size	s

i	Inclination	<i>rad or deg</i>
I_{sp}	Specific impulse	<i>s</i>
M	Mean anomaly	<i>rad or deg</i>
m	System mass	<i>kg</i>
$q_{dyn,max}$	Maximum dynamic pressure	<i>Pa</i>
Q_{max}	Maximum heat load	<i>J/m²</i>
r	Radius	<i>m</i>
r_1	Radius of the inner planet	<i>m</i>
r_2	Radius of the outer planet	<i>m</i>
S_{EV}	Surface area of the entry vehicle	<i>m²</i>
t_0	Current time	<i>s</i>
V	Velocity	<i>m/s</i>
v_1	Velocity increment required at inner planet (Hohmann)	<i>m/s</i>
v_2	Velocity increment required at outer planet(Hohmann)	<i>m/s</i>
V_f	Desired final velocity	<i>m/s</i>
x_C	x-axis of the Earth-centred Earth-fixed frame	—
x_E	x-axis of the Vehicle-carried normal Earth frame	—
x_I	x-axis of the Earth-centred inertial frame	—
y_C	y-axis of the Earth-centred Earth-fixed frame	—
y_E	y-axis of the Vehicle-carried normal Earth frame	—
y_I	y-axis of the Earth-centred inertial frame	—
z_C	z-axis of the Earth-centred Earth-fixed frame	—
z_E	z-axis of the Vehicle-carried normal Earth frame	—
z_I	z-axis of the Earth-centred inertial frame	—

ABBREVIATIONS

AB4	Adams-Bashforth 4	MAV	Mars Ascent Vehicle
AB6	Adams-Bashforth 6	MPF	Mars Pathfinder
ABM4	Low-order Predictor-Corrector	MRO	Mars Reconnaissance Orbiter
ABM12	High-order Predictor-Corrector	MSL	Mars Science Laboratory
BF	Boy-fixed	MSR	Mars Sample Return
CM	Command Module	PICA	Phenolic Impregnated Carbon Ablator
CSM	Command and Service Module	RCS	Reaction control system
DE	Shampine-Gordon	RF	Frame of Reference
DGB	Disk-Gap Band	RKF45	Runge-Kutta-Fehlberg
ECEF	Earth-centred Earth-fixed	RHA	Rover Hazard Avoidance
ECI	Earth-centred inertial	RK4	Runge-Kutta 4
EDL	Entry, descent and landing	RKN12	High-order Runge-Kutta-Nyström
EoM	Equations of Motion	s/c	Spacecraft
FPB	Aerodynamic (or flight-path) body	SC14	Störmer-Cowell
GLOM	Gross Lift-Off Mass	SCI	Solar system (sun-centred) inertial
GMT	Greenwich Mean Time	SLA	SuperLight Ablative
IAD	Inflatable Aerodynamic Decelerator	SM	Service Module
JPL	Jet Propulsion Laboratory	SRC	Sample Return Capsule
JVSRP	JPL Visitor Student Research Program	TPS	Thermal protection system
LAM	Lunar Ascent Module	TRW	Thompson Ramo Wooldridge inc.
LM	Lunar Module	VCNE	Vehicle-carried normal Earth
MA	Martian Ascent		

1

INTRODUCTION

This document has been written to help formulate thesis topic opportunities and provide general information on different subjects that shall have to be used during the thesis work that will be done at NASA [JPL](#). The thesis work at [JPL](#) is made possible through the JPL Visitor Student Research Program ([JVSRP](#)), which has given the opportunity to do research at [JPL](#) during a period of 10.5 months. This time will be used to perform a detailed literature study and thesis work. It was decided that a clear selection and description of thesis topics is needed in order to provide [JPL](#) with different research opportunities and have flexibility when it comes to choosing the right topic. It was given that the focus has to be on Mars missions, and therefore three different subjects were selected: Mars Sample Return trajectories, Mars Science Laboratory 2 descent and rover hazard avoidance. The reason for choosing these different subjects is explained in Chapter [2](#). These subjects are the starting point of the preparation research, resulting in a general search area. In Chapter [3](#) different reference missions for each of the subjects are given to get an idea of what has already been done and which missions could be used when designing the different missions that correspond with the subjects. It is also very important to have a general idea about different mathematical concepts that will have to be used during the thesis work. For this purpose Chapter [4](#) on optimization, Chapter [5](#) on integrators and Chapter [6](#) on reference systems and transformations between these systems were written and form the basic understanding that is necessary. In the optimization chapter, different optimization methods are described and eventually a selection is made of the optimization methods that will be useful in the case of the chosen subjects. The same is done for the different integrators. Chapter [6](#) on reference systems and transformations contains clear example transformations and describes different reference frames that are used in space applications. Because the general subjects are already known, information on different aspects of missions based on these subjects has to be provided as well. Therefore, Chapter [7](#) describes the entry and descent of previous missions and the restrictions as well. It also provides alternative technologies that are either already available or have to be researched. In Chapter [8](#) a summary is given of the different Martian launcher methods that have already been researched and possible alternatives to those methods. And finally Chapter [9](#) describes the different transfer orbits and possible return orbits for the return of a Martian sample back to Earth. From the information provided in Chapters [3](#) to [9](#) a refinement on the subjects is performed resulting in different research topics for each of the different subjects. The research opportunities are identified in Chapter [10](#) and properly formulated in Chapter [11](#). These final topics are the topics that will be proposed at [JPL](#) to serve as the thesis topic.

2

OVERVIEW OF THE SUBJECTS

In Chapter 1 it was already mentioned that this literature study will focus on three different subjects; two specifically and one as an extra option. This chapter will explain where the ideas for these three subjects came from and what the initial general research concept was.

2.1. SEARCHING FOR SUBJECTS

Since the thesis research is going to be done at NASA [JPL](#) under their supervision it made sense to look at the different missions that they have planned for the near future. A nice overview was found on the [JPL](#) website [48]. Here I looked at the future missions and the proposed missions to Mars and the two missions available were [MSR](#) and [Mars 2020](#). There is another mission planned to go to Mars called InSight, but that mission is set to launch in March 2016, which means that I would not be able to have any real contribution to this mission.

The [MSR](#) mission is described as a mission that would return samples to Earth using an ascent rocket to launch from the Martian surface. It would contain rock, soil and atmospheric samples to be analysed back on Earth.

The [Mars 2020](#) mission (also sometimes referred to as the [MSL 2](#) mission) will be the next rover mission to Mars. Its prime goal will be to investigate the (past) habitability of Mars, and assess natural resources and possible hazards in order to help in the preparation of future human expeditions according to [48]. It is in its concept similar to the current Curiosity mission.

Given these two missions, it was then decided to formulate thesis subjects to fit within these missions but also correlate to my own interests.

2.2. INITIAL CONCEPTS

The first subject was based on the [MSR](#) mission and incorporated the desire to work on both launcher trajectory and orbit optimization. Therefore this subject was called "***Mars Sample Return launch trajectory***". The goal would be to optimize the whole journey of the samples back to Earth starting with a Martian launch, then performing the transfer orbits to get it back to Earth, and finally re-entry to land the samples safely on Earth.

The second subject was based on the [MSL 2](#) mission and was mainly focussed on a Martian descent similar to the [MSL 1](#). This was interesting because the [MSL 1](#) mission had a very interesting descent phase consisting of several stages. The challenge here would be to see if this would be useful for a second mission as well, if so; where could it be improved. If not, what would be a better solution for [MSL 2](#) instead. This second subject is therefore called "***Mars Science Laboratory 2/Mars 2020 descent analysis***".

The final subject was also based on the [Mars 2020/MSL 2](#) mission but focussed more on the rover aspect. In this case a hazard avoidance system for the new rover would be developed to try and optimize the avoidance of rocks and craters on the Martian surface. This subject, called "***Rover Hazard Avoidance (RHA) System***", is however the spare/extra subject because it does not necessarily have to be on Mars, but it could also be applied on the moon for example. Furthermore, the other two subjects have trajectories, orbits and descent problems in them which is something I am personally more interested in.

These are the initial subjects that were used during this literature study. In Chapter 11 these subjects are refined into final master thesis subjects.

3

MISSION HERITAGE

With the three different subjects defined as in Chapter 2, it is now important to look into what has already been done and what is currently being worked on. This is called researching the missions heritage and is done for every of the three subjects. To keep an overview, the reference missions will be discussed per subject and in the same order as mentioned in Section 2.2. This means that the sections will respectively discuss the different missions that have to do with [MSR](#), [MSL 2](#) and [RHA](#).

3.1. SAMPLE RETURN REFERENCE MISSIONS

In early 2012 a group of scientists and engineers was set-up to devise an approach for the continuing exploration of Mars [49]. They had to combine all the requirements set by President Obama (to have humans in Mars orbit in the 2030s) and the 2011 NRC Decadal Survey for Planetary Science (science goals) while still keeping to the new proposed budget of the FY2013 Budget Submittal.

Their conclusion was that a sample return mission would be the best option, because they deemed it to be the best combination between Human Exploration, Science and Technology. It is the most logical next step. They also suggest different mission architectures to perform a [MSR](#) mission; using three, two or one launch(es). The first concept would first launch a rover to collect samples, then a [MAV](#) and a so-called *Fetch* rover to collect the sample case from the first rover and launch them into orbit, and the final launch would then send a sample return orbiter to collect the [MAV](#)/sample case and safely return them to Earth. The second concept would combine the last two launches into one providing using a smaller return orbiter propelled by a solar electric propulsion system. Finally, the third concept is to put all of these aspects into one launch, resulting in a sample collection rover with an on board [MAV](#) system and again a small return orbiter [49].

Given the proposed NASA missions mentioned in Section 2.1 it seems that the two and three launches options are being pursued.

Now this might explain why it needs to be done and why these missions are envisioned, but it does not say anything about what has already been tried before. Therefore, it is best to take a step back and first look at general sample return missions.

There are different kind of sample return missions, but in this case it means returning soil and rock samples from the surface of Mars back to Earth. Therefore all reference missions will be focused on missions that have done this for different solar system bodies. A nice overview of all the sample return missions is given by [6] for both manned and unmanned missions. All successful soil and rock sample return missions were performed on the moon by the Soviet Union (robotic) and the United States (manned). An overview is given in Table 3.1.

All these missions had in common that they first had a craft land on a different body, collect samples and then return these samples back to Earth by launching a [S/C](#) back into space.

There were four other sample return missions, but they were based on the return of small particles (see Table 3.2). One of these missions was to collect space debris from Earth orbit by mounting a collection devise on the outside of the MIR space station. These samples were then returned back to Earth in a manned capsule. The other three missions all returned their samples in an unmanned return capsule. Both the Stardust and the Hayabusa mission capsules made a soft landing on Earth, unfortunately because of incorrectly installed

Table 3.1: Previous Missions

Launch date	Country	Mission	Returned mass
16 July 1969	United States	Apollo 11	22 kg
14 November 1969	United States	Apollo 12	34 kg
12 September 1970	Soviet Union	Luna 16	101 g
31 January 1971	United States	Apollo 14	43 kg
26 July 1971	United States	Apollo 15	77 kg
14 February 1972	Soviet Union	Luna 20	55 g
16 April 1972	United States	Apollo 16	95 kg
7 December 1972	United States	Apollo 17	111 kg
9 August 1976	Soviet Union	Luna 24	170 g

accelerometers in the Genesis capsule [7], the parachute never deployed and thus performed a hard landing on Earth. Luckily, they were able to retrieve most of the samples. However, all these three missions can be used as reference when looking at the autonomous return of collected samples should that be required.

Table 3.2: Particle Return Missions

Launch date	Country	Mission	Target	Return date
22 March 1996	United States & Russia	MIR	Orbital Debris	6 October 1997
7 February 1999	United States	Stardust	Comet 81P/Wild 2	15 January 2006
8 August 2001	United States	Genesis	Solar wind	9 September 2004
9 May 2003	Japan	Hayabusa	Asteroid Itokawa	13 June 2010

Because of the differences in all the missions mentioned, it is good to take a closer look at the different missions/programmes. Therefore, each will be discussed a bit further in Sections 3.1.1 to 3.1.3. Besides past missions it is also useful to look into the missions that are planned for the future, besides the JPL missions. These future missions are summarised in Section 3.1.4.

3.1.1. APOLLO

The Apollo programme was the first and only manned lunar programme. It started in 1961 and lasted till 1972 [1]. The first few missions were designed as tests and demonstrators for the actual lunar landings. The first manned lunar landing was performed by the Apollo 11 crew in the 5th Lunar Module (LM) on the 20th of July 1969 [50]. Five successful manned lunar missions were performed after that: Apollo 12, 14, 15, 16 and 17. All Apollo missions were able to bring back tens of kilograms of soil and rock samples because the astronauts also needed to return back to Earth. Both the astronauts and the samples ascended from the lunar surface using the Lunar Ascent Module (LAM), which was the upper part of the LM as shown in Figures 3.1 and 3.2.

Once back in lunar orbit, the LAM would then rendezvous with the Command and Service Module (CSM) at which time the astronauts and all the samples were transferred to the command and service module. The CSM incorporated an Earth return capsule (Command Module (CM)) for Earth re-entry in the 'nose' of the vehicle, as can be identified in Figure 3.3. The CM would separate from the Service Module (SM) just before entering the atmosphere. Figure 3.4 shows a photo of the Apollo return capsule after re-entry.

The details of the Apollo (and the other) missions will be discussed in the corresponding subject chapters later in this report.

3.1.2. LUNA

The Luna programme was a Soviet lunar exploration programme between 1958 and 1976 [51]. It was first proposed by Sergei Korolev on the 28th of January 1958. The programme started with some early probing between 1958 and 1960 by the Luna 1, 2 and 3 probes, followed by a proof of technology by the Luna 4 through 14 missions between 1963 and 1968. On the 3rd of February 1966, Luna 9 performed the first successful soft lunar landing. Following this successful mission, 6 more lunar landing missions were completed successfully: Luna 13, 16, 17, 20, 21 and 24. Luna 23 did land on the moon, but was not able to perform its mission after

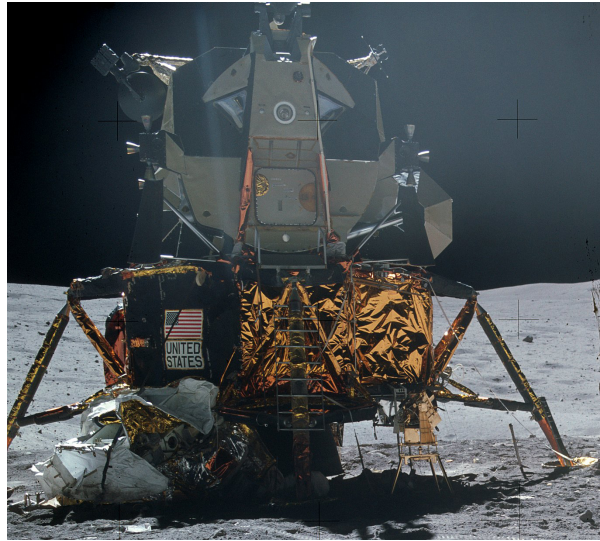


Figure 3.1: Lunar Module [1]



Figure 3.2: Lunar Ascent Module [2]

that because of damage which occurred during this landing.

As mentioned in Table 3.1 Luna 16, 20 and 24 were sample return missions (also see [52]). These three missions were virtually identical in their architecture and s/c design. The s/c consisted of a descent stage and a smaller ascent stage [53]. General information on the s/c itself can be found in [54]. The s/c had a drill on board that was attached to an arm that could be rotated in one direction. Basically it could lower down to the surface to drill and collect the samples and then move up towards the ascent stage to deposit the samples. The ascent stage would then lift-off with the samples contained in a spherical re-entry capsule (also see Figure 3.5). This spherical capsule would then perform a ballistic re-entry and land in Soviet controlled territory.

3.1.3. PARTICLE RETURN MISSIONS

In 1999 NASA launched its first SRM, called Stardust, to an asteroid. Its objective was to perform a fly by of the comet 81P/Wild 2 and collect samples from the coma (tail) of the comet [5]. It also collected some interstellar particles during its travel. The collection was done using aerogel attached to a paddle. The paddle had two sides, one for the comet particles and one for the interstellar particles, and could thus be turned around for

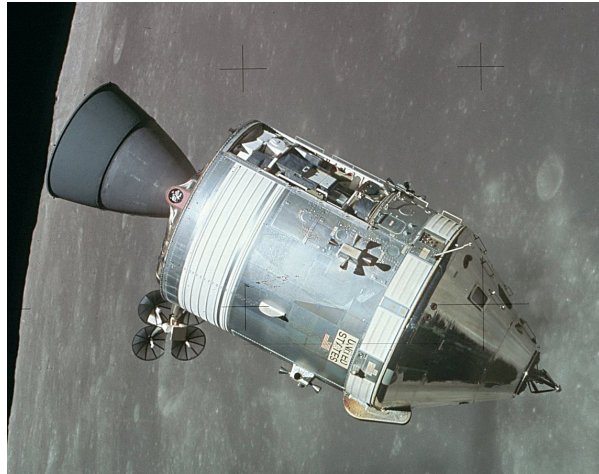


Figure 3.3: Apollo Command and Service Module [3]



Figure 3.4: Apollo re-entry capsule [3]

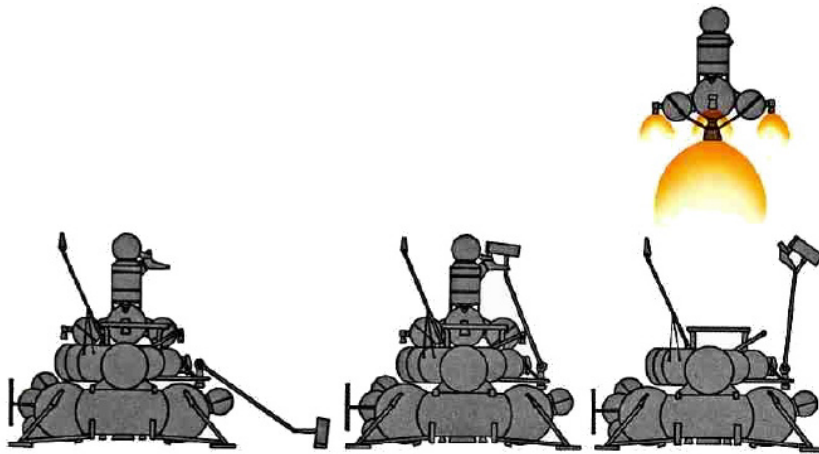


Figure 3.5: Luna SRM sequence [4]

the different mission phases. When the paddle was not in use it was safely stored back in the re-entry capsule. An artists impression of the s/c during the comet collection phase can be seen in Figure 3.6.

At the end of the final collection phase, the paddle was permanently placed back in the re-entry capsule.

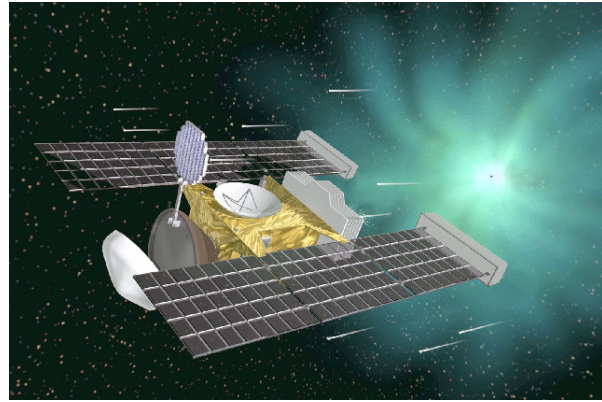


Figure 3.6: Artists impression of the collection of coma samples by Stardust [5]

The [s/c](#) then performed an Earth fly-by to deliver the re-entry capsule back to Earth. A detailed look of the 0.8 m diameter Stardust [SRC](#) is given in Figure 3.7.

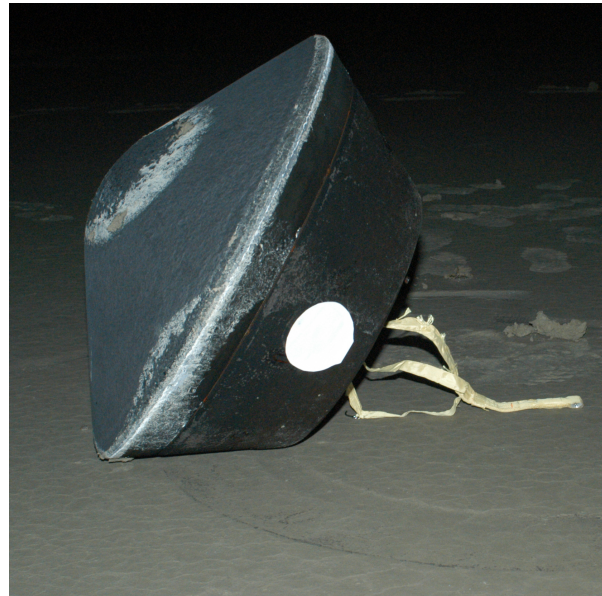


Figure 3.7: SRM after return to Earth [6]

The second SRM of NASA, called Genesis, was launched in 2001 and was set to collect Solar wind samples. Its destination was a halo orbit around the Sun-Earth Lagrangian libration point L1 [7]. The [s/c](#) carried three honeycomb collection discs similar to Stardust, but made from different materials to optimise the collection of solar particles. Once in the halo orbit, the discs were deployed for a period of over 30 months. Figure 3.8 gives a good idea of what this might have looked like.

After this period, the discs were stored back into the re-entry capsule for return to Earth. During the following Earth fly-by of Genesis, the capsule was released and sent back to Earth. Unfortunately, the parachutes never deployed and the capsule made a hard landing at 311 km/hr. An after image of the 1.5 m diameter capsule is shown in Figure 3.9. Fortunately, some of the samples could still be recovered.

Japan is the only other nation that has successfully returned samples from another body besides the Soviet Union and the United States. This was done with the Hayabusa mission that was launched back in 2003. Its primary mission was to collect surface samples and return them safely to Earth [9]. Hayabusa was the first mission to land and ascent from another body besides the moon, and was done at least two times successfully. During these touchdowns, samples were collected using the long sample collector visible in Figure 3.10. The idea was that two 'bullets' would fire and create an upwards dust cloud. This dust could then be collected by the [s/c](#). These bullets were however never fired due to malfunctions, but fortunately the [s/c](#) was still able

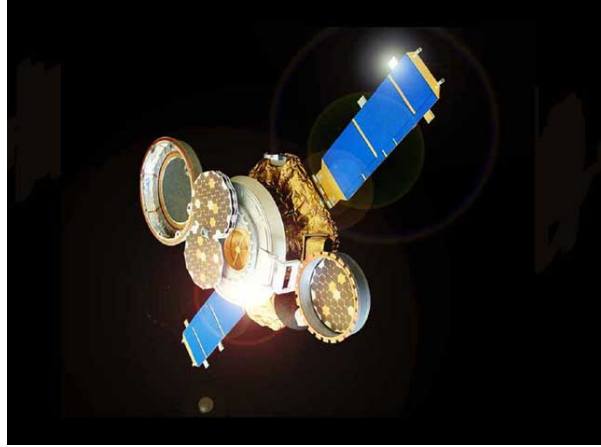


Figure 3.8: Artists impression of Genesis during its collection period [7]



Figure 3.9: Genesis SRC after crash landing [8]

to collect surface dust samples due to dust that was displaced when the s/c landed on the surface of the asteroid. These samples were then brought back to Earth using a small re-entry capsule shown in Figure 3.11. This capsule only had a diameter of 0.4 m, but was still able to make a soft landing in Australia back in 2010.

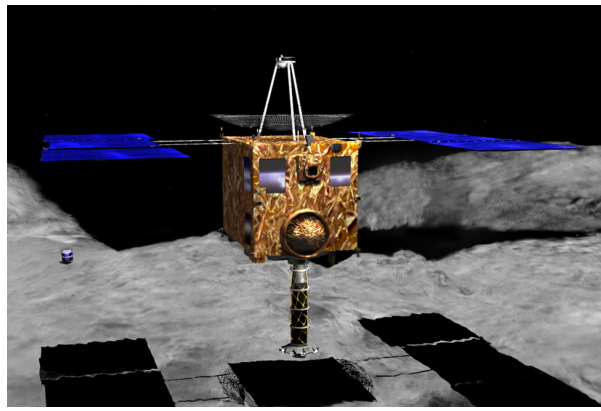


Figure 3.10: Artists impression of Hayabusa during its 'landing' on the asteroid [9]

3.1.4. PLANNED MISSIONS

Two of the planned missions to Mars were already discussed earlier, the MSL 2 deploying a rover that will collect samples, and the MSR mission to bring samples back to Earth. Both of these missions are under

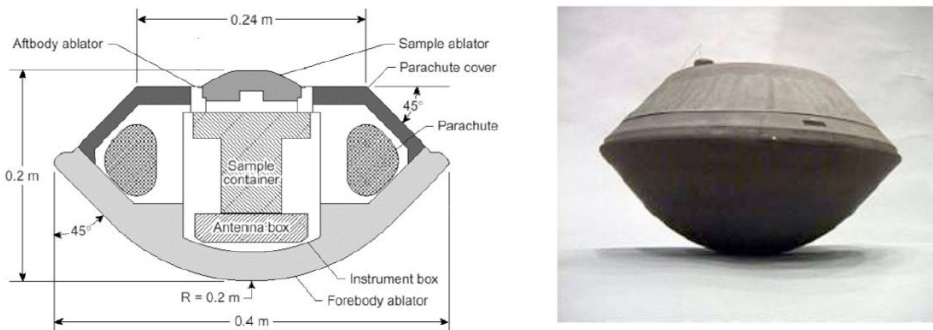


Figure 3.11: Hayabusa re-entry capsule and schematic [10]

consideration by JPL. However, besides these mission, there are other SRM planned by the United States and other countries. An overview of the other missions is given in Table 3.3. The last mention is based on SpaceX technology and is not an official running programme at this time but could be interesting in the future.

Table 3.3: Other planned SRMs

(Proposed) Launch date	Country	Mission	Target	Kind of SRM
3 December 2014	Japan	Hayabusa 2	Asteroid 1999 JU3	Surface samples [55]
3 September 2016	United States	OSIRIS-REx	Asteroid Bennu	Surface samples up to 2 kg [56]
2017	China	Chang'e 5	Moon	At least 2 kg of soil and rock samples [57]
2022	United States	Red Dragon	Mars	Soil and rock samples [58]

3.2. MARS ENTRY AND DESCENT REFERENCE MISSIONS

In order to have useful information, it is better to look at successful Martian lander and rover missions. In this section an overview will be given of previous missions to Mars that had to perform an entry and descent to the Marian surface and did so successfully. A summary of these missions is given in Table 3.4 and is based on the list of Mars missions given in [13].

Table 3.4: Previous Mars Entry and Descent Missions

Launch date	Country	Mission	Type
19 May 1971	Soviet Union	Mars 3	Lander (and failed rover)
20 August 1975	United States	Viking 1	Lander
9 September	United States	Viking 2	Lander
4 December 1996	United States	Mars Pathfinder/Sojourner	Lander and rover
2 June 2003	Europe and United Kingdom	Mars Express/Beagle 2	Lander
10 June 2003	United States	Mars Exploration Rover - A/Spirit	Rover
7 July 2003	United States	Mars Exploration Rover - B/Opportunity	Rover
4 August 2007	United States	Phoenix	Lander
26 November 2012	United States	Mars Science Laboratory/Curiosity	Rover

For each of these missions it is important to know what kind of entry and descent they had and how they eventually landed. Therefore, these parts of the mission will be discussed further in the next few sections.

3.2.1. MARS 3

The Mars 3 lander made its descent to the Marian surface on the 2nd of December 1971 and was the first soft landing on Mars [11]. It started with the firing of the main descent engine. This turned the heat shield in the flight direction. After entering the atmosphere, the braking parachute was deployed and a few seconds later the main chute was deployed as well. This main chute was reefed and was completely opened as soon as

the capsule velocity dropped below supersonic. At the same time the heat shield was ejected from the craft revealing the radar altimeter and the final retro rockets. At an altitude of about 20 metres, the main parachute was cut-off and pulled away from the craft by a small rocket. At this time the retro rockets were fired to lower the speed of the capsule and safely land it on the Martian surface. A model of the Mars 3 lander is shown in Figure 3.12. The landing was successful, but still after approximately 20 seconds the signal was lost. It is suspected that the storm that was acting up at that time damaged the communication system.

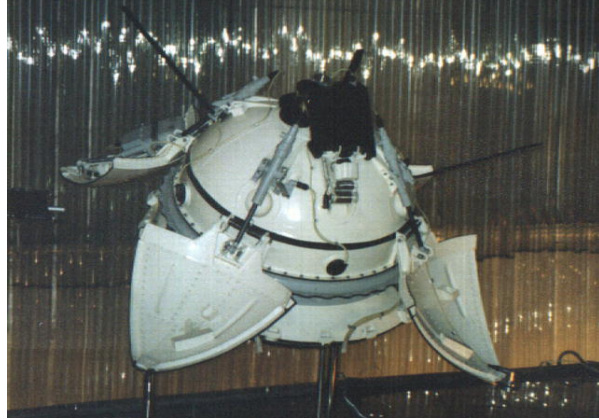


Figure 3.12: Mars 3 lander [11]

3.2.2. VIKING

The Viking lander mission architectures were virtually identical. The descent sequence was started after the landing craft was separated from the orbiter in Mars orbit [12]. At this point the main rockets were fired to decelerate and de-orbit the craft. When it reached an altitude of approximately 300 km the lander was oriented with the heat shield into the flight direction. The shield was used in the atmosphere to decelerate the craft such that it reached a velocity of about 250 m/s at an altitude of 6 km at which the parachute was deployed. A few seconds later the heat shield was jettisoned and a few seconds after that the landing legs were deployed. The retro rockets were ignited at an altitude of 1.5 km and fired for 40 seconds until the lander landed with a speed of 2.4 m/s. A model of the Viking lander is given in Figure 3.13.

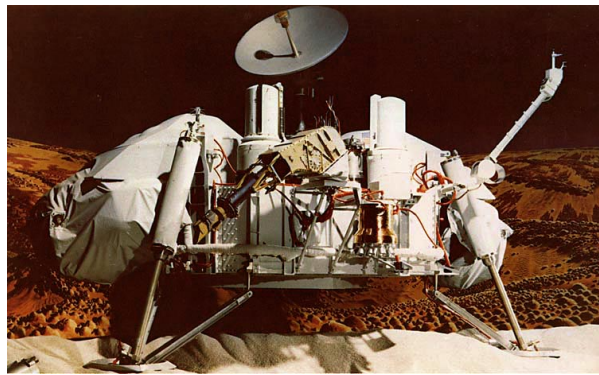


Figure 3.13: Viking lander [12]

3.2.3. PATHFINDER

The MPF performed a direct approach into the Martian atmosphere, so without first going into an orbit around Mars, on the 4th of July 1997 [59]. During the first phase of the atmospheric descent, the s/c velocity was reduced to about 400 m/s using a heat shield. At this velocity, the (main) parachute was deployed and 20 seconds later the heat shield was jettisoned. Then a 20 m long tether, called a bridle, was released from the bottom of the craft and a few seconds later the lander part of the s/c travelled to the bottom of the bridle. At this point the complete contraption first had a parachute, then the back-shell of the s/c, a bridle and the

lander at the end of it. At about 10 seconds before landing, four air bags surrounding the lander were inflated creating an impact resistant sphere around the lander. Then four seconds after that, three retro rockets that were attached to the back-shell of the *s/c* fired to slow the lander down even more. About four seconds before touchdown at an altitude of 21.5 m the bridle was cut, and the lander surrounded by air-bags was released. The lander then bounced around the surface for about 2.5 minutes having travelled a horizontal distance of 1 km before coming to a complete stop. A few seconds later the air bags were deflated and the Pathfinder opened its three panels. After two days, on the 6th of July 1997, the lander Sojourner was deployed and set on an exploratory path on the surface of Mars. A well known image taken of the rover can be seen in Figure 3.14.



Figure 3.14: Sojourner rover on the Martian surface [13]

3.2.4. BEAGLE 2

On the 19th of December 2003 the Beagle 2 was separated from its mother-ship Mars Express and set on a ballistic trajectory towards the red planet [14]. On the 25th of December it entered the Martian atmosphere, but no signal was ever received from the craft itself and it was assumed that the lander was lost. The landing should have had a close resemblance to the Pathfinder descent sequence; first deceleration using a heat shield, followed by a parachute deployment. Air-bags would then inflate around the *s/c* approximately 1 km above the surface, but would simple use them as impact reducers once it touched the ground (which means it would not have been cut and bounced around the surface like Pathfinder did). However, since no data was received, it is unsure what really happened during the descent.

But then on the 16th of January 2015 it was announced by the Mars Reconnaissance Orbiter (MRO) team that the Beagle 2 was found on the surface of Mars using the HiRISE camera [60]. After the first few images showed an interesting spot on the surface of Mars, the Beagle 2 team was able to confirm that it was indeed their lander. From the images it was determined that not all of the four solar panels had been deployed causing a blockage of the communication system and thus preventing the lander from communicating. This did however proof that the lander made a proper soft landing and is thus the first European soft landing on Mars. The images also showed that the parachute was likely still attached to the lander and landed a few metres away. A model of the lander is given in Figure 3.15.

3.2.5. MARS EXPLORATION ROVERS

The Mars Exploration Rover missions consisted of two rover missions called Spirit and Opportunity. Since again these missions were identical, only the descent sequence of Spirit will be discussed here. Spirit entered the Martian atmosphere on the 20th of January 2004 [15]. In the early phase of the descent, the heat shield of the *s/c* decelerated the craft to approximately 445 m/s at which point the parachute was deployed. Similar to the Pathfinder, a bridle was lowered with the lander at the end of it. At an altitude of 100 m the retro rockets were fired and the air-bags were inflated. The bridle was cut and the craft bounced around on the surface until it came to a full stop. At this point, the air-bags were deflated and the landers opened up revealing the rover. The rover deployed its solar arrays and started transmitting back to Earth. An animated model of the complete deployed rover is given in Figure 3.16.

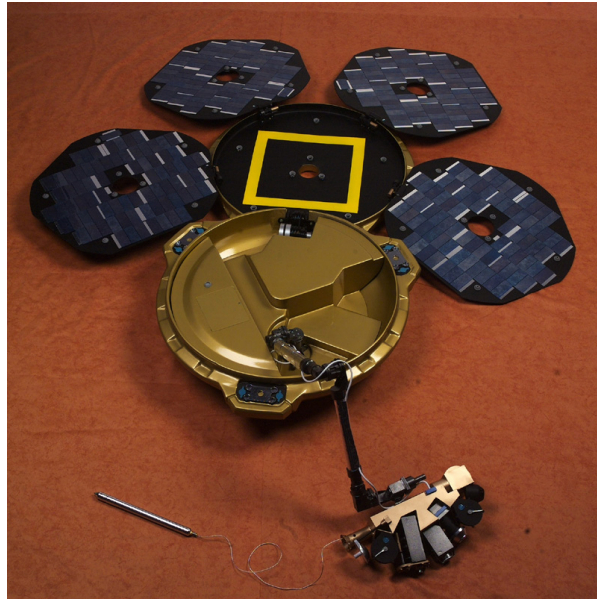


Figure 3.15: A model of the deployed Beagle 2 lander, how it should have happened [14]

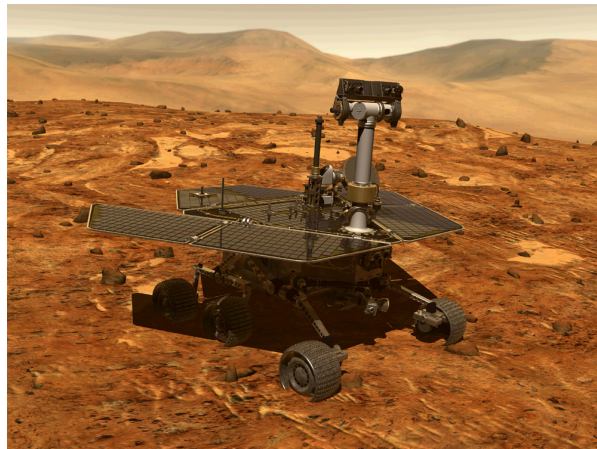


Figure 3.16: A computer model of the deployed Spirit/Opportunity rover on Mars [15]

3.2.6. PHOENIX

The Phoenix lander started its descent to the surface on the 25th of May 2008 [16]. The heat shield slowed the s/c down during the first three minutes, after which the parachute was deployed. Jettison of the shield happened 15 seconds after this, followed by the deployment of the landers' legs. At an altitude of approximately 1 km the lander separated from the back-shell and the parachute and started a drop with a retro rocket descent. After touchdown was detected by the footpads, the rockets were shut-down. After the soft landing, the Phoenix lander deployed its solar arrays, communication systems and cameras. An animated model of the craft is given in Figure 3.17.

3.2.7. MARS SCIENCE LABORATORY

The descent sequence of the latest Mars mission, the MSL, was a very impressive one. It basically combined the tethered descent of the MERs with the controlled powered descent of the Phoenix lander. The MSL entered the Martian atmosphere on the 6th of August 2012 [17]. With use of its heat shield and some S-curve manoeuvres the s/c velocity was reduced. Then about three minutes before touchdown the parachute was deployed and after that the heat shield was jettisoned. During the next phase, the descent module housing the lander was detached from the back-shell and parachute and started a powered descent. The descent module then hovered a few metres above the Martian surface in order to lower the rover to the ground using

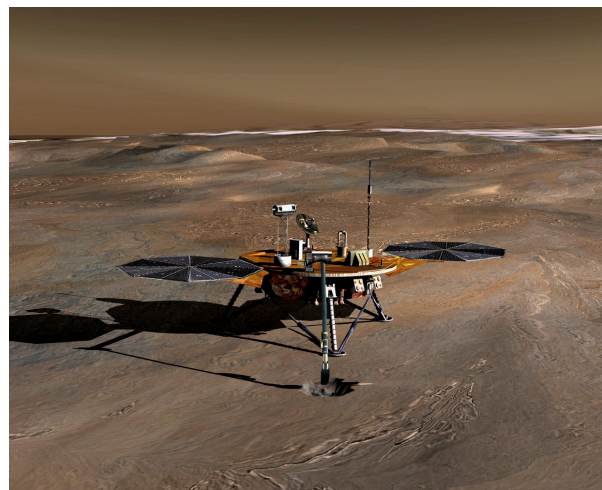


Figure 3.17: A computer model of the deployed Phoenix lander on Mars [16]

a tether system. During this time the legs of the Curiosity rover were deployed as well. Once touchdown of Curiosity was detected, the tether was cut at the rover side and the descent module flew off into the distance to make a hard landing away from the rover. A 'selfie' of the fully deployed Curiosity rover on the surface of the red planet is given in Figure 3.18.

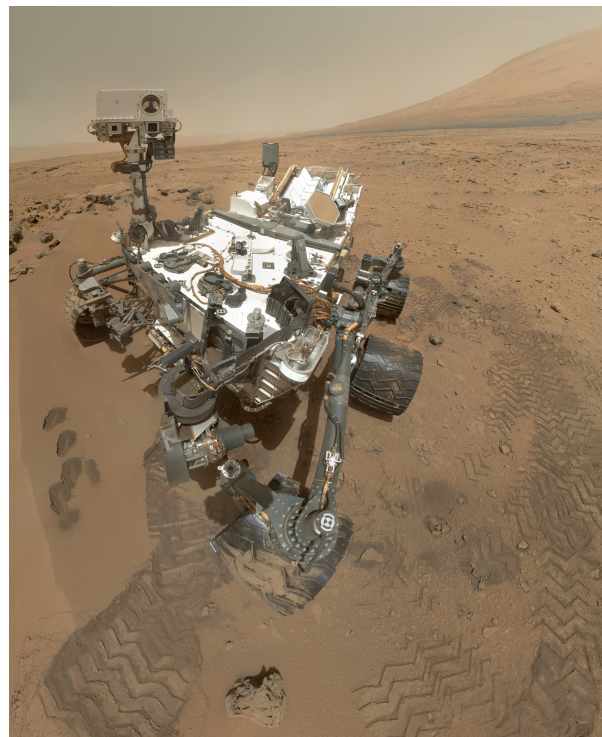


Figure 3.18: A 'selfie' of the deployed Curiosity rover on Mars [17]

3.3. HAZARD AVOIDANCE REFERENCE MISSIONS

The Mars 3 lander also carried a small rover called the PROP-M [11]. Unfortunately, because of the loss of signal of the lander, the rover was never deployed. However, this would have been the first rover on Mars to use a sort of automated hazard avoidance system. It basically used two detection sticks placed on the front of the box to detect obstacles.

Looking at the rovers that have already been mentioned, Sojourner is discussed first. This rover had an au-

tomated hazard avoidance system that used both cameras and lasers [61]. This system was used to detect objects, craters and steep slopes. Accelerometers were used to detect excessive tilts and the rover would turn back if the slope was more than 30° . Finally, the rover was also equipped with contact sensors that would trigger if it touched something that it was not expected to touch.

Spirit, Opportunity, Curiosity and Yulu (the Chinese lunar rover deployed from the Chang'e 3 lander) all used Hazcams, hazard avoidance cameras [62]. These cameras are used for autonomous hazard avoidance by the rovers using specific programs. Figure 3.19 shows a photo of two of the 8 Hazcams that were used on the Curiosity rover. Two other successful rover missions were performed on the Lunar surface by the Lunokhod 1 and 2 (respectively brought there by Luna 17 and 21) back in the 70s. However, compared to all the rovers that would follow, these two did not have a RHA system on board [63]. Instead they were directly controlled from the ground, which is unfortunately not an option for Martian rover missions.

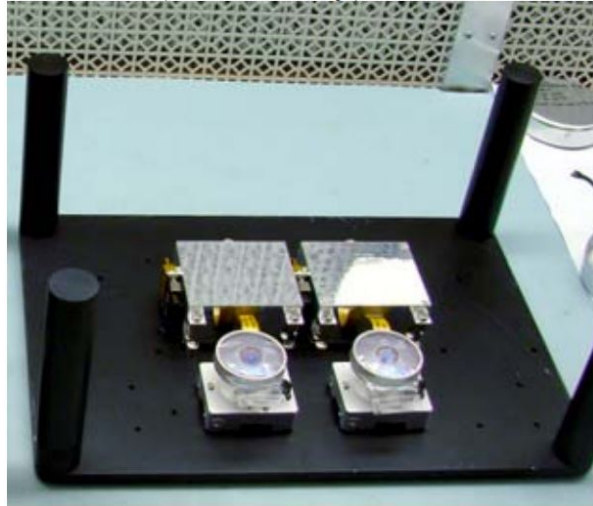


Figure 3.19: Two Hazcams with corresponding electronics used on Curiosity [18]

4

OPTIMIZATION

In this chapter, different mission design optimization techniques will be discussed. There are two different kinds of optimizations: local optimization, where a minimum (or maximum) is found but is only the minimum for a small 'area', and global optimization, where the found minimum (or maximum) is the minimum value of the entire function space [64]. Such a function space can have multiple local minimums but only has one global minimum, that means that one of the local minimums is also the global minimum. First a general description of the local and global optimization techniques is given in Sections 4.1 and 4.2 respectively. Examples of a combination of these techniques and advanced techniques are given in Section 4.3. Then the different optimization techniques will be compared in Section 4.4 and finally, the most appropriate method for each of the subject problems is given in Section 4.5. When it comes to the optimization of a problem, it basically means that the problem comes down to a certain corresponding function. This function is then optimized either analytically or numerically. There are two ways a function can be optimized; analytically, resulting in a direct solution, or numerically, approaching the exact solution [65]. Depending on the problem, one method might be better than the other. Also, the chosen method can be used based on the cpu time or the final accuracy of the result. Often a more accurate result takes more time and thus increases the cpu time needed. Also, every time an optimization is used to find a minimum, the same method can be used to find a maximum as well, however from now on only the minimum is mentioned.

4.1. DIFFERENT LOCAL OPTIMIZATION METHODS

Local optimization locates the local minimum of a function. The methods used are called **Nelder-Mead**, **Newton-Raphson** (1D), **steepest descent** (either along the axes or in an arbitrary direction), **Sequential Quadratic Programming** and **Monotonic Basin Hopping** [65] and [66]. They might get stuck at the local minimum, but sometimes can find several local minimums and thus also find the global minimum. Local optimization methods are usually fast and accurate, producing good results in a short time. But they do only focus on a small area of the function space [67]. Therefore it is important to define a proper initial value for the local methods. Convex optimization can help in this case, even if the problem is non-convex. In convex optimization, there is a maximum of one global minimum and every local minimum is a global minimum. So if a convex approximation is taken for a non-convex problem and this convex approximation is solved, it will result in an accurate result for the approximation of the non-convex problem. This value can then be used as the initial input for the local optimization providing a quicker and more accurate result in the end, which could even lead to the global minimum.

4.2. DIFFERENT GLOBAL OPTIMIZATION METHODS

In [65], three different numerical global optimization categories are given: sampling methods, metaheuristics, and special. In global optimization the actual minimum value of the complete function is obtained, or at least an approximation of this value. Global optimization is usually used for problems that only have a few variables, because the computation time using these methods can be very long [67].

4.2.1. SAMPLING METHODS

The sampling methods are based on choosing a value for the variable(s) in the function and then evaluating the function. This is done for many different values until a minimum is found and can be done randomly (**Monte Carlo**) or using a certain pattern (**grid search** and **Latin hypercube sampling** [68]). Then there is also a way of generating variable values called quasi-random, which usually means generating all the different values at the same time and then going through them one by one. This is done with **Sobol sequencing** [69], which also uses a hypercube design to generate quasi-random values such that the values are spread evenly among the function space. Sampling methods can be used to reduce the search space first and then use another method to precisely get to the final answer, since the resolution of sampling methods can be limited. However, if the sampling is done on a small function space accurate results can still be obtained, which is why it can also be used for local optimization.

4.2.2. METAHEURISTICS

Metaheuristics are numerical optimization techniques that directly go towards the solution. Unfortunately, convergence cannot always be detected. Usually it requires a local optimization gradient method to refine the final solution. The different methods are: **Genetic Algorithm**, **Differential Evolution**, **Particle Swarm Optimization**, (Adaptive) **Simulated Annealing**, **Ant Colony Optimization**, **Dynamic Programming** and **Interval Analysis** [65] and [66](usually using a branch and bound method [70]). Most of the times these methods need a lot of iterations to get to a proper solution, but they are very robust and do not need a good initial value.

4.2.3. SPECIAL TECHNIQUES

The final special techniques are called **Primer vector theory** and **Q Law**. These techniques are used to optimize thrust and coast arcs for low-thrust trajectories for instance.

4.3. ADVANCED AND HYBRID TECHNIQUES

When it comes to advanced techniques and hybrid techniques, experience with different problems is desired. Every problem needs a different combination of techniques to find the most optimal solution and these combinations of techniques depend on the judgement of the person solving the problem. Usually a combination of global and local optimization methods is used to first find a general solution and then refine this solution to find an exact or close to exact solution. Some of these techniques are: hybrids different metaheuristics, **separate evolution/branching**, combination of sampling and local optimization methods, combination of metaheuristics and local optimization methods, and **search space pruning** (often used in interval analyses [70]).

4.4. TECHNIQUE COMPARISON

In order to get a better understanding of the different methods mentioned in bold in Sections 4.1 to 4.3, a comparison is made between all these methods. In the case of launch trajectory and transfer orbit optimization, a global minimum solution is wanted. Therefore, getting stuck at a local minimum is not advantageous. Table 4.1 shows the advantages and disadvantages of each method similar to how it is done in [65] to give a clear and quick overview.

Table 4.1: Optimization method comparison

Method	Type	Advantage	Disadvantage
Nelder-Mead	Local	simple	converges to local minimum
Newton-Raphson	Local	simple	convergence is slow near a flat optimum and converges to local minimum

Steepest descent	Local	simple, always finds a minimum and only requires previous gradient information (arbitrary direction results in better conversion)	can oscillate around minimum, has a slow convergence and goes to a local minimum (needs second derivatives/Hessian matrix for arbitrary directions)
Sequential Quadratic Programming	Local	works well on non-linearly constrained problems and neither initial point or iterate points have to be feasible [71]	converges to local minimum
Monotonic Basin Hopping	Local	can locate several local minimums that are close together [66]	no guarantee that best found local minimum is also global minimum and normal Basin Hopping works better if just looking for the value of one local minimum [72]
Monte Carlo	Global/sampling	simple to implement and does not depend on derivatives	only simple problems (otherwise very slow), it is based on luck and can have bad resolution (approximation of value)
Grid search	Global/sampling	simple to implement and does not depend on derivatives	slow and can have bad resolution (approximation of value)
Latin hypercube sampling	Global/sampling	simple to implement, does not depend on derivatives and it provides more regular sampling	only simple problems (otherwise very slow), it is based on luck and can have bad resolution (approximation of value)
Sobol sequencing	Global/sampling	good uniform distribution (regular sampling), faster convergence and does not depend on derivatives	all sampling values are generated at once [69]
Genetic Algorithm	Global	robust, does not depend on derivatives, does not require a good initial value and always directly works towards a solution	needs many iterations, convergence is unclear and becomes very slow for a large number of variables

Differential Evolution	Global	(same as for Genetic Algorithm)	(same as for Genetic Algorithm)
Particle Swarm Optimization	Global	(same as for Genetic Algorithm)	(same as for Genetic Algorithm)
Simulated Annealing	Global	(same as for Genetic Algorithm)	(same as for Genetic Algorithm)
Ant Colony Optimization	Global	(same as for Genetic Algorithm)	(same as for Genetic Algorithm)
Dynamic Programming	Global	(same as for Genetic Algorithm)	(same as for Genetic Algorithm)
Interval Analysis	Global	(same as for Genetic Algorithm)	(same as for Genetic Algorithm)
Primer vector theory	Global	specific applications for space problems, precise and can be used for many general cases [66]	can become sensitive if more gravity assists are added
Q law	Global	specific applications for space problems	needs metaheuristics for optimization [73]
Separate evolution/branching	Global	spreads optimization over several processors and more computations done [66]	refinement of solution might be needed and requires several processors
Search space pruning	Local and Global	more focussed search (quicker)	requires good knowledge of the problem and can become very complex if number of levels increase [66]

Also, the metaheuristic (and other global) methods usually require extra optimization by using a gradient technique to get (close to) the exact minimum value.

4.5. CHOSEN METHODS

To be able to choose one or several of these methods to be used in the subject problems given in Chapter 2, it is useful to know what has been done in the TU Delft Space department. Basing the decision on what knowledge already exists in the department will allow for use of resources that are already in place and will make it easier to learn from experienced people. However, other used methods for similar subject problems should also not be ignored, since one might be better suited for the problem than the other. But a general decision can already be made. Therefore, Section 4.5.1 first shows a collection of methods that are frequently used for these kind of problems (basically showing a selection of the methods mentioned in Table 4.1) and then Section 4.5.2 will discuss the methods used in the Space department. With both these information sources, a final decision will be made in Section 4.5.3.

4.5.1. FREQUENTLY USED METHODS

In order to be able to quickly see who used what method for what particular purpose, it is best to have an overview such as was done in Section 4.4. Therefore Table 4.2 has been set-up to show the methods used in the past. They are mentioned in chronological order of publication; earliest publication first.

All the problems mentioned in Table 4.2 require metaheuristic methods. [82] mentions that Differential Evolution is very popular resulting in good results and being very robust, but that Monotonic Basin Hopping might be a better alternative because it can give better results.

When looking at the problem of ascent launch trajectory optimization again metaheuristics can be used, because they are easy to implement. However, there are some ([83]) who say that when looking at an ascent

Table 4.2: Previous methods used for trajectory and orbit transfer optimization problems

Who	What	Which method
P.J. Gage et al. [74]	Interplanetary Trajectory (Mars missions)	Genetic Algorithm
Y.H. Kim and D.B. Spencer [75]	Spacecraft Rendezvous	Genetic Algorithms
G.A. Rauwolf and V.L. Coverstone-Carroll [76]	Low-thrust orbit transfers (to Mars and Mercury)	Genetic Algorithm
D.R. Myatt et al. [77]	Mission Analysis and Design (transfer orbits)	Differential Evolution (most robust)
S. Lee et al. [73]	Low-thrust orbit transfers	Q-law with Genetic Algorithm and G-law with Simulated Annealing
O. Abdelkhalik and D. Mortari [78]	Transfer orbits	Genetic Algorithms
M. Vasile et al. [79]	Space trajectories	Monotonic Basin Hopping
J.A. Garcia et al. [80]	Optimization of Mars entry vehicle for a mass of 40 tons	(Multi Objective) Genetic Algorithm
L. Shuang and P. Yuming [81]	Mars entry and descent	Sequential Quadratic Programming and Monte Carlo
B. Addis et al. [82]	Space trajectories	Monotonic Basin Hopping

problem, trajectory optimization will give the best results when performed analytically (as also done in [64]). This because ascent trajectory optimization problems do not have discrete variables according to [83].

4.5.2. TU DELFT OPTIMIZATION HERITAGE

At the Space department of the TU Delft, a toolbox was developed called Tudat. This toolbox can be used to solve and create programs for all kinds of astrodynamical problems. Since the introduction of this toolbox, students have been working on optimization programs within this toolbox mainly based on Differential Evolution [84]. Such a program was developed by [66]. These developed programs were also adjusted to incorporate specific problem needs such as was done by [85] where the original program used Differential Evolution and Particle Swarm Optimization was added to get a better solution.

4.5.3. CHOSEN CANDIDATE METHODS

As mentioned earlier in this section, the decision of which method to use would primarily be based on TU Delft heritage. Currently, the method that is used most (and the method that most existing programs in the Tudat toolbox are programmed for) is Differential Evolution. Therefore it is logical to use the Differential Evolution optimization method for the current subjects problems. However, as [85] also showed, depending on the problem, it might be better to incorporate other methods as well. Based on the previously used methods given in Section 4.5.1 it is clear that even though Differential Evolution is very popular even outside of the TU Delft, Monotonic Basin Hopping might be a good alternative to explore.

Therefore it is decided that at this point Differential Evolution seems to be the best option, keeping Monotonic Basin Hopping and analytical methods for launch trajectories in mind as well.

5

INTEGRATORS

Integration can be used to model/predict the way a function will progress (in time) usually given an initial condition. In orbital computations, integration is often used to model the stability of an orbit or predict where an object or spacecraft will be after a certain time or given a certain disturbance. Because orbits and launch trajectories are multi-dimensional problems, the functions cannot be integrated analytically and have therefore be approximated using numerical integration methods [86]. A short summary of available integration methods will be given in Section 5.1. When it comes to choosing a certain integration method, it is important to look at what the accuracy of the results should be and the amount of (cpu-)time is available. In order to get an accurate result, usually a lot of cpu-time is needed. But often a good solution indication/approximation can be given in a shorter time, but with a lower accuracy. Therefore, a trade off between accuracy and time is often made [87]. In Section 5.2 a comparison will be made between the given integration methods, which will give an idea of the accuracy and time efficiency. At the end of this chapter (Section 5.3) a selection is made of the best integrators based on the TU Delft heritage and external experience with problems similar to the subjects given in Chapter 2. Unfortunately, because the methods are numerical, and thus never give an absolute accurate answer, there is always a sudden inaccuracy. This inaccuracy is represented by a certain error called the truncation error. These truncation errors are usually the biggest errors, however there can also be an additional error caused by the fact that computers round-off values up to a certain amount of decimal figures. The more computations are done in sequence, the bigger this round-off error will become. There are also specific errors that come with the integration of a space related problem as described in [88]. If the simulated system is chaotic or if the step-size is too large, instability errors can occur. There can also be errors in the physical model used to simulate the system caused by mistakes in the assumptions made to make up the physical model such as forces and disturbances that are not (properly) taken into account. Many methods exist to deal with, or at least give an approximation of, these errors. These methods are then sometimes combined with integration methods to create new integration methods. This chapter will thus focus on the different integration methods and not the different methods of determining the different errors.

5.1. DIFFERENT INTEGRATORS

There is a whole range of different integration methods available. Therefore it is best to split them up into different categories. In this section the methods have been split into single-step (Section 5.1.1) and multi-step (Section 5.1.2) based on [87]. The methods can further be categorised by either having a fixed or a variable step-size and by being explicit or implicit. An explicit method only uses the information of the current \mathbf{x}_i (and sometimes past) point(s) to determine the next point value \mathbf{x}_{i+1} . In addition an implicit method also uses the next point value to determine this next point value, which requires iteration. Numerical integration to the next point can be defined by the current point plus the step-size h times the increment function Φ as given in Equation (5.1). The increment function changes depending on the used method. Here, η represents the numerical approximation.

$$\mathbf{x}(t_0 + h) \approx \mathbf{x}_0 + h\Phi = \eta(t_0 + h) \quad (5.1)$$

5.1.1. SINGLE-STEP

In single-step methods, only the information at the current (starting) point is taken into account and the information of previous points is neglected and not saved [87]. Some simple explicit, fixed step-size, single-step methods are **Euler**, **Mid-point** and **Runge-Kutta 4 (RK4)** [86]. Euler simply takes the properties of the initial point to directly calculate the value at the next point. Mid-point already takes an extra point at half a step-size into account, and RK4 takes the weighted average of four points (the starting point, two mid-points and a final point) into account. Many derivative methods exists based on these functions. A method based on the Mid-point method for instance is the **high-order extrapolation (a.k.a. DIFEX2)** (explicit) [89]. And some examples based on the original RK4 integrator are **Runge-Kutta-Nyström (a.k.a. DOPRIN)** (implicit) [90], **High-order Runge-Kutta-Nyström (RKN12)** (implicit) [90] and **Runge-Kutta-Fehlberg (RKF45)** [91, 92]. This last one is slightly different since it is still explicit, but uses a variable step-size.

5.1.2. MULTI-STEP

A multi-step method uses the information from the current point and the information of previous points, usually going as far back as the previous three points such as the **Adams-Bashforth 4 (AB4)** method [87]. This explicit method is similar to RK4 where it uses a weighted average of four points, but in this case uses three previous points. A derivative of this method is the **Adams-Bashforth 6 (AB6)** (explicit) method. An implicit, fixed step-size, multi-step method is the **Adams-Moulton** method which uses a polynomial to interpolate the function values [87]. Combining both these explicit and implicit methods creates what is called a Predictor-Corrector where the initial guess for the next point value is given by the explicit function and the implicit function is then used to correct or improve the estimate. Such methods are **Low-order Predictor-Corrector (ABM4)** and **High-order Predictor-Corrector (ABM12)** [87, 90]. These all use a fixed step-size, however there are also variable step-size methods based on these previous methods such as **Shampine-Gordon (DE)**, which is an explicit method [93, 94] and **Störmer-Cowell (SC14)**, which is again both implicit and explicit (based on Predictor-Corrector) [90, 93].

5.2. TECHNIQUE COMPARISON

In order to get a better understanding of the different methods mentioned in bold in Sections 5.1.1 and 5.1.2, a comparison is made between all these methods. A representation (based on [87]) of the mentioned methods is given in Table 5.1. The sources for these advantages and disadvantages are the same as mentioned in Sections 5.1.1 and 5.1.2, and should an extra source be used, it will be mentioned separately. Also, please note that the comparison is sometimes based on astrodynamical problems specifically and do not necessarily hold true for other physical problems.

Table 5.1: Integration method comparison

Method	Type	Advantage	Disadvantage
Euler	Single-step, fixed step-size, explicit	simple, easy to implement	poor accuracy, for better solution it requires very small step-sizes, so an increase in cpu time
Mid-point	Single-step, fixed step-size, explicit	simple, easy to implement	still not very accurate
RK4	Single-step, fixed step-size, explicit	simple, stable, and has small round-off error accumulation	step-size has to be determined through trial and error which required a lot of cpu time
DIFEX2	Single-step, fixed step-size, explicit	useful for numerically stable second order differential equations	not that accurate and not very fast

DOPRIN	Single-step, fixed step-size, implicit	includes local truncation error estimate [95], can be used for a wide range of accuracies [19]	not very accurate and not very fast either
RKN12	Single-step, fixed step-size, implicit	high accuracy, efficient (fast)	high order (can be complex) and not the best method if the system is velocity dependent [19]
RKF45	Single-step, variable step-size, explicit	includes local truncation error estimate	poor accuracy and slow
AB4	Multi-step, fixed step-size, explicit	simple, stable, efficient if previous results are stored, faster than RK4 for identical step-size and has small round-off error accumulation	step-size has to be determined through trial and error which required a lot of cpu time, and needs a different technique to determine the previous point values at the beginning
AB6	Multi-step, fixed step-size, explicit	very fast	very poor accuracy and instability at large step-sizes [19]
Adams-Moulton	Multi-step, fixed step-size, implicit	accurate, stable, and has small round-off error accumulation	step-size has to be determined through trial and error which required a lot of cpu time, and needs a different technique to determine the previous point values at the beginning
ABM4	Multi-step, fixed step-size, both implicit and explicit	very fast and includes local truncation error estimate	poor accuracy and not efficient if high accuracies are required
ABM12	Multi-step, fixed step-size, both implicit and explicit	fast, has a high accuracy and includes local error estimate	not efficient if low accuracies are required
DE	Multi-step, variable step-size, explicit	very accurate, high efficiency, includes local truncation error estimate and stable [19]	not very fast
SC14	Multi-step, variable step-size, both implicit and explicit	very accurate, fast and very stable [19]	can be complex

A graphic performance comparison, performed by [19], was made between these methods for single-step (Figure 5.1) and multi-step (Figure 5.2). It should be mentioned though that the graphs show more methods than mentioned in this and the previous section, because more variations exist but it was chosen to give

discuss a selection of different methods only.

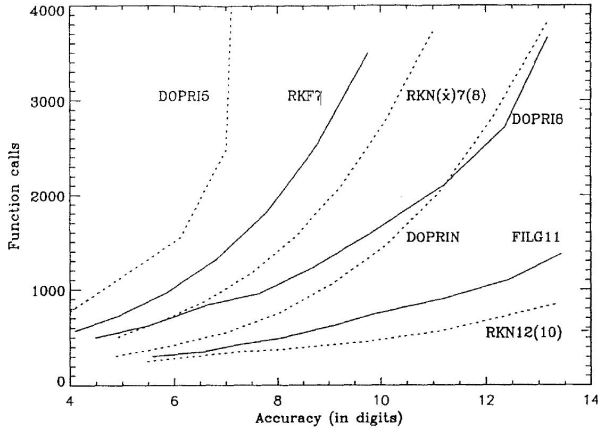


Figure 5.1: Comparison of single-step methods for an eccentricity of 0.1 [19]

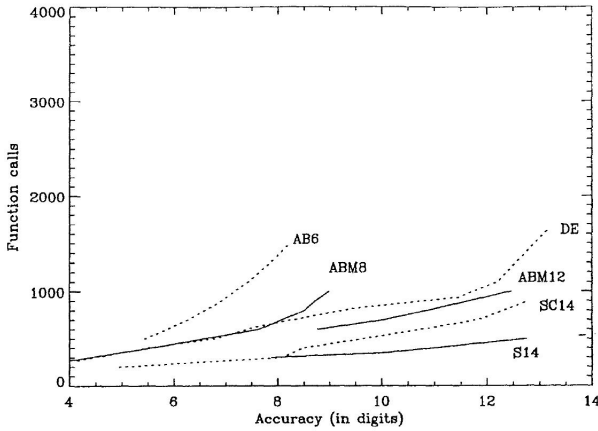


Figure 5.2: Comparison of multi-step methods for an eccentricity of 0.1 [19]

5.3. CHOSEN METHODS

In order to again choose one or several of the mentioned integration methods, it is useful to know which methods are being used in industry and which methods have already been used within the space department at the TU Delft. Some of the references used in Sections 5.1 and 5.2 were already focussed on space missions but discussed a whole selection of different methods. Some elaboration on the used methods for space problems is done in Section 5.3.1. Then the past TU Delft experience is given in Section 5.3.2. It is important to look at the experience that already exists within the department because that way it will be easier to learn from the people there, which is why the heritage will mainly decide the main methods. However, new developments or different theories from outside of the department should not be neglected, which is why these are also still considered as alternatives.

5.3.1. FREQUENTLY USED METHODS IN RELATED SPACE PROBLEMS

To give a quick overview of who used what method for what particular purpose, Table 5.2 has been set-up. Should a reference discuss different methods, then the method that the author deems best for a space related mission will be chosen. However, in some cases several methods are mentioned, since the detailed scope of the subjects is not set yet. In those cases, the proper application of the methods will be given as well. The references mentioned in Table 5.2 are mentioned in chronological order of publication; earliest publication first.

Table 5.2: Previous integration methods used for trajectory and orbit (transfer) problems

Who	What	Which method
T.R. Quinn et al. [96]	Orbit propagation	Störmer (so without Cowell implicit correction)
O. Montenbruck [19]	Orbital motion (very low and very high elliptic orbits)	RKN12 (if EoM $\neq f(V)$) else DE
P.J. van der Houwen et al. [97]	High-precision orbit computations	Störmer-Cowell
A.B. González et al. [98]	long-term satellite orbit prediction	high order RKN
M.M. Berry [93]	Space surveillance	Störmer-Cowell

Unfortunately, often in literature, it is simply mentioned that an integration was performed, but then they fail to mention which method it was.

A completely different category of integrators is the symplectic integration methods. These are used in orbit mechanics when dealing with a pure Hamiltonian system [86] and in the case of very long term orbit integrations. However, since they deal with such a specific problem they are not yet considered useful.

5.3.2. TU DELFT INTEGRATION HERITAGE

Within the space department, integration work has been performed by Van Kints in 2005 [87] (with SC14 performing best with Cartesian coordinates), Gondelach in 2012 [99] (using RK4) and Hofsteenge in 2013 [86] (recommends DOPRI8, which is similar to DOPRIN). Although most methods used here are quite different, it is still important to know what has been done in the past.

5.3.3. CHOSEN CANDIDATE METHODS

Considering the different methods mentioned in Section 5.3.2 the choice will also highly depend on the methods mentioned in Section 5.3.1. Therefore, at this point the best method considered is Störmer-Cowell. Still however taking into account the existing experience of the space department.

6

REFERENCE SYSTEMS AND TRANSFORMATION

If someone drives too fast in their car they might risk getting a ticket. This is because the speed of the car can be measured by the police. Also, when you get the ticket, the police might point to the fact that there is a speedometer build into the dashboard of the car and the driver could have known that he was driving too fast. This can be done because it is all measured in the same [RF](#); the car is travelling with respect to the Earth. However, in space it works a bit different. When talking about the position, speed and acceleration of a space vehicle, different reference frames are usually used. Why there are different frames, which frames there are, what they are used for and how to transfer from one frame to the other will be discussed in Sections [6.1](#) and [6.2](#). When looking back at the example of the speeding car, a certain coordinate system has to be used in order to measure the speed in a certain direction. In this case for instance it can be said that a Cartesian system was used with x in the direction of motion, z pointing towards the ground and y then pointing to the right if looking in the direction of motion (using a so-called right-hand rule to complete the frame). In this case the speed is then measured and expressed in the x -direction. This works well when a vehicle is travelling in a straight line or on a flat plane, but in orbital mechanics the motion usually has to be described around a sphere or in an orbit around that sphere. Therefore it is important to know which coordinate system is used and how to change between these coordinate systems should the other system become more convenient to use at some point. In Section [6.3](#) the difference between these coordinate systems and how to get from one to the other is explained.

6.1. DIFFERENT REFERENCE FRAMES

In the example of the speeding car, the frame of reference is fixed to the Earth. However, if you look at two cars driving on the same road (for instance the police car trying to intercept the speeding car) it might be better to look at the difference in speed of the two cars. In that case a [RF](#) is chosen that is fixed to one of the two cars. This way it is easier to determine the relative speed of one car with respect to the other car. The same can be done for [s/c](#) (think of formation flying). There are therefore a number of different [RFs](#) that can be used. In this chapter the most commonly used [RFs](#) and their use will be presented.

6.1.1. ECI RF

The Earth-centred inertial reference frame is a [RF](#) that is, as the name already implies, fixed to the centre of mass of the Earth [\[20\]](#). It is a frame in which the Earth still rotates with respect to that frame, or in other words it is an inertial frame with respect to Earth. The z -axis is pointed north through the rotational axis of the Earth as it was on the 1st of January 2000 at 12:00 Greenwich Mean Time ([GMT](#)). The x -axis is defined through the vernal equinox of that same year. The vernal equinox is the point in the northern hemisphere spring where the solar ecliptic and the Earth equator cross. On that day, the night lasts precisely 12 hours. Finally, the y -axis is added using the right hand rule as depicted in Figure [6.1](#). The centre of the frame is given by the letter 'A'. The reason why this date is so important is because a standard was established on that date. Also, due to nutation, the rotation axis of the Earth changes, which is not useful if you want to use an inertial frame. Therefore, the International Celestial Reference System was set-up. This standard uses the mean equator and

the vernal equinox of the so-called J2000 standard. It is called J2000 because the standard was set on the Julian date of 2451545.0 or 01-01-2000 at 12:00 [GMT](#).

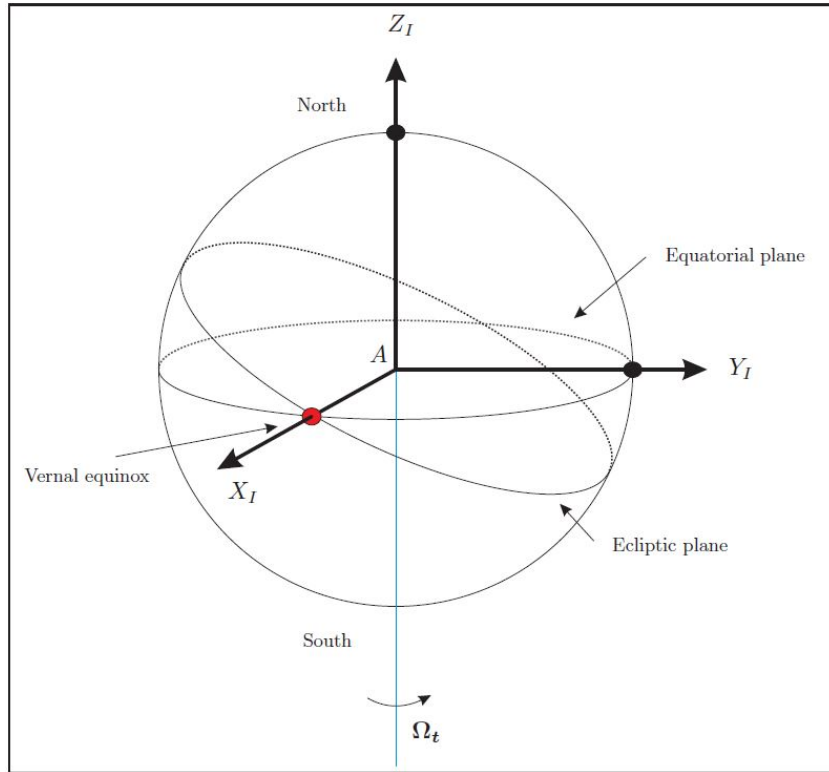


Figure 6.1: Graphical definition of the Earth-centred inertial reference frame [20]

This reference system is very useful if the motion of the [s/c](#) with respect to the [s/c](#) ground track is not important.

6.1.2. SCI RF

The sun-centred inertial reference frame is similar to the [ECI](#) in that it is again inertial and the x-axis is pointed through the vernal equinox. However, in this case the [RF](#) is positioned in the centre of mass of the Sun and the z-axis goes through the north pole of the Sun. Also, the y-axis now lies on the solar ecliptic instead of on the equatorial plane as it did in the [ECI RF](#) [26]. A graphic representation of the [SCI RF](#) is given in Figure 6.2.

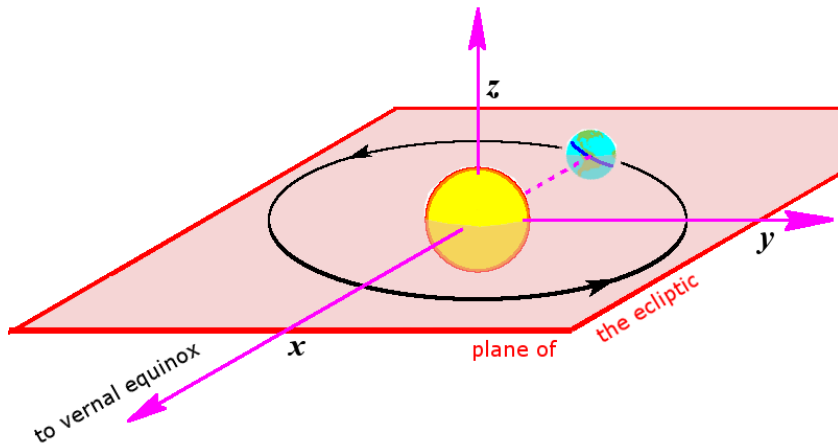


Figure 6.2: Graphical definition of the Sun-centred inertial reference frame [21]

6.1.3. ECEF RF

The Earth-centred Earth-fixed frame is exactly the same as the [ECI](#) frame except for one distinct difference. Where the x-axis of the [ECI](#) frame (x_I) was set in the celestial sphere pointing through the vernal equinox, the x-axis of the [ECEF](#) frame (x_C) goes through the point on the equator where the Greenwich meridian crosses [20]. And thus, because the Greenwich meridian is fixed to the surface of the Earth and rotates around the Earth rotational axis (in both [ECI](#) and [ECEF](#) the z-axis), the [ECEF](#) is also a rotational frame. This frame rotates with the Earth and can therefore be very useful for ground observation purposes. A graphical representation of the [ECEF](#) frame is shown in Figure 6.3.

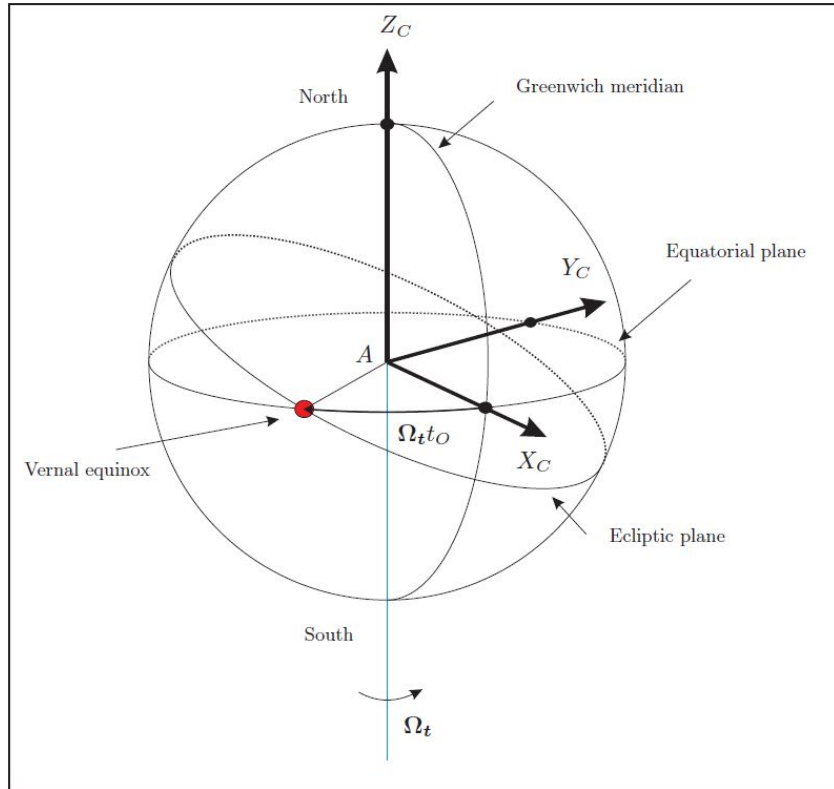


Figure 6.3: Graphical definition of the Earth-centred Earth-fixed reference frame [20]

6.1.4. VCNE RF

This next frame of reference is not often used in space applications but is still worth mentioning due to its usefulness in serving as an intermediate step when transforming from a [s/c](#) frame to a planet frame. The centre of this [VCNE](#) frame is set in the centre of gravity of the [s/c](#) [20] but is not rotationally fixed to it. This means that the frame can rotate with respect to the [s/c](#) itself. This is because the x-axis is set to point to the north pole of the planet the [s/c](#) is orbiting (in this case Earth). The z-axis points to the centre of the Earth (assuming the Earth is a sphere for now) and the y-axis then points due East. The x-y plane is given to be tangent to the Earth geoid. Figure 6.4 shows the [VCNE](#) frame denoted by the letter 'E' at an arbitrary position around the Earth compared to the [ECI](#) frame. Also, the centre of the [VCNE](#) frame is given by the letter 'G'.

6.1.5. BF RF

As can already be determined by the name of this [RF](#), the body-fixed frame is fixed to the [s/c](#) body and therefore rotates with the [s/c](#) as well. The origin of the [BF RF](#) is usually chosen to be in the centre of mass (most of the times equal to the centre of gravity) [20]. The nice thing about this frame though is the fact that the axis orientation can be chosen to be in any direction. In case of a 3U-cubesat orbiting Earth for example, it is useful to define the x-axis to go through the longest part of the satellite. Also, the y-axis and the z-axis are then chosen to go through the 'right' and 'bottom' side of the satellite. This situation is depicted in Figure 6.5.

It is very common to use a self defined [BF](#) frame for [s/c](#) in order to, for instance, compute disturbances and vibrations. Another example of a [BF RF](#) is given in Figure 6.6. Here, the used [BF RF](#) of the Apollo Command

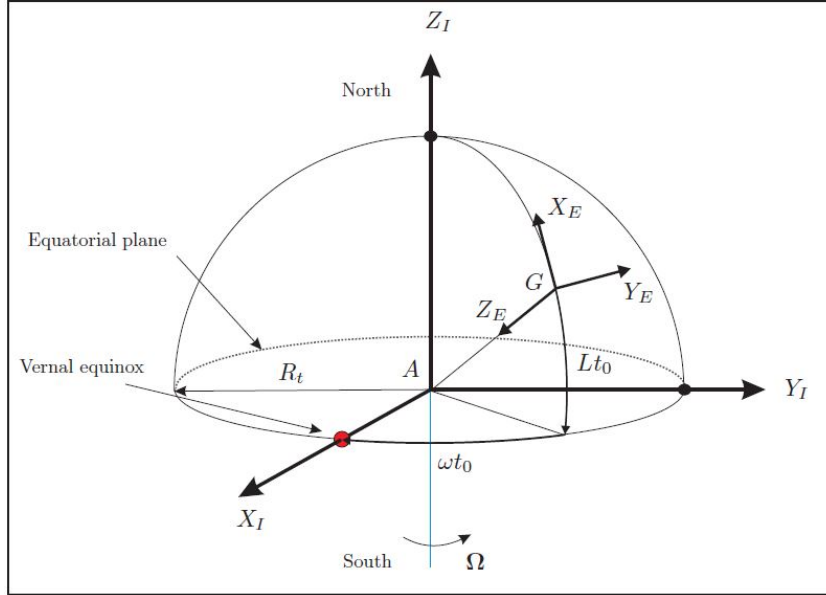


Figure 6.4: Graphical definition of the Vehicle-carried normal Earth reference frame compared to the Earth-centred inertial frame [20]

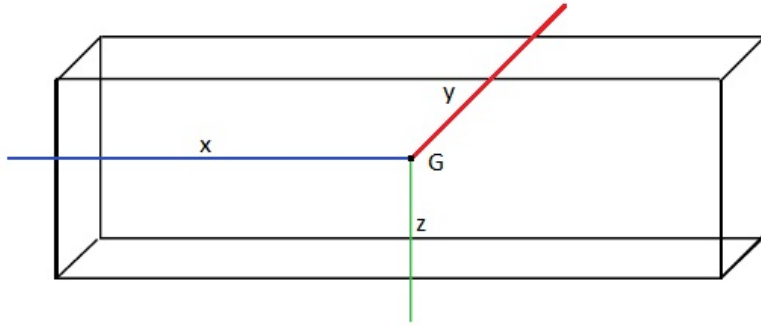


Figure 6.5: Graphical example of a Body-fixed reference frame for a 3U-cubesat adapted from [22]

and Service module was defined by the nose of the vehicle and the main hatch.

6.1.6. FPB RF

This type of vehicle frame is commonly used in orbit mechanics (where the [s/c](#) is often simulated as a point mass). The origin of the frame is set in the centre of mass and the x-axis is pointed in the direction of flight (based on [20]). If the [s/c](#) is orbiting Earth for example, the z-axis will be pointed towards the Earth and the y-axis is defined through the right hand rule to complete the [RF](#). In case of a perfectly circular orbit, this means that the x-axis is parallel to the planet surface (assuming a sphere) and the z-axis is pointed directly into the direction of the planet centre. In this case the [FPB](#) frame can be represented by Figure 6.7.

6.2. TRANSFORMATION BETWEEN REFERENCE FRAMES

Because different problems and situations are easier to understand and to formulate in different [RFs](#), it is important to understand how to go from one [RF](#) to the other. Or in other words, how to transform from one [RF](#) to the other. This is first done for a set point in time, which is then called a static transformation, and is described in Section 6.2.1. Then in Section 6.2.2 the dynamic transformations, transformations over time, will be discussed.

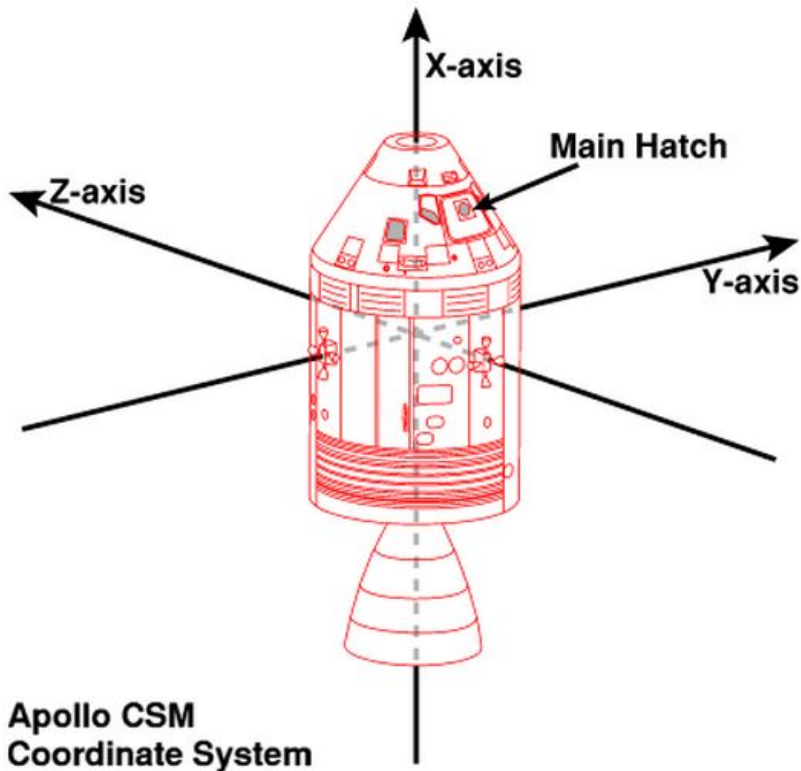


Figure 6.6: Graphical example of a Body-fixed reference frame used on the Apollo Command and Service module [23]

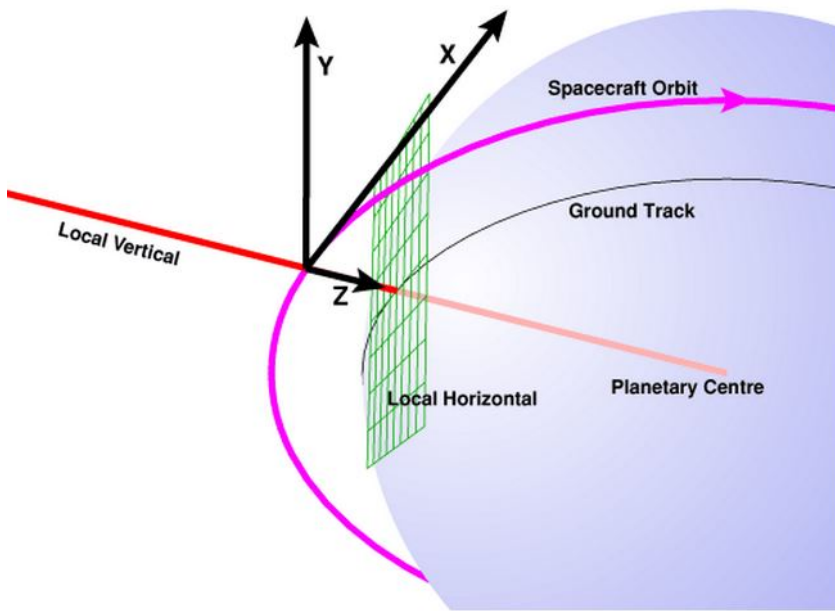


Figure 6.7: Graphical definition of the Flight-path body reference frame for a circular orbit [24]

6.2.1. STATIC REFERENCE FRAME TRANSFORMATIONS

Before a transformation can take place from one RF to the other, a correlation between the two RFs has to exist. This correlation (orientation) is described using a set of angles, called the Euler angles, that can be described between the different RFs [25]. In a 3 dimensional space, there are three axis, so in order to get from one RF to the other, a maximum of 3 rotations (translations/transformations) have to take place; one over each axis. However, it could happen that less rotations are needed because some of the axes are already prop-

erly aligned. Since a 3 dimensional space is described, three dimensional coordinates have to be translated to the next reference frame. This has to be done using a set of equations. A rotation around the x-axis can be described by the change in the y and z coordinates due to an angle ϕ in the y-z plane a visualized in Figure 6.8. The rotation around the x-axis follows the right hand rule of rotation, which states that if the thumb of your right hand is pointed in the axis direction, then the rest of your fingers show the direction of positive orientation. In this case it can thus be seen that the rotation described is positive. Also, because ϕ is defined to be positive in the direction of rotation, it will have a positive sign. Should the rotation have been to the other direction (clockwise around the x-axis as seen in Figure 6.8) or if the angle ϕ would have been defined positive from the z_j -axis to the z_i -axis (so the other way around), the angle would have been negative. This is very important when dealing with transformations, but becomes clearer when more transformations are done after each other. But first a system of equations is needed to transform from the 'i' frame to the 'j' frame.

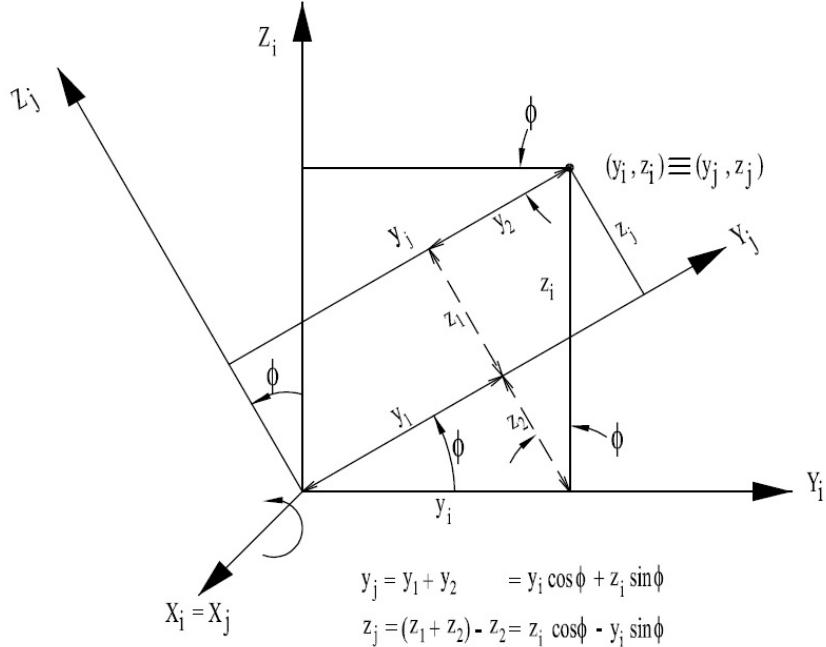


Figure 6.8: General rotation around the x-axis [25]

From Figure 6.8 a relation can be found between the coordinates in the 'i' frame and the 'j' frame in matrix form. This relation (convention found in [25]) is given by Equation (6.1). Here \mathbf{r} is the state vector containing the coordinate values and $T_x(\phi)$ represents the x-axis transformation matrix and is the standard matrix to be used if a transformation around an x-axis is performed. The only parameter that changes is the angle (and sometimes the sign of the angle as mentioned earlier).

$$\begin{pmatrix} x \\ y \\ z \end{pmatrix}^j = \begin{bmatrix} 1 & 0 & 0 \\ 0 & \cos(\phi) & \sin(\phi) \\ 0 & -\sin(\phi) & \cos(\phi) \end{bmatrix} \begin{pmatrix} x \\ y \\ z \end{pmatrix}^i \Rightarrow \mathbf{r}^j = T_x(\phi)\mathbf{r}^i \quad (6.1)$$

This rotation described by Figure 6.8 and Equation (6.1) can also be done for the y-axis and the z-axis. The complete set of axis transformation matrices is then given by Equation (6.2).

$$T_x(\phi) = \begin{bmatrix} 1 & 0 & 0 \\ 0 & \cos(\phi) & \sin(\phi) \\ 0 & -\sin(\phi) & \cos(\phi) \end{bmatrix}, T_y(\phi) = \begin{bmatrix} \cos(\phi) & 0 & -\sin(\phi) \\ 0 & 1 & 0 \\ \sin(\phi) & 0 & \cos(\phi) \end{bmatrix}, T_z(\phi) = \begin{bmatrix} \cos(\phi) & \sin(\phi) & 0 \\ -\sin(\phi) & \cos(\phi) & 0 \\ 0 & 0 & 1 \end{bmatrix} \quad (6.2)$$

The order, or sequence, in which these transformations are performed is very important. This is because the sequence results in a matrix multiplication equation, and from linear algebra it is known that $\mathbf{A} \cdot \mathbf{B} \neq \mathbf{B} \cdot \mathbf{A}$. Therefore, if the sequence of transformations is not correct, the resulting RF will not be the desired RF. Also, it is not always possible or easy to go from one RF directly into the other, so usually one of the afore

mentioned RF is used as an intermediate RF. It could therefore be possible to transform from the ECI matrix all the way to the FPB matrix using almost all the other mentioned RFs with a maximum of three rotations between each frame. To make the equation formulation a bit easier however, it has been chosen to adopt the convention mentioned in [20] and [25]. Therefore the ECI, SCI, ECEF, VCNE, BF and FPB frames will be known as F_I , F_{SI} , F_C , F_E , F_b and F_a respectively when used to indicate the RFs in equations. And because these equations involve matrix multiplications, they always have to be read from right to left. When looking at Equation (6.1) it can be seen that in order to go from one state vector with x, y and z coordinates to the other requires a transformation matrix. But this transformation matrix could actually be comprised of several other transformation matrices that transition between different RFs in order to get to the final one. Therefore it can be said that the transformation matrix to go from $F_I \rightarrow F_E$ for example is $\mathbb{T}_{EI} = \mathbb{T}_{EC}\mathbb{T}_{CI}$. This transformation is depicted in Figure 6.9.

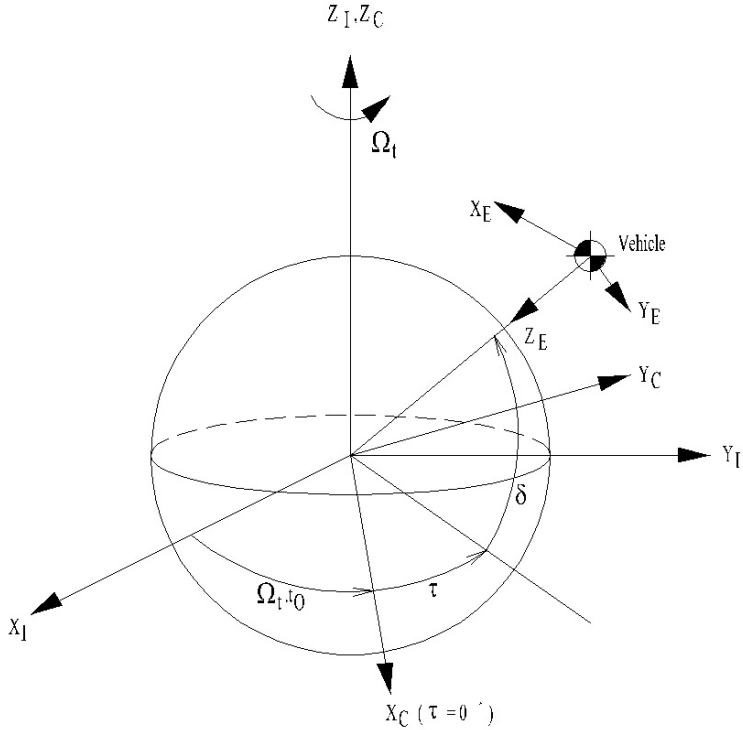


Figure 6.9: Rotation from the ECI to the VCNE frame [25]

However, even these two transformation matrices might comprise of several axis transformation matrices (at most three) with either a positive or negative angle. Therefore it is useful to express the transition matrix as shown by Equation (6.3) (based on [100]). Here the vertical lines with the letter designations depict when a certain reference frame is reached. The looking at the angles from right to left, first a transition is made from $F_I \rightarrow F_C$. This is done over the angle $\Omega_t t_O$ as defined in Figures 6.3 and 6.9. Ω_t is the rotational velocity of Earth and t_O is the time from J2000 till the current time. Also, it can be noted that this angle is positive, because it is defined to be positive going from x_I to x_C and that is also the positive rotational direction of the rotation around the z-axis according to the right hand rule for rotation. The same is done for τ , again a positive angle. Please note that both these rotations can be done at once by adding the two angles together (for proof that either way still results in the same transformation matrix see lines 2, 3 and 4 of Equation (6.4)), but this notation helps to keep a clear overview. The final rotation that is done is over the y-axis in F_C . In this case it can be seen that the angle δ is negative because the rotation is done in the negative rotational direction of the y-axis of F_C (and it is not a double negative, so positive angle again, because the angle is defined positive from $F_C \rightarrow F_E$).

$$\mathbb{T}_{EI} = \mathbb{T}_{EC}\mathbb{T}_{CI} = \left| \begin{array}{c} \mathbb{T}_y(-\pi/2 - \delta)\mathbb{T}_z(\tau) \\ \mathbb{T}_z(\Omega_t t_O) \end{array} \right|_I \quad (6.3)$$

As an expansion on this example, the transformation matrices have been written out and combined to

form the final transformation matrix as shown in Equation (6.4).

$$\begin{aligned}
 T_{EI} &= \begin{bmatrix} \cos(-\pi/2 - \delta) & 0 & -\sin(-\pi/2 - \delta) \\ 0 & 1 & 0 \\ \sin(-\pi/2 - \delta) & 0 & \cos(-\pi/2 - \delta) \end{bmatrix} \begin{bmatrix} \cos(\tau) & \sin(\tau) & 0 \\ -\sin(\tau) & \cos(\tau) & 0 \\ 0 & 0 & 1 \end{bmatrix} \begin{bmatrix} \cos(\Omega_t t_O) & \sin(\Omega_t t_O) & 0 \\ -\sin(\Omega_t t_O) & \cos(\Omega_t t_O) & 0 \\ 0 & 0 & 1 \end{bmatrix} \\
 &= \begin{bmatrix} -\sin(\delta) & 0 & \cos(\delta) \\ 0 & 1 & 0 \\ -\cos(\delta) & 0 & -\sin(\delta) \end{bmatrix} \begin{bmatrix} \cos(\tau) & \sin(\tau) & 0 \\ -\sin(\tau) & \cos(\tau) & 0 \\ 0 & 0 & 1 \end{bmatrix} \begin{bmatrix} \cos(\Omega_t t_O) & \sin(\Omega_t t_O) & 0 \\ -\sin(\Omega_t t_O) & \cos(\Omega_t t_O) & 0 \\ 0 & 0 & 1 \end{bmatrix} \\
 &= \begin{bmatrix} \sin(\delta) & 0 & \cos(\delta) \\ 0 & 1 & 0 \\ -\cos(\delta) & 0 & -\sin(\delta) \end{bmatrix} \begin{bmatrix} \cos(\tau) \cos(\Omega_t t_O) - \sin(\tau) \sin(\Omega_t t_O) & \sin(\tau) \cos(\Omega_t t_O) + \cos(\tau) \sin(\Omega_t t_O) & 0 \\ -\sin(\tau) \cos(\Omega_t t_O) - \cos(\tau) \sin(\Omega_t t_O) & -\sin(\tau) \sin(\Omega_t t_O) + \cos(\tau) \cos(\Omega_t t_O) & 0 \\ 0 & 0 & 1 \end{bmatrix} \\
 &= \begin{bmatrix} \sin(\delta) & 0 & \cos(\delta) \\ 0 & 1 & 0 \\ -\cos(\delta) & 0 & -\sin(\delta) \end{bmatrix} \begin{bmatrix} \cos(\tau + \Omega_t t_O) & \sin(\tau + \Omega_t t_O) & 0 \\ -\sin(\tau + \Omega_t t_O) & \cos(\tau + \Omega_t t_O) & 0 \\ 0 & 0 & 1 \end{bmatrix} \\
 &= \begin{bmatrix} -\sin(\tau) \cos(\tau + \Omega_t t_O) & -\sin(\tau) \sin(\tau + \Omega_t t_O) & \cos(\delta) \\ -\sin(\tau + \Omega_t t_O) & \cos(\tau + \Omega_t t_O) & 0 \\ -\cos(\delta) \cos(\tau + \Omega_t t_O) & -\cos(\delta) \sin(\tau + \Omega_t t_O) & -\sin(\delta) \end{bmatrix} \quad (6.4)
 \end{aligned}$$

6.2.2. DYNAMIC REFERENCE FRAME TRANSFORMATIONS

The difference between the static and the dynamic RF transformations is that time is now taken into account as well. In [20], two different dynamics are mentioned: motion and rotation. By default, the inertial reference frames will not move (but the ECI moves with respect to the SCI and vice versa). However, when comparing two RFs and expressing the motion and rotation to one of these RFs, it can be said that this RF is inertial with respect to the other RF which is then moving. In general any RF can be described by the origin and its unit vectors. In case of the defined inertial RF the origin would be called O and the unit vectors would be I, J and K respectively in the x, y and z direction [20]. For the moving RF the origin would be defined as G with unit vectors i, j and k . For the purpose of this explanation the inertial reference frame is taken to be F_I and the moving reference frame is F_b . Then if an arbitrary point P is taken, the position of this point can be described in both frames using position vectors as shown in Figure 6.10.

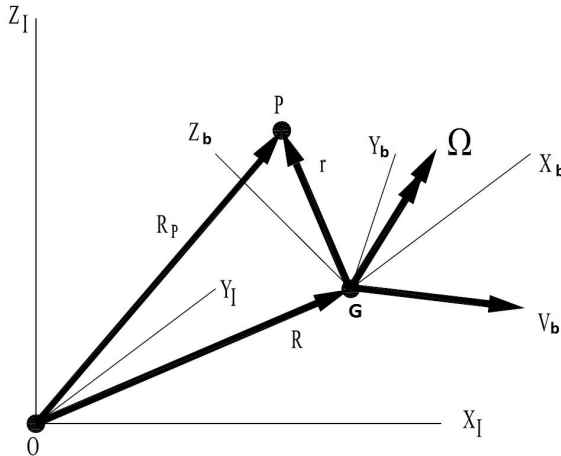


Figure 6.10: Motion and rotation of point P described in an inertial and moving frame adapted from [20]

In Figure 6.10 R is the position vector of origin G with respect to origin O , r is the position vector of point P in F_b and \mathbf{R}_P is the position vector of point P in F_I . Also, because all movements and rotations need to be expressed in F_I , it can be seen that $\mathbf{R}_P = \mathbf{R} + \mathbf{r}$. Now the velocity of point P with respect to F_I can be expressed by Equation (6.5) where the I at the bottom of the vertical line represents the RF in which the derivative is taken and the superscript represents the RF in which the derivative is eventually expressed [20, 100].

$$\frac{d\mathbf{R}_P}{dt} \Big|_{\mathbf{I}}^{\mathbf{I}} = \frac{d\mathbf{R}}{dt} \Big|_{\mathbf{I}}^{\mathbf{I}} + \frac{d\mathbf{r}}{dt} \Big|_{\mathbf{I}}^{\mathbf{I}} \quad (6.5)$$

In Equation (6.5) the motion of F_b with respect to F_I is given by $\frac{d\mathbf{R}}{dt}$, which is V_b in Figure 6.10. Also, the velocity that point P has with respect to F_b is expressed in F_I . However, this velocity can also be expressed in F_b frame when the rotational velocity of F_b with respect to F_I (Ω_{Ib}) is added. This then leads to the expression found in Equation (6.6) [100].

$$\frac{d\mathbf{r}}{dt} \Big|_{\mathbf{I}}^{\mathbf{I}} = \frac{d\mathbf{r}}{dt} \Big|_{\mathbf{b}}^{\mathbf{I}} + \Omega_{\mathbf{b}\mathbf{I}}^{\mathbf{I}} \times \mathbf{r}^{\mathbf{I}} \quad (6.6)$$

Then combining Equation (6.5) and Equation (6.6) results in Equation (6.7) where the first two terms are motion terms (first one between the two RFs and the second of point P within F_b) and the last term is the rotation term.

$$\frac{d\mathbf{R}_P}{dt} \Big|_{\mathbf{I}}^{\mathbf{I}} = \frac{d\mathbf{R}}{dt} \Big|_{\mathbf{I}}^{\mathbf{I}} + \frac{d\mathbf{r}}{dt} \Big|_{\mathbf{b}}^{\mathbf{I}} + \Omega_{\mathbf{b}\mathbf{I}}^{\mathbf{I}} \times \mathbf{r}^{\mathbf{I}} \quad (6.7)$$

A more detailed derivation and explanation can be found in [20].

When taking a closer look at the rotational velocity (or rotational rate vector) Ω it can be seen that this reflects the rotation by a certain angle in a certain amount of time (in the case of Ω_t it represents the *rad/s*, rotational speed, of the Earth), or a part of that angle every time-step. When looking at the transformation done over the angle τ in Equation (6.3), the associating rotational rate of the angle itself would be $\dot{\tau} = \frac{d\tau}{dt}$. The vector notation of this rotational rate would then be $\Omega_{C'C} = \dot{\tau}\mathbf{z}_C$ with C' representing the intermediate RF between F_C and F_E . If the rotation from this intermediate RF to F_E is added the total rotation rate vector from $F_C \rightarrow F_E$ can be represented by Equation (6.8).

$$\Omega_{EC} = (-\pi/2 - \delta)\mathbf{y}_{C'} + \dot{\tau}\mathbf{z}_C = \Omega_{EC'} + \Omega_{C'C} \quad (6.8)$$

The rotational rates can simple be added to get to the final rotational rate. Which means that the total rotation rate vector for Equation (6.3) can be represented by Equation (6.9).

$$\Omega_{EI} = (-\pi/2 - \delta)\mathbf{y}_{C'} + \dot{\tau}\mathbf{z}_C + (\Omega_t t_O)\mathbf{z}_I = \Omega_{EC'} + \Omega_{C'C} + \Omega_{CI} \quad (6.9)$$

Again, the subscripts note a transformation/rotation from right to left. However, in Equation (6.6) it can clearly be seen that it is written that the rotation should be from $F_I \rightarrow F_b$, which is not the case (it goes from $F_b \rightarrow F_I$). This notation can easily be explained if you consider point P to be stationary in F_I and only F_b is rotating. Then a positive rotation in F_b will have to be translated back using that same rotation rate but then negative (in order to get a stationary point P in F_I). So it is expected to write $-\Omega_{Ib}^{\mathbf{I}}$. But because the rotational rate is simply an addition of all rotational rates, it holds that $-\Omega_{Ib}^{\mathbf{I}} = \Omega_{bI}^{\mathbf{I}}$, which explains the notation.

6.3. TRANSFORMATION BETWEEN DIFFERENT COORDINATE SYSTEMS

In the previous sections the different RF and transformations were always expressed using x, y and z-axes. These x, y and z coordinates belong to the Cartesian coordinate system. However, during an integration, simulation or analysis it might be more useful and meaningful to have the position (and velocity) expressed in a different coordinate system. Two other systems are the Spherical and Keplerian coordinate systems. How to transform back and forth from the Cartesian system to these other two systems will be explained in ??subsec:sphercart,subsec:keplcart) respectively and are based on [26]. Keplerian elements are very useful for orbit computations, unfortunately singularities can occur if this coordinate system is used. Therefore Section 6.3.3 will discuss a Non-singular form of the Kepler elements.

6.3.1. SPHERICAL AND CARTESIAN

Spherical coordinates can be very useful in order to determine the rough location of a satellite above Earth assuming that Earth is a perfect sphere. The coordinate relation between spherical and Cartesian coordinates can be seen in Figure 6.11. Based on this diagram, the relations to get from the spherical system to the Cartesian system are derived and are given in Equation (6.10).

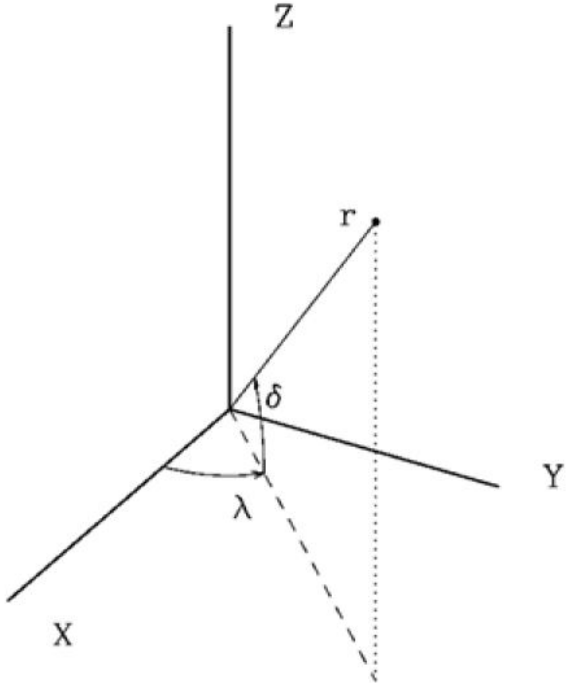


Figure 6.11: Relation between spherical position coordinates and Cartesian position coordinates [26]

$$\begin{aligned} x &= r \cos(\delta) \cos(\lambda) \\ y &= r \cos(\delta) \sin(\lambda) \\ z &= r \sin(\delta) \end{aligned} \quad (6.10)$$

Then the velocities can be obtained by taking the time derivatives of these functions, resulting in the velocity expressions in x, y and z direction given in Equation (6.11). And differentiating those expressions again will result in the accelerations.

$$\begin{aligned} \dot{x} &= \dot{r} \cos(\delta) \cos(\lambda) - r \dot{\delta} \sin(\delta) \cos(\lambda) - r \dot{\lambda} \cos(\delta) \sin(\lambda) \\ \dot{y} &= \dot{r} \cos(\delta) \sin(\lambda) - r \dot{\delta} \sin(\delta) \sin(\lambda) + r \dot{\lambda} \cos(\delta) \cos(\lambda) \\ \dot{z} &= \dot{r} \sin(\delta) + r \dot{\delta} \cos(\delta) \end{aligned} \quad (6.11)$$

Going back from Cartesian coordinates to spherical coordinates can again be done by looking at Figure 6.11, resulting in the expressions given in Equation (6.12).

$$\begin{aligned} r &= \sqrt{x^2 + y^2 + z^2} \\ \delta &= \arcsin\left(\frac{z}{r}\right) \\ \lambda &= \arctan\left(\frac{y}{x}\right) \end{aligned} \quad (6.12)$$

However, the expression for λ only results in a value between $-\pi/2$ and $\pi/2$. In order to solve this issue, the so-called 'atan2' function can be used. This function incorporates both sin and cosine values to give a value for λ between 0 and 2π [26]. In most programming languages, this function is already incorporated and thus the expression in Equation (6.13) can simply be used in the programming.

$$\lambda = \text{atan2}(y, x) \quad (6.13)$$

The actual definitions behind atan2 are given in Figure 6.12.

$$\text{atan2}(y, x) = \begin{cases} \text{atan}\left(\frac{y}{x}\right) & x > 0 \\ \pi + \text{atan}\left(\frac{y}{x}\right) & y \geq 0, x < 0 \\ -\pi + \text{atan}\left(\frac{y}{x}\right) & y < 0, x < 0 \\ \frac{\pi}{2} & y > 0, x = 0 \\ -\frac{\pi}{2} & y < 0, x = 0 \\ \text{Undefined} & y = 0, x = 0 \end{cases}$$

Figure 6.12: atan2 function evaluation conditions adapted from [27]

Then again the time derivatives of the functions given in Equation (6.12) can be taken to find the velocity expressions. Fortunately, the velocity is not quadrant related. The resulting velocity expressions are shown in Equation (6.14).

$$\begin{aligned} \dot{r} &= \frac{x\dot{x} + y\dot{y} + z\dot{z}}{\sqrt{x^2 + y^2 + z^2}} \\ \dot{\delta} &= \frac{x\dot{y} - y\dot{x}}{x^2 + y^2} \\ \dot{\lambda} &= \frac{r\dot{z} - z\dot{r}}{r^2 \sqrt{1 - \left(\frac{z}{r}\right)^2}} \end{aligned} \quad (6.14)$$

6.3.2. KEPLERIAN AND CARTESIAN

The relations described in Section 6.3.1 were very elementary, unfortunately the relation between the Keplerian and Cartesian systems is slightly more complex. Figure 6.13 shows the Kepler elements: a (semi-major axis), e (eccentricity, not shown but is a ratio that shows how elliptic an orbit is), i (inclination), ω (argument of perigee), Ω (right ascension of the ascending node) and M (Mean anomaly). The mean anomaly is defined to be the angle between the semi-major axis and line between the centre of the orbit and the mean position of the orbiting body in the auxiliary circle that can be drawn around the orbit. The mean position of the orbiting body is determined by assuming a constant rotational speed in this circular orbit with the same orbital time as the actual orbit. These elements can now be converted to Cartesian coordinates.

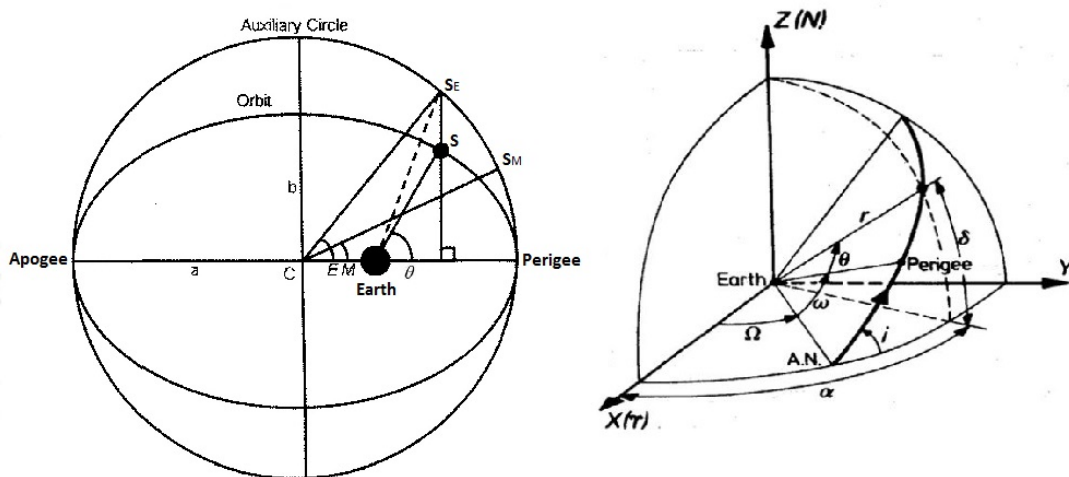


Figure 6.13: Definition of the Kepler elements in 2D (left) and 3D (right) [26, 28]

The transformation from Kepler to Cartesian consists of a few steps starting with the mean anomaly and eccentricity. Both these values have to be used to determine the eccentric anomaly E and in turn the true anomaly θ . The eccentric anomaly is computed by rewriting the first expression of Equation (6.15) into the second expression such that E can be determined [26].

$$\begin{aligned} M &= E - e \cdot \sin E \\ E_{i+1} &= E_i + \frac{M - E_i - e \cdot \sin E_i}{1 - e \cdot \cos(E_i)} \end{aligned} \quad (6.15)$$

As can be seen, the determination of E is an iterative process. First a decent estimate of E has to be given (it is best to use the value for M for this) and then a new E value can be computed. This has to be done until the desired level of precision is reached. Then the true anomaly can be computed using this E as given by Equation (6.16).

$$\theta = 2 \cdot \arctan \left[\tan \left(\frac{E}{2} \right) \sqrt{\frac{1+e}{1-e}} \right] \quad (6.16)$$

With the true anomaly known, the radial distance from the orbiting body to the centre of Earth r can be determined using Equation (6.17)

$$r = \frac{a \cdot (1 - e^2)}{1 + e \cos(\theta)} \quad (6.17)$$

The Cartesian coordinates can now be computed using the expression in Equation (6.18) with the matrix entries given by Equation (6.19)[26].

$$\begin{pmatrix} x \\ y \\ z \end{pmatrix} = \begin{bmatrix} l_1 & l_2 \\ m_1 & m_2 \\ n_1 & n_2 \end{bmatrix} \begin{pmatrix} r \cos(\theta) \\ r \sin(\theta) \end{pmatrix} \quad (6.18)$$

$$\begin{aligned} l_1 &= \cos(\Omega) \cos(\omega) - \sin(\Omega) \sin(\omega) \cos(i) \\ l_2 &= -\cos(\Omega) \sin(\omega) - \sin(\Omega) \cos(\omega) \cos(i) \\ m_1 &= \sin(\Omega) \cos(\omega) + \cos(\Omega) \sin(\omega) \cos(i) \\ m_2 &= -\sin(\Omega) \sin(\omega) + \cos(\Omega) \cos(\omega) \cos(i) \\ n_1 &= \sin(\omega) \sin(i) \\ n_2 &= \cos(\Omega) \sin(i) \end{aligned} \quad (6.19)$$

Equation (6.20) provides the final expressions for x , y and z when Equation (6.18) and Equation (6.19) are combined.

$$\begin{aligned} x &= r \cdot [\cos(\Omega) \cos(\omega + \theta) - \sin(\Omega) \sin(\omega + \theta) \cos(i)] \\ y &= r \cdot [\sin(\Omega) \cos(\omega + \theta) - \cos(\Omega) \sin(\omega + \theta) \cos(i)] \\ z &= r \sin(i) \sin(\omega + \theta) \end{aligned} \quad (6.20)$$

For the velocity values, an extra parameter is needed. This parameter is called the specific relative angular momentum h . Assuming that the mass of the orbiting body can be neglected with respect to the planet (or other celestial body) it is orbiting, h can be expressed as a function of the standard gravitational parameter of that planet μ , a and e as shown by Equation (6.21).

$$h = \sqrt{\mu a \cdot (1 - e^2)} \quad (6.21)$$

Then with h and the expression given in Equation (6.19), the velocities can be expressed as given by Equation (6.22).

$$\begin{aligned}\dot{x} &= \frac{\mu}{h} [-l_1 \sin(\theta) + l_2 \cdot (e + \cos(\theta))] \\ \dot{y} &= \frac{\mu}{h} [-m_1 \sin(\theta) + m_2 \cdot (e + \cos(\theta))] \\ \dot{z} &= \frac{\mu}{h} [-n_1 \sin(\theta) + n_2 \cdot (e + \cos(\theta))]\end{aligned}\quad (6.22)$$

It is also possible to convert from the Cartesian system back to Kepler system, however, this requires more steps and intermediate expressions. First, it is convenient to express the position and velocity both in one vector each as given by Equation (6.23).

$$\begin{aligned}\mathbf{R} &= [x \quad y \quad z] \\ \mathbf{V} &= [\dot{x} \quad \dot{y} \quad \dot{z}]\end{aligned}\quad (6.23)$$

The cross product of these two will then give the specific relative angular momentum vector \mathbf{H} and the scalar values, or lengths, can then be represented by $r = \|\mathbf{R}\|$, $v = \|\mathbf{V}\|$ and $h = \|\mathbf{H}\|$. Also, a vector \mathbf{N} can be defined as given by Equation (6.24)[26].

$$\mathbf{N} = \begin{pmatrix} 0 \\ 0 \\ 1 \end{pmatrix} \times \mathbf{H} \quad (6.24)$$

With these parameters set, the first four Kepler elements (a , e , i and Ω) can be computed as shown by the expressions given in Equation (6.25). Here, the value for the eccentricity can be obtained by taking the length of the vector: $e = \|\mathbf{e}\|$. Also, $\mathbf{H}(3)$ is the third value of the specific relative angular momentum, so the value in the z-direction. The same principle holds for the values from \mathbf{N} .

$$\begin{aligned}a &= \left(\frac{2}{r} - \frac{v^2}{\mu} \right)^{-1} \\ \mathbf{e} &= \frac{\mathbf{V} \times \mathbf{H}}{\mu} - \frac{\mathbf{R}}{r} \\ i &= \arccos\left(\frac{\mathbf{H}(3)}{h}\right) \\ \Omega &= \text{atan2}(\mathbf{N}(2), \mathbf{N}(1))\end{aligned}\quad (6.25)$$

Then, in order to compute the values for ω and θ , three unit vectors are needed: $\hat{\mathbf{N}} = \frac{\mathbf{N}}{\|\mathbf{N}\|}$, $\hat{\mathbf{e}} = \frac{\mathbf{e}}{\|\mathbf{e}\|}$ and $\hat{\mathbf{R}} = \frac{\mathbf{R}}{\|\mathbf{R}\|}$. This leads to the conditional expressions seen in Equation (6.26).

$$\begin{aligned}\omega &= \begin{cases} \arccos(\hat{\mathbf{e}} \cdot \hat{\mathbf{N}}), & \text{if } (\hat{\mathbf{N}} \times \mathbf{e}) \cdot \mathbf{H} > 0 \\ -\arccos(\hat{\mathbf{e}} \cdot \hat{\mathbf{N}}), & \text{otherwise} \end{cases} \\ \theta &= \begin{cases} \arccos(\hat{\mathbf{R}} \cdot \hat{\mathbf{e}}), & \text{if } (\mathbf{e} \times \mathbf{R}) \cdot \mathbf{H} > 0 \\ -\arccos(\hat{\mathbf{R}} \cdot \hat{\mathbf{e}}), & \text{otherwise} \end{cases}\end{aligned}\quad (6.26)$$

The eccentric anomaly can now be computed using θ and e as shown by Equation (6.27), which is the rewritten form of Equation (6.16).

$$E = 2 \cdot \arctan \left[\tan\left(\frac{\theta}{2}\right) \sqrt{\frac{1-e}{1+e}} \right] \quad (6.27)$$

And finally, the mean anomaly can then be found using the earlier mentioned first expression in Equation (6.15)[26].

6.3.3. NON-SINGULAR KEPLER ELEMENTS

Unfortunately, some of the Kepler elements mentioned in Section 6.3.2 can not assume every value. Singularities thus occur when $e = 0$, or $i = 0$. There are several ways these singularities can be avoided, and usually depends on the problem. An example of non-singular values is given in [101]. In this case, all the Kepler elements (except for the semi-major axis) are used to describe six new parameters: $\underline{\lambda}$ (mean longitude), $\underline{\omega}$ (longitude of pericentre, not to be confused with ω the argument of pericentre), ξ , η , \underline{P} and \underline{Q} . The set of corresponding expressions is given in Equation (6.28).

$$\begin{aligned}\underline{\lambda} &= M + \omega + \Omega \\ \underline{\omega} &= \Omega + \omega \\ \xi &= e \cos(\underline{\omega}) \\ \eta &= e \sin(\underline{\omega}) \\ \underline{P} &= \sin\left(\frac{i}{2}\right) \cos(\Omega) \\ \underline{Q} &= \sin\left(\frac{i}{2}\right) \sin(\Omega)\end{aligned}\tag{6.28}$$

And then these can be reverted back into normal Keplerian elements by using the expressions given in Equation (6.29), which are simply the previous equations rewritten.

$$\begin{aligned}M &= \underline{\lambda} - \underline{\omega} \\ e &= \frac{\xi}{\cos(\underline{\omega})} \\ i &= 2 \cdot \arcsin\left(\sqrt{\underline{P}^2 + \underline{Q}^2}\right) \\ \Omega &= \arccos\left(\frac{\underline{P}}{\sin\left(\frac{i}{2}\right)}\right) \\ \omega &= \underline{\omega} - \Omega\end{aligned}\tag{6.29}$$

7

MARS ENTRY AND DESCENT

Several missions have already performed entry and descent successfully on the Martian surface. A short overview of these missions and how they descended to the surface was already given in Section 3.2. But for easy reference, the table with all the reference missions is given again (see Table 7.1, same as Table 3.4).

Table 7.1: Previous Mars Entry and Descent Missions

Launch date	Country	Mission	Type
19 May 1971	Soviet Union	Mars 3	Lander (and failed rover)
20 August 1975	United States	Viking 1	Lander
9 September	United States	Viking 2	Lander
4 December 1996	United States	Mars Pathfinder/Sojourner	Lander and rover
2 June 2003	Europe and United Kingdom	Mars Express/Beagle 2	Lander
10 June 2003	United States	Mars Exploration Rover - A/Spirit	Rover
7 July 2003	United States	Mars Exploration Rover - B/Opportunity	Rover
4 August 2007	United States	Phoenix	Lander
26 November 2012	United States	Mars Science Laboratory/Curiosity	Rover

Also, another overview can be used to quickly show the different techniques that were used on each mission. This overview is given in Table 7.2 and is based on the information provided in Section 3.2.

Table 7.2: Previous entry, descent and landing methods

Mission	Entry phase	Atmospheric descent phase	Landing phase
Mars 3	Separated from s/c (before entering orbit [11], semi-direct entry), main descent engine fire to point heat shield	Heat shield, braking parachute and reefed main parachute [102]	Retro rockets (in back-shell) and drop with air-bags [103]
Viking(s)	Separated from orbiter, main descent engines to de-orbit	Heat shield and parachute	Drop with retro rockets
Mars Pathfinder	Direct entry	Heat shield and parachute	Lowering cable, retro rockets (in back-shell) and air-bags
Mars Express/Beagle 2	Separated from orbiter	Heat shield, pilot parachute and main parachute [38]	Air-bags and main parachute (still attached)

Mars Exploration Rover(s)	Direct entry	Heat shield and parachute	Lowering cable, retro rockets (in back-shell) and air-bags
Phoenix	Direct entry	Heat shield and parachute	Drop with retro rockets
Mars Science Laboratory	Direct entry	Heat shield, manoeuvres and parachute	Drop with powered descent followed by hovered descent and deployment on surface through lowering cable

The [EDL](#) phases all show similarities between the different missions and also some distinct differences. The used methods, general theory and alternative methods will be discussed in this chapter per [EDL](#) phase.

In order to visualize the events described in Table 7.2, the [EDL](#) sequences of the Viking, MPF, Beagle 2 and MSL missions are given in Figures 7.1 to 7.4 respectively.

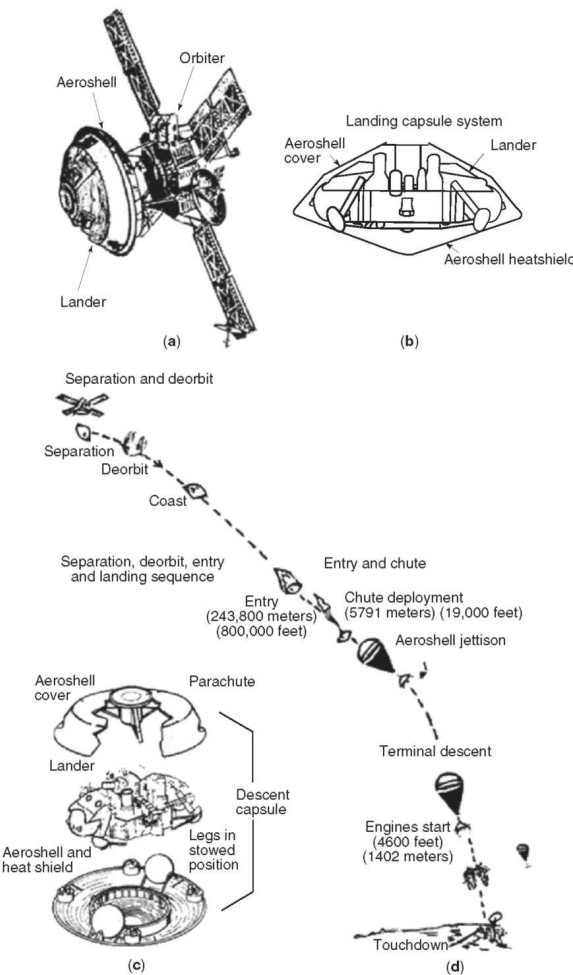


Figure 7.1: Illustration of the Viking 1 [29]; a) the complete [s/c](#), b) the entry vehicle, c) exploded view and d) [EDL](#) sequence

7.1. ENTRY PHASE

Given the previous missions seen in Table 7.2, it is clear that a distinction can be made between orbital entry and direct entry, with the exception of Mars 3 which performed a semi-direct entry where the entry vehicle was released before the [s/c](#) entered orbit around Mars [11]. During the direct entry, a spacecraft intercepts Mars and enters the atmosphere with speeds higher than escape velocity (around 7.26 km/s in the case of Pathfinder compared to 4.7 km/s in the case of the Viking missions [104], Mars escape velocity is around

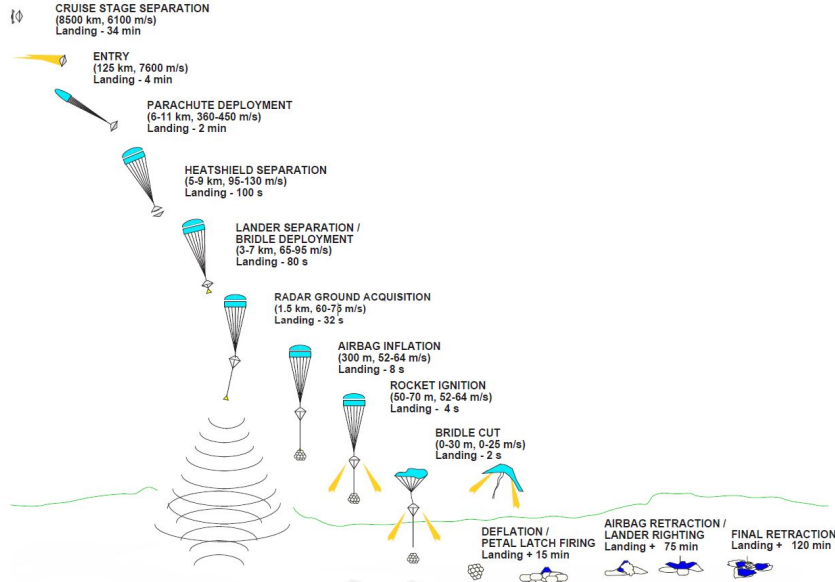


Figure 7.2: Illustration of the MPF EDL sequence [30]

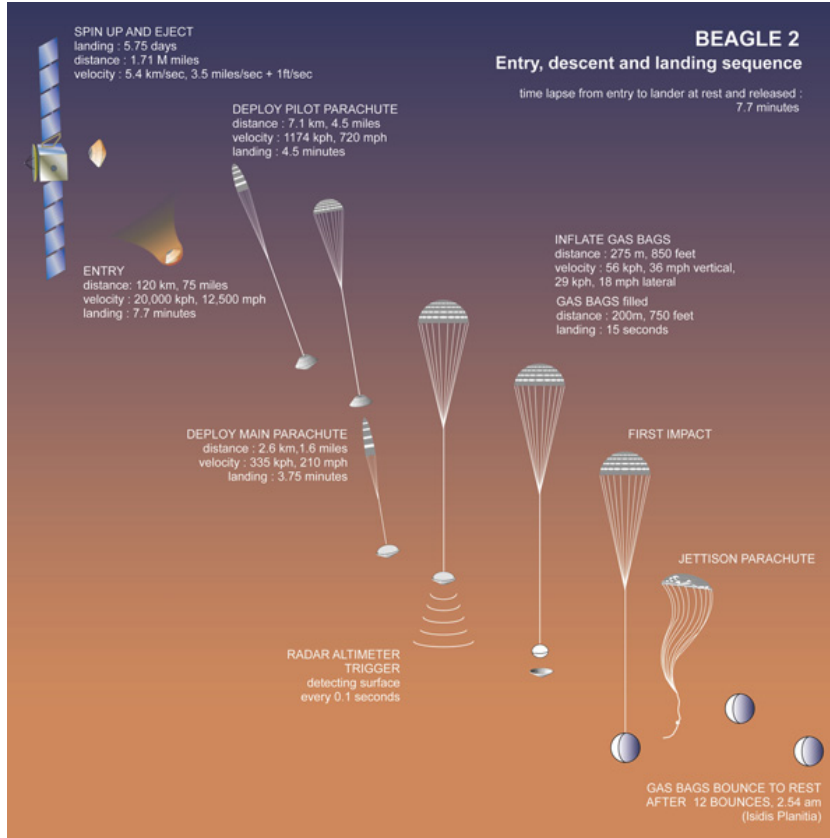


Figure 7.3: Illustration of the Beagle 2 EDL sequence [31]

5.027 km/s [105]. When the spacecraft uses an orbital entry, the speeds are much lower, however in this case usually main engines are fired to decelerate and rotate the capsule such that the heat shield is pointed in the proper direction. The MPF, Beagle 2 and MER missions all had no guidance and no centre of mass offset, and thus performed a purely ballistic entry [34]. In their case, they entered the atmosphere with an angle of attack of 0° [104, 106]. The MPF and MER were spin stabilized at entry [107]. The Viking, Phoenix and MSL entry

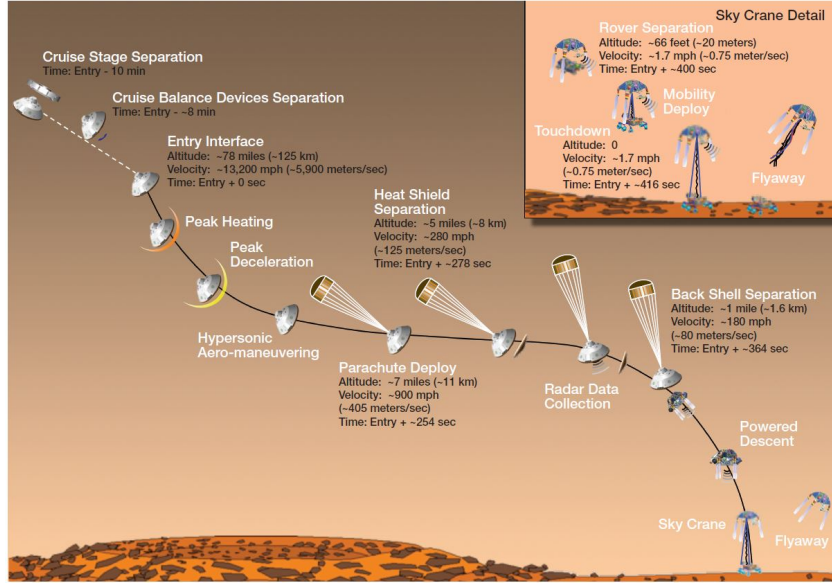


Figure 7.4: Illustration of the MSL EDL sequence [32]

vehicles all used a centre of mass offset in order to create lift and thus control the entry [104] (semi-ballistic [34]). In the case of MSL, active guidance in the form of thrusters were also used to have more control over the entry of the vehicle.

During the entry phase the Reaction control system (RCS), usually thrusters, helps to assure the proper attitude of the capsule. Together with the mass and aerodynamic properties of the capsule, they make sure that the heat shield is pointed in the right direction (ballistic and semi-ballistic entry [34]).

7.2. ATMOSPHERIC DESCENT PHASE

The actual atmospheric descent phase of the EDL is in this case defined to be the phase where the atmosphere is first 'touched' by the entry vehicle. The first part of this phase is performed using a protective heat shield, and the rest of the vehicle is protected by means of an Aero-shell. More on both these aspects of the vehicle will be discussed in Section 7.2.1. The second part of the atmospheric descent usually consists of deceleration through the use of a parachute. Some general theory and a description of the parachutes used in the reference missions will be given in Section 7.2.2. However, there are currently also alternative atmospheric decelerators that could be used instead of the traditional heat shield and parachutes. Section 7.2.3 provides a short overview of the different alternatives and likely candidate technologies that have already been under consideration for use in future Mars missions.

7.2.1. AERO-SHELL AND HEAT-SHIELD

When looking at the entry vehicle a distinction can be made between the lander (and/or rover) and the protective cover. This protective cover is called the Aero-shell and protects the lander during the cruise to Mars and during the entry and descent. It usually consists of two different segments: a heat shield in the front and a back-shell [33]. A graphic representation of the aero-shell for the MER missions is given in Figure 7.5. The back-shell can house the parachute(s), extra decelerators, in this case solid rocket motors, and other subsystems such as release mechanisms for the lander.

The heat shield acts both as thermal protector as well as main decelerator. Different thermal protectors exist, but in case of Mars missions, ablative thermal protection systems TPS are used [33, 104]. The idea behind an ablative heat shield is that energy is taken away from the vehicle by losing the shield material while it burns. Due to the hypersonic speeds ($>$ Mach 5) a bow-shock is present in front of the vehicle during entry, resulting in aerodynamic heating of the air [34]. In Figure 7.6 a graphic representation is given of what happens when a (semi-)ballistic vehicle enters the Martian atmosphere.

As can be seen in this figure, the hot air can re-attach after flow separation behind the vehicle. This is why the back-shell also requires a thermal protective layer, but not has different requirements because of the lower energy in the re-attached flow. For the design of a TPS for a ballistic entry, three different parameters

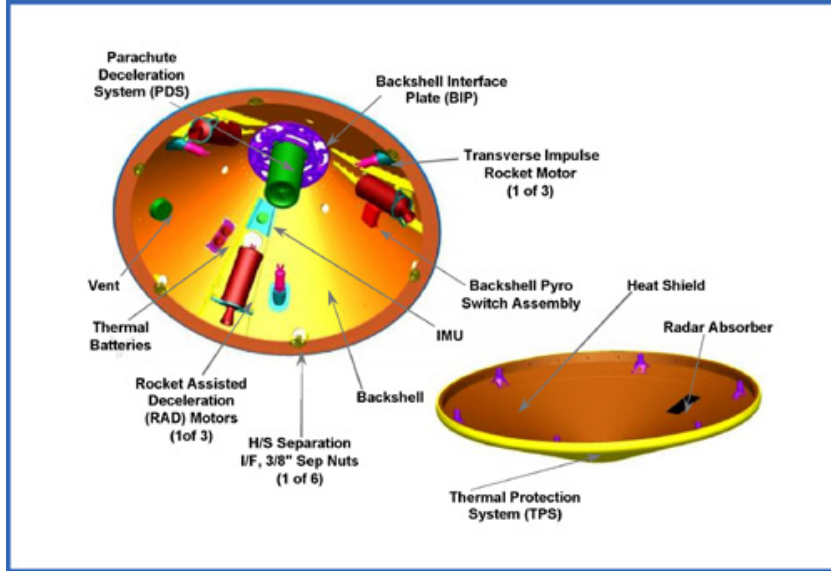


Figure 7.5: Graphic representation of the MER aero-shell [33]

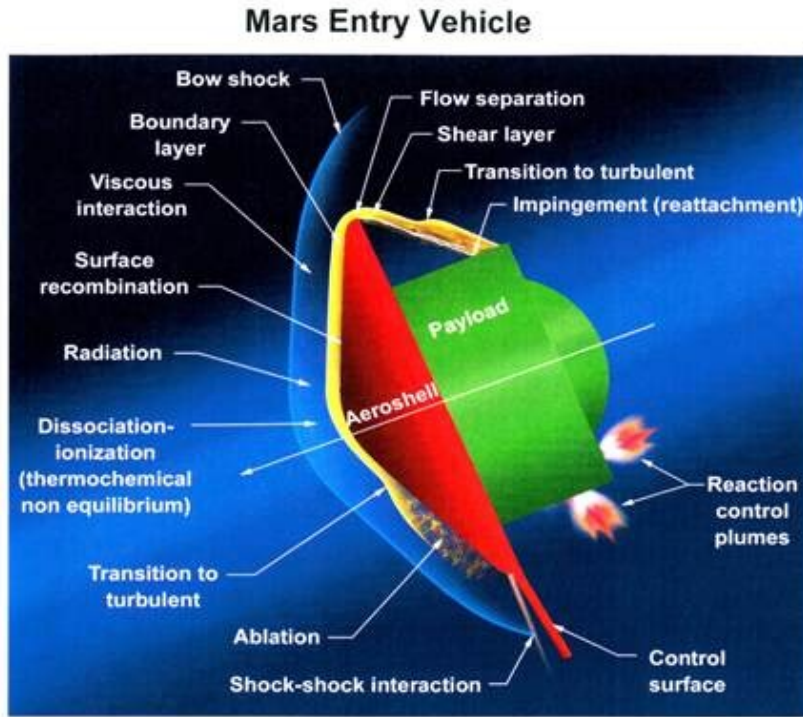


Figure 7.6: Graphic representation of a Martian entry [34]

are very important: the maximum dynamic pressure ($q_{dyn,max}$), the maximum heat flux (\dot{Q}_{max}) (which is the energy per time per square metre) and the integrated heat flux or maximum heat load (Q_{max}). These maxima occur in the stagnation point on the vehicle and determine the type of TPS material and the thickness. Another important system requirement is the maximum deceleration ($g_{load,max}$) [34]. Figure 7.7 shows the general graphs for the density, vehicle velocity, deceleration and the heat flux as a function of altitude, and it is interesting to note that the peak deceleration happens at an altitude lower than the peak heat flux. More information on how to determine these maxima and how they are affected by design choices such as entry angle and entry velocity can be found in [34].

The ablative material for the TPS is therefore chosen based on the mission characteristics during entry.

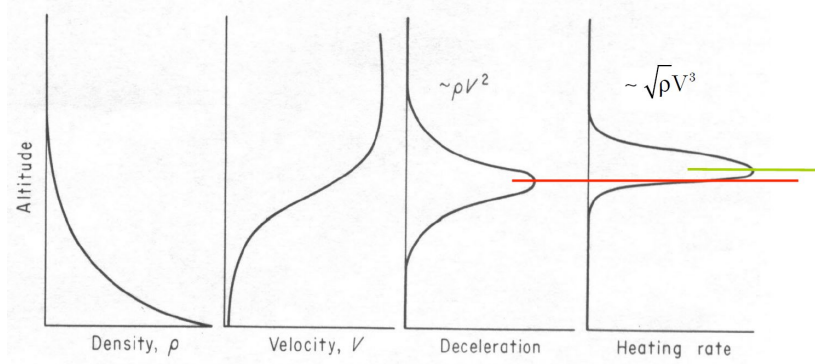


Figure 7.7: Typical entry characteristic graphs [34]

An overview of the ablative materials and the dimensions of the heat shields that were used in the reference missions is given in Table 7.3 and are mostly based on [104] unless mentioned otherwise. Also, a comparison of the different NASA mission aero-shells is visualized in Figure 7.8.

Table 7.3: Previous Mars mission heat shield characteristics

Mission	Shield diameter [m]	TPS material	TPS thickness [cm]
Mars 3	2.9 [11]	unknown	unknown
Viking(s)	3.5	SLA-561V	1.37
Mars Pathfinder	2.65	SLA-561V	1.91
Beagle 2	0.9 [106]	Norcoat Liège FI [108]	0.8 [108]
Mars Exploration Rover(s)	2.65	SLA-561V	1.57
Phoenix	2.65	SLA-561V	1.40
Mars Science Laboratory	4.6	PICA (SLA-561 back-shell) [109]	2.29

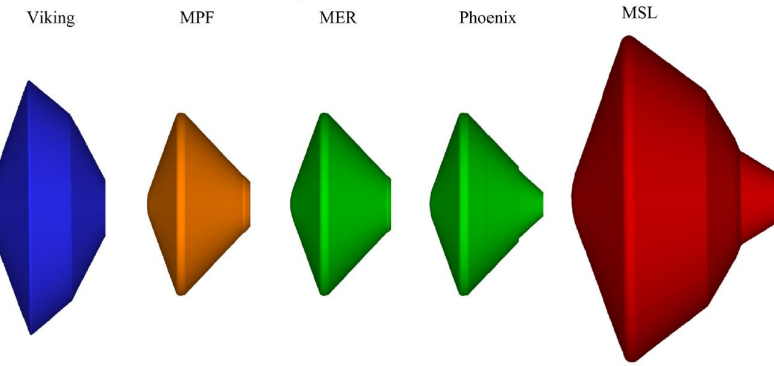


Figure 7.8: Aero-shell comparison of the different NASA Mars entry vehicles [35]

The mentioned Norgot Liège TPS used on Beagle 2 was originally developed for the Ariane 4 [110] and the French military by EADS Launch Vehicles (before called Aerospatiale, currently Airbus Defence and Space) back in the '70s [108]. The Norgot Liège TPS is produced in panels and is made from cork powder and phenolic resin. The SLA-561V was developed by the Martin company (now Lockheed Martin) back in the '60s specifically for a mission to Mars [111]. The SuperLight Ablative (SLA) material is a combination of elastomeric silicone and cork [112] and the original SLA-561 was used for the Space Shuttle External tank as well. And finally, the Phenolic Impregnated Carbon Ablator (PICA) was developed by NASA in the '90s and was first successfully used for re-entry on the Stardust mission [109].

7.2.2. PARACHUTES

Parachutes are traditional aerodynamic decelerators that are used for atmospheric deceleration starting at supersonic or subsonic speeds (< Mach 5) [38]. In 1978 the third United States Air Force Parachute Handbook was published containing information on numerous parachute designs [36]. From this collection, four types of parachutes have been flown in space [38] and two were used for Mars missions: the Disk-Gap Band (DGB) (see Figure 7.9) and the Ringsail Parachutes (see Figure 7.10).

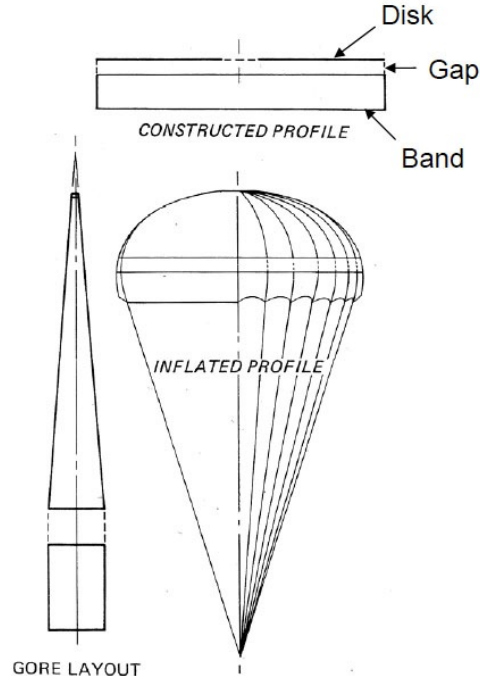


Figure 7.9: Disk-Gap Band parachute [36]

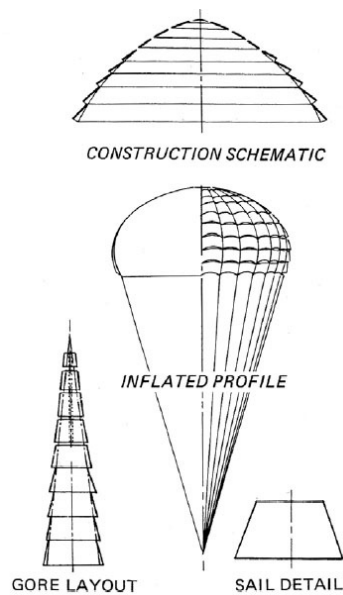


Figure 7.10: Ringsail parachute [36]

The size of the parachute needed can be determined through the terminal descent conditions (or the specified conditions at a certain altitude). Assuming a circular parachute surface, the chute diameter d_p can be determined using the expression given by Equation (7.1).

$$d_P = 2 \sqrt{\frac{1}{\pi C_{D_P}} \left(2 \frac{m g_{0,mars}}{\rho_0 V_f^2} - C_{D_{EV}} S_{EV} \right)} \quad (7.1)$$

Here, C_{D_P} is the drag coefficient of the parachute determined by the parachute type and given in [36], m is the mass of the entire system (so both entry vehicle and parachute system), $g_{0,mars}$ is the gravitational acceleration at the Martian surface, ρ_0 is the air density at the Martian surface, V_f is the desired final velocity, S_{EV} is the surface area of the entry vehicle and $C_{D_{EV}}$ is the drag coefficient of the entry vehicle. These last two parameters can be combined with the mass m to give the ballistic coefficient $\beta = \frac{m}{C_{D_{EV}} S_{EV}}$, which is a characteristic parameter of the entry vehicle. In that case the equation for the chute diameter can be written as given by Equation (7.2).

$$d_P = 2 \sqrt{\frac{1}{\pi C_{D_P}} \left(2 \frac{m^2 g_{0,mars}}{\rho_0 V_f^2} - \beta \right)} \quad (7.2)$$

As a reference, the characteristic parameters and type of parachute(s) used in the given reference missions are shown in Table 7.4. The data in the table was obtained from [104, 113] unless mentioned otherwise. Also, given the lack of information on the Mars 3 mission, this mission will not be used as reference here.

Table 7.4: Previous Mars Mission parachute and entry vehicle characteristics

Mission	Parachute type	d_P [m]	C_{D_P} [-]	β [kg/m^2]
Viking(s)	DGB	16.2	0.67	64
Mars Pathfinder	DGB	12.7	0.4	63
Beagle 2	DGB (Pilot), Ringsail (Main)	3.2 (Pilot), 10.0 (Main)	0.52 to 0.58 [36](Pilot), 0.92 [114] (Main)	73 [115]
Mars Exploration Rover(s)	DGB	14.1	0.48	94
Phoenix	DGB	11.7	0.67	65 [115]
Mars Science Laboratory	DGB	19.7	0.67	140 [115]

In case of the Beagle 2, a DGB pilot chute was used for the initial deceleration and stabilization after the heat shield deceleration and it was also used to deploy the main parachute. Also, please note that the ballistic coefficients mentioned are those at atmospheric entry.

7.2.3. SPECIAL AERODYNAMIC DECELERATORS

The parachutes have thus far worked because the vehicle mass and speeds were low enough, however when the masses and speeds become higher for say a manned mission to Mars, the traditional aerodynamic decelerators will simply not be sufficient to make a soft landing on the Martian surface [116]. Also, because of the surface elevation, it is currently impossible to reach approximately half of the surface with the currently used techniques. Fortunately other high speed (far into the hypersonic regime) alternatives have been envisioned and tested in as early as the '50s. These alternative decelerators can be divided up into three categories: hypersonic parachutes (made out of fabric and have a close resemblance to traditional parachutes) [37], trailing inflatable aerodynamic decelerators IAD (are parachute like inflatable devices) and attached IADs (have a close resemblance to inflatable heat shields but are not always used for the initial deceleration from high hypersonic speeds; around Mach 30).

Two examples of hypersonic parachutes are the hyperflo and the supersonic-x parachutes. The hyperflo parachute was developed in the '60s and is described by [117]. It is a flat circular ribbon weaved parachute capable of resisting aerodynamic heating and can be deployed at speeds up to at least Mach 6 [37]. A photo and graphic representation of the chute if given in Figure 7.11.

The other hypersonic parachute, the supersonic-x, was also developed in the '60s [118], and has been tested up to Mach 8 [36]. Its main use would be as a drogue parachute because of the parachute stability but only average drag. It has a close resemblance to a reversed bell nozzle as can be seen in Figure 7.12.

Both of these designs were rigorously tested in the '60s but seem not to have any merit in current investigations into Martian decelerators. IADs on the other hand seem to have gained much popularity in the past

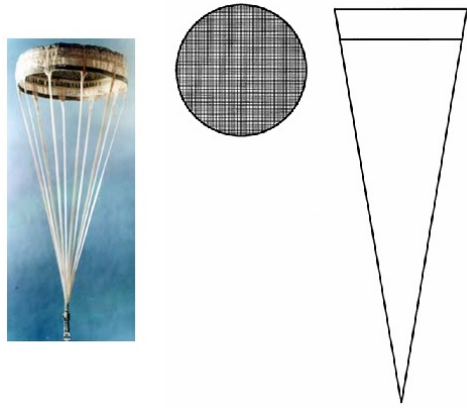


Figure 7.11: Hyperflo parachute [37]

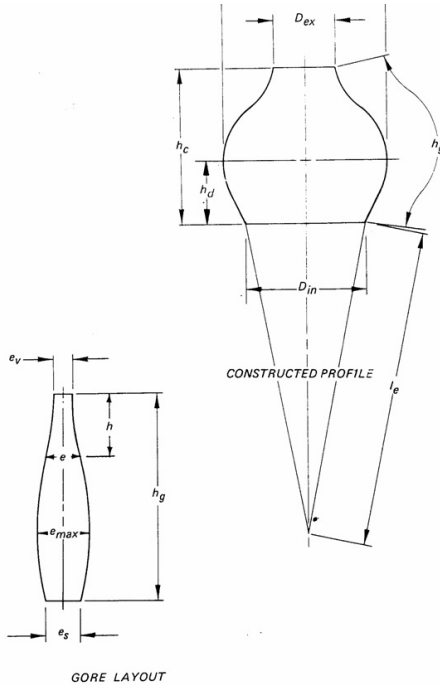


Figure 7.12: Supersonic-x parachute [36]

few years (see for instance [38, 39, 116, 119–122]). The earliest trailing IAD developed was the so called ballute (a balloon parachute) by Goodyear in the '50s and was part of the Gemini escape system [38]. A photo of the original design is shown in Figure 7.13. Currently, the design is under consideration to perform as a drogue chute for hypersonic Mars entries combined with an improved supersonic ringsail main parachute and an attached IAD [119].

Other examples of trailing IADs currently under consideration are shown in Figure 7.14.

One of the earliest examples of an attached IAD was developed in the '60s as well [40] and underwent several supersonic tests. A graphic representation of such a decelerator is given in Figure 7.15.

Another supersonic attached IAD is the tension cone [121, 122] (see Figure 7.16 for examples of attached IADs). This supersonic IAD could be used in combination with a hypersonic heat shield IAD (stacked toroid blunted cone in the figure) to perform a Martian re-entry [120].

Considering all the different possible alternatives for aerodynamic decelerators it is clear that there are currently plenty of options under development, but it is unclear at the moment which (combination) of these will perform best in case of for instance the MSL 2 mission.



Figure 7.13: The original ballute by Goodyear [38]

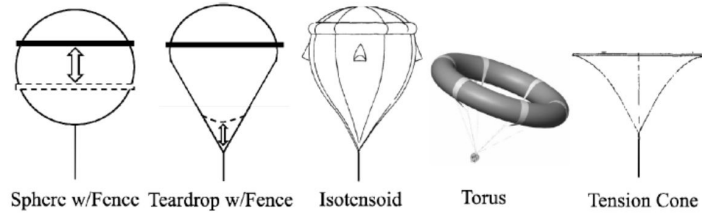


Figure 7.14: Selection of trailing IADs under investigation [38, 39]

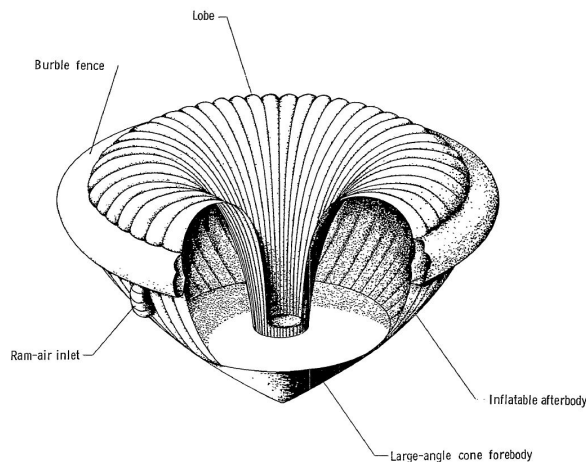


Figure 7.15: Earliest design of an attached IAD [40]



Figure 7.16: Different attached IADs[38]

7.3. LANDING PHASE

The landing is defined as the final approach to the surface. In this phase, the final velocity is brought down to the required touchdown speed using the final deceleration systems. In this phase, there are several methods of getting the lander/rover safely on the planet surface. These methods were already mentioned in Table 7.2, and usually involved a combination of the different methods. In this section, the methods are divided up into

the use of retro rockets, lowering cable(s) and air-bags. A clearer overview of the different methods used per reference mission is shown in Table 7.5.

Table 7.5: Landing methods used by previous Mars missions

Mission	Method used		
	Retro rockets	Lowering cable(s)	Air-bags
Mars 3	Yes (in back-shell)	No	Yes
Viking(s)	Yes	No	No
Mars Pathfinder	Yes (in back-shell)	Yes	Yes
Beagle 2	No	No	Yes
Mars Exploration Rover(s)	Yes (in back-shell)	Yes	Yes
Phoenix	Yes	No	No
Mars Science Laboratory	Yes (in hover-crane)	Yes	No

In the next subsections, the use of the different methods will be discussed in case of the different reference missions.

7.3.1. RETRO ROCKETS

Retro rockets were used in almost all of the reference missions. The reason to use them is to provide high final deceleration and controlled descent [38]. The Mars 3 lander used gunpowder engines to perform a final deceleration before the lander was dropped [103]. Both the MPF and the MER missions used solid retro rockets to decelerate during final approach [123, 124]. On the Viking, and MSL missions the retro rockets were liquid monopropellant engines that could be throttled for better control of the precise landing [35, 125]. The Phoenix engines were also liquid monopropellant engines, but instead it was decided to go for a pulse mode modulated system [126].

7.3.2. LOWERING CABLE

In three cases, lowering cables (or bridles) were used during the final approach phase. For the MPF and MER missions the lowering cable acted as a tether and provided space for the air-bags to deploy, a safe distance from the solid retro rockets and increased stability [123]. In case of the MSL, the lowering cables were used slightly differently. MSL had three of them, and they were used for controlled descent unto the Martian surface rather than a tether [35]. Only when it was confirmed that the rover had landed on the surface (cables would have less tension on them), the cables were cut and moved away with the hovering crane. The lowering of the rover on the surface via cables was preferred because this would minimize soil contamination and provide less risk to the rover itself.

7.3.3. AIR-BAGS

And finally, four missions (the smaller landers/rovers) used air-bags to dampen the impact on the Martian surface. This does not guarantee a precise landing but does provide protection for the on-board electronics and is simpler and has a lower mass compared to a powered descent unto the surface. However, when looking at future missions with higher mass requirements, air-bags might not be a viable option anymore [49].

8

MARTIAN LAUNCHER METHODS

Martian sample return has never been attempted, as a matter of fact a sample return from a celestial body with an atmosphere has never been done before. When designing a sample return missions for Mars, a vital part of it is getting the samples off of the planet. This can then either be send directly to Earth or rendezvous with a [s/c](#) (either orbiting the planet or not), but either way, the samples have to be able to get there first. This chapter will focus on the different possibilities of Martian Ascent ([MA](#)) that have already been investigated and/or proposed (Section 8.1) and other (advanced, unconventional or futuristic) ideas for a Martian application described in Section 8.2.

8.1. PREVIOUS INVESTIGATIONS

Many studies have already been done focused on a [MAV](#). A number of these studies have been gathered and are shown in Table 8.1. For each study, the main launch concept is given and the kind of propellant(s) as well. They are presented in order of publication year.

Table 8.1: Previous [MAV](#) studies

Who	Which method	Kind of propellant(s)
J.C. Whitehead [127]	two stage rockets (comparison study)	solid and liquid (and gel recommended too)
C.S. Guernsey [128]	two stage rocket	2x liquid
P.N. Desai et al. [129]	two stage rocket	2x liquid
C. Stone [130]	two stage rocket	hybrid
D.D. Stephenson [43]	two stage rocket (three different designs)	2x Solid (Best), Solid and liquid or hybrid and 2x gel (Best)
J.C. Whitehead [131]	one, two and three stage rockets (variational study)	solid and liquid
D.D. Stephenson and H.J. Willenberg [132]	two stage rocket	2x solid
A. Sengupta et al. [133]	two stage rocket	2x liquid
M.A. Trinidad et al. [41]	two stage rocket	2x liquid
G. Mungas et al. [42]	single stage rocket	liquid mono-propellant
Mars Program Planning Group [49]	undefined rocket	solid and liquid

From the table it is clear that all studies envision a rocket to bring the samples either into Martian orbit or back to Earth. Also, four clear propellant types have been investigated: the traditional solid and liquid propellant engines, the hybrid engine (which is a combination of a solid fuel and a liquid oxidizer) and the gel engine. The gel engine uses a gel as a propellant. A gel propellant behaves as a viscoelastic solid when stored and burns as a liquid when pressure is applied and the gel is atomized [134]. It was developed as a

stable propellant for missiles and the first successful missile was launched in 1999 by TRW (now Northrop Grumman). It is rather important to know the amount of stages and the kind of propellant because that also determines the ascent trajectory and the final orbit the MAV can reach. A good overview of stages versus propellants is given by [41] (see Figure 8.1) for a hypothetical scenario where the payload to orbit is 31 kg. This table is meant as a comparison for the four different propellant types.

Propellant Type	# Stage Vehicle	Stage Mass (kg)						Stage Mass Fraction			
		1	2	3	4	Payload	GLOM	1	2	3	4
SOLID	1										
	2	242.63	29.48			31.00	303.11	0.818	0.612		
	3	159.18	79.82	17.23		31.00	287.23	0.788	0.727	0.540	
	4	122.45	79.82	44.90	4.99	31.00	283.15	0.767	0.727	0.664	0.500
LIQUID	1	290.04	0.00	0.00		31.00	321.04	0.777			
	2	143.64	69.52	0.00		31.00	244.16	0.734	0.675		
	3	130.75	75.96	18.42		31.00	256.13	0.727	0.684	0.481	
	4	105.89	64.45	46.04	6.91	31.00	254.29	0.711	0.668	0.633	0.347
GEL	1	290.25				31.00	321.25	0.797			
	2	151.93	61.68			31.00	244.60	0.762	0.696		
	3	131.52	76.19	14.97		31.00	253.67	0.752	0.713	0.500	
	4	104.31	63.49	45.35	6.80	31.00	250.95	0.737	0.698	0.667	0.383
HYBRID	1	295.69				31.00	326.69	0.803			
	2	151.47	68.48			31.00	250.95	0.766	0.704		
	3	136.05	77.55	13.61		31.00	258.21	0.758	0.715	0.500	
	4	113.83	61.68	44.90	6.80	31.00	258.21	0.745	0.694	0.662	0.401
SOLID- Stage 1 GEL – Stage 2	1										
	2	157.37	68.03			31.00	256.39	0.787	0.705		
	3	126.98	83.45	20.41		31.00	261.84	0.770	0.721	0.563	
	4	128.00	76.19	51.25	6.80	31.00	294.04	0.771	0.713	0.679	0.383

Figure 8.1: Image of comparison table for different stages with different propellants[41]

This particular study showed that the Gross Lift-Off Mass (**GLOM**) would be lowest when using a two stage liquid rocket. However, a two stage gel rocket would be a close second. A low **GLOM** is however not the only requirement which is why at this point no one particular solution can be selected. A visual representation of some of the described designs is given in Figure 8.2.

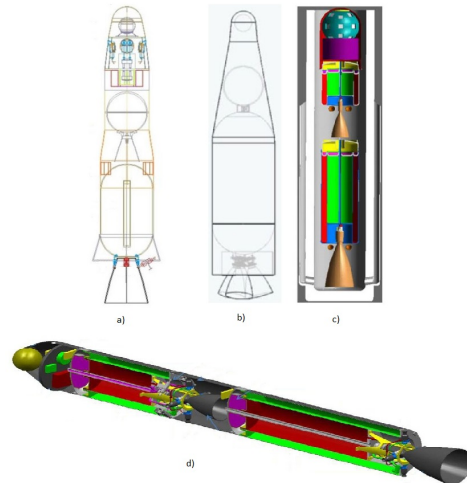


Figure 8.2: Some rocket concepts visualized. a) Two stage solid rocket by Lockheed Martin /citestephenson2002, b) Single stage mono-liquid rocket by Firestar Technologies [42], c) Two stage gel rocket by TRW [43] and d) Two stage bi-liquid rocket by Boeing [41]

8.2. FUTURISTIC IDEAS

Only rockets have been under consideration so far, however other solutions exist as well. These are slightly more exotic and are currently ideas meant for Earth, but it is good to have an overview of everything that is possible. Table 8.2 shows different ideas (order based on publication date) that have been proposed for Earth

launches. For all of these systems it should be investigated if and how these methods could be applied on Mars.

Table 8.2: Futuristic non-rocket launch methods for Earth

Who	Which method
J. Pearson [135]	Space elevator: A counterweight far from Earth would allow a vehicle to travel on a cable between that counterweight and the Earth
K.H. Lofstrom [136]	Launch loop: A launch cable that remains stable due to the rotation of the Earth
R.H. Frisbee [137]	Microwave propulsion: Based on heat/energy exchange of a ground based microwave generator to heat on-board propellants
J.T. Kare [138]	Laser launch: Based on the heat/energy exchange of a ground laser to heat on-board propellants
J. Hunter [139]	Space gun: A water based space gun based on rapid gas propulsion
Zero2infinity [140]	Balloon launch: Balloon carrying rocket and ignited in the stratosphere

At this point in time most of these systems cannot be applied on Mars because it either involves creating a large infrastructure or demands a lot of energy. However, a balloon launch could be possible and might be worth investigating.

9

TRANSFER ORBITS

For a MSR mission, the most important part would be to actually get the samples back to Earth for detailed analysis. Therefore, the *s/c* carrying the samples will have to travel from Mars back to Earth using what is called an interplanetary transfer orbit. Several methods exist in order to reach such a transfer orbit and the application depends highly on mission requirements. Therefore this chapter will explain the basic concepts behind every different method and what it can be used for. A difference can be made with respect to the level of thrust that needs to be applied, which is why Section 9.1 will focus on (traditional) high-thrust orbits and Section 9.2 will discuss low-thrust possibilities.

9.1. HIGH-THRUST

Two types of high-thrust transfer orbits are high energy transfer and minimum energy transfer orbits [141]. This last transfer method is referred to as a Hohmann transfer [45] and is the most common transfer orbit, which is thus often used as a benchmark. It is a direct transfer method, which means that it will directly transfer a *s/c* from one planet to the other by travelling less than 360° around the Sun. In case of a Hohmann transfer, the *s/c* travels 180° around the Sun before arriving at the destination planet. A Hohmann transfer orbit is characterized by two propulsive shots, one at the departing planet and one at the destination planet as illustrated in Figure 9.1. It can be seen that the elliptic orbit touches both the departing and destination planet orbits.

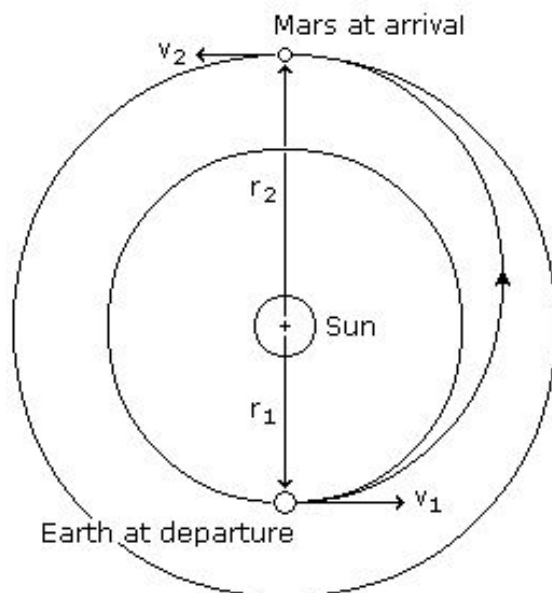


Figure 9.1: Graphical representation for Earth-Mars Hohmann transfer propellants[44]

It is also clear that the planets have to be aligned such that the angle between the departing planet at the time of departure and the destination planet at the time of arrival is 180° which only happens every so often. In order to have more opportunities to reach a planet, and faster as well, high energy transfer orbits can be applied. In Figure 9.2 the four different trajectory types for the ordinary two dimensional case are given for a transfer from Earth to a planet further from the Sun.

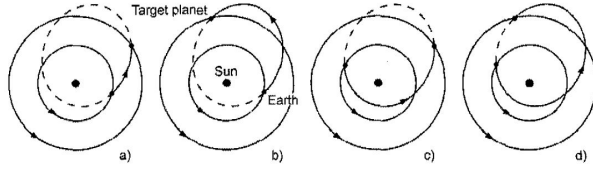


Figure 9.2: Graphical representation of the four different high energy transfer orbit possibilities based on an arbitrary ellipse crossing both orbits[45]

Looking at figure a), it is clear that this is the fastest trajectory and is called a type I trajectory. Figure b) represents a so called type II trajectory where the planet is intercepted at the second crossing of the orbit. Figures c) and d) are similar but for a different starting position of the Earth. Even though the type I trajectory requires more energy, it might still be a very good option if time is a major factor. A good example of the benefits is given by [45], where it is said that a flight time reduction of 50% only requires an increase in ΔV of 19% but reduces the transferable payload mass by 27%. This does not however include the plane change that needs to be performed. More information on the associated equations for both Hohmann and high energy transfer orbits can be found in [45].

A final type of (high-thrust) transfer orbit that has not been mentioned yet is transfer over invariant manifolds. These manifolds are basically low energy paths between celestial bodies that can be travelled like flowing river. Once a thrust is given in such a manifold direction, a s/c would simply travel along this manifold [45]. A good illustration of such manifolds is given in Figure 9.3 and was obtained from a Master thesis from the Delft University of Technology space department [46]. This is one of many written using this type of transfer orbit and thus there is already existing experience.

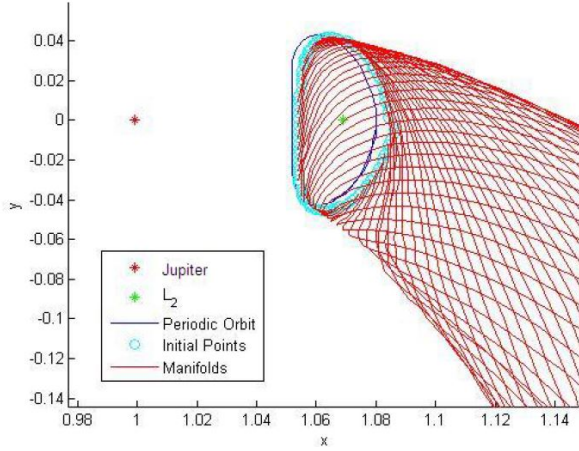


Figure 9.3: Example manifold in the Jupiter-Sun system[46]

These manifolds are attached to Lagrange points and periodic orbits which is why there can be so many of them around in this case the L2 point of Jupiter in the Jupiter-Sun system.

9.2. LOW-THRUST

The low thrust category can be divided up into two characteristic groups: low thrust chemical propulsion and Electric propulsion [141]. The low thrust chemical propulsion can be used to get from one orbit to the destination orbit using several impulsive shots. This creates different Hohmann transfer segments and thus takes longer than an ordinary Hohmann transfer. In some cases the s/c will have to travel several times around the

Sun before a certain planet can be reached as shown in Figure 9.4. In this case the inner circle represents the Earth orbit around the Sun and the outer circle the orbit of a desired destination planet that is further away from the sun.

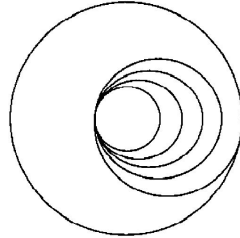


Figure 9.4: Example low thrust transfer trajectory using Hohmann segments[47]

The electric propulsion group consists of different types of propulsion methods. A differentiation is made in [45] between electrothermal, electrostatic and electromagnetic propulsion. All these different electric propulsion methods result in a high specific impulse (I_{sp}) but very low thrust levels. They are very useful for long duration missions and can thrust continuously if necessary. This continuous thrusting would result in a spiral orbit as depicted in Figure 9.5, however the thrust can also be applied in increments where there are thrusting periods and coasting periods in the transfer orbit. This was for instance done by the Dawn spacecraft in combination with gravity assists (see Figure 9.6).

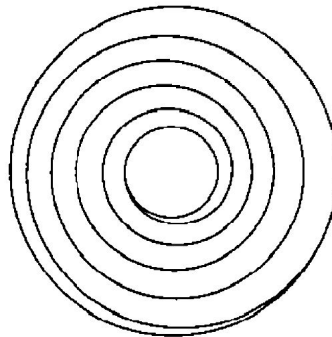


Figure 9.5: Example of continuous low thrust trajectory[47]

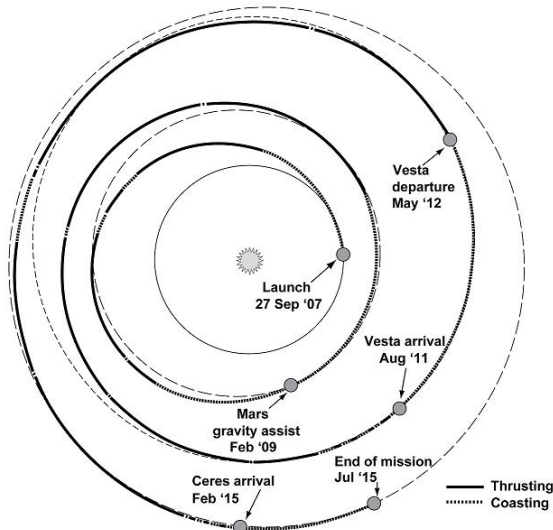


Figure 9.6: Example of a segmented low thrust interplanetary trajectory: the Dawn spacecraft[45]

9.3. REFERENCE RESEARCH

The most important difference is time; high-thrust orbits have a lower transfer time (usually) and low-thrust orbits require more time to reach the same point in space. In order to get an idea of the different transfer methods that have been under consideration already when looking at MSR return orbits, an overview has been created and is given in Table 9.1. Sometimes the transfer trajectory method is a combination of the different transfer orbits mentioned before. The investigations are given in order of publication year starting with the earliest one. Overall, the Mars-Earth transfer problem is rather interesting because it involves travelling from a planet further away from the Sun to a planet that is closer to the Sun. The same transfer orbits have thus also been used for missions to Mercury and Venus.

Table 9.1: Reference Mars-Earth transfer studies

Who	Which trajectory	For what purpose
P.F. Wercinski [142]	high energy transfer	MSR in less than 1.5 years
M.R. Patel et al. [143]	free return (based on planet alignment and gravity assist)	To get from Earth to Mars and back to Earth in a short period and with only one thrusting manoeuvre at the beginning
A. Miele and T. Wang [144]	(near) Hohmann transfer	Round-trip Mars mission
R. Mattingly et al. [145]	high energy and continuous electrical low thrust (several different studies)	Mars-Earth transit for MSR
R. Mattingly et al. [146]	high energy transfer	MSR (to and from Mars)
R. Mattingly and L. May [147]	high energy transfer	MSR (to and from Mars)
T. Engelhardt [148]	direct Hohmann transfer	MSR (ideal simulation)
D.A. Tito et al. [149]	free return	Manned Mars missions

It is interesting to note that [145] shows that different studies performed by different companies. In the early phase of the studies there was no requirement on mission time, and therefore two companies opted to go for electric propulsion. However, when the requirements changed and were set for a mission time of less than 5 years, only one company decided to keep the electric propulsion. So the optimal return trajectory will highly depend on the mission time requirements.

10

RESEARCH OPPORTUNITIES

Throughout this literature study there have been mentions of where the current research done could be or has to be improved. This can either be based on mission requirements that have to be fulfilled or new methods that have not been thoroughly investigated yet. In this chapter, different research opportunities per proposed subject will be given.

10.1. MARS SAMPLE RETURN RESEARCH

In Chapter 4 it was already concluded that Differential Evolution and Monotonic Basin Hopping would be the most interesting choice when it comes to optimization of trajectories. Given the different possible ascent and Mars-Earth return trajectories, it might be interesting to perform a comparison of both these methods in these two trajectory cases for a Mars Sample Return mission. It would in the end provide an optimal solution as a result of both these methods. However, considering the different possibilities for return trajectories, a combination of the different methods mentioned in Chapter 9 could be optimized on itself using (either of) these two optimization methods. This could even be done by choosing different propellants and engine/rocket configurations mentioned in Chapter 8 (maybe combining it with a balloon launch) in order to include the optimization of Mars ascent trajectories. Or, if done separately, design the optimum MAV with the corresponding ascent trajectory and final orbital conditions. In the case of a long duration return flight (for instance when electric propulsion is used for the return journey back to Earth) the trajectory can be integrated using Störmer-Cowell as was concluded in Chapter 5. Again a comparison could be made between the different integration methods for a low thrust trajectory back to Earth. Störmer-Cowell can also be used for the integration of the ascent trajectories and different combination of return trajectories.

10.2. MARS ENTRY AND DESCENT RESEARCH

According to [120], with the current EDL technologies, only 50% of the Martian surface is accessible through direct landing (also see Chapter 7). And if the landing masses increase, it won't be possible to use the current technology to soft land on Mars. Therefore new technologies and strategies have to be investigated. A lot of research has already been performed on new entry methods and aerodynamic decelerators and even a combination of these has been investigated to create different EDL architectures, but mostly for generic missions. Therefore it could be useful to look at the optimal EDL sequence specifically for the MSL 2 rover or even for a specified manned mission to Mars. Using the same optimization methods mentioned in Section 10.1 an EDL trajectory can be optimized to find out what it will take in order to be able to land (almost) everywhere on Mars. Another possibility would be, either in combination with this trajectory optimization or not, to optimize the heat shield and other decelerators for different entries. Thus a feasibility study of the different IADs could be done as well, in order to determine which one would be best suited for what kind of mission. In that case a differentiation can be made between hypersonic IADs and supersonic IADs, both of which have high priority when it comes to development according to the Mars Program Planning Group [49]. They also mention that the development of high-thrust liquid supersonic retro-propulsion systems should be investigated and could be seen as a stand-alone option or might be used in combination with other decelerators.

10.3. HAZARD AVOIDANCE RESEARCH

Finally, when it comes to hazard avoidance, there are two possible applications and thus main research areas. An improved hazard avoidance system could be investigated for use on rovers and automated manoeuvring on the Martian surface through optimized paths, or a hazard avoidance system for the automated and guided landing of a Mars lander/rover could be interesting to look into which has a high priority according to the Mars Program Planning Group [49]. Both these systems could be designed for different main requirements such as: lowest propellant/power usage or path/landing area with the least amount of rocks.

11

FINAL SUBJECT DEFINITION

The final subject definitions are based on the research opportunities described in Chapter 10. In this chapter the final definitions are given as different topics under the three different subjects. Each topic is represented by a title and a short description. In each case, if the topic does not involve a comparison, the optimization can be done using either Differential Evolution or Monotonic Basin Hopping and the integration can be done using either Störmer-Cowell or any of the other integration methods that have been used in the space department. At the end of each topic definition, an overview is given of the relevant chapters and sections within this report.

11.1. MSR FINAL RESEARCH TOPICS

A Mars Sample Return mission involves many different mission phases. In Chapter 2 it was already mentioned that the focus of the subject would lie on the return of the sample back to Earth from the Martian surface. Therefore the research topics mentioned below will incorporate either a certain part of the return, or the entire return phase of the mission.

- **"Trajectory optimization for the return of a Martian sample from the Martian surface back to Earth"** *This would involve the optimization of the ascent trajectory and the Mars-Earth return trajectory in one go using both Differential Evolution and Monotonic Basin Hopping. This would involve a branched optimization where there are three possible scenarios: direct transfer from the surface back to Earth, or first into Mars orbit and then back to Earth, or first to L1 and then back to Earth. Other possibilities could be considered as well. Chapters 2, 4 to 6, 8 and 9 and Section 3.1*
- **"Low-thrust Mars-Earth trajectory optimization using different integration methods"** *This would involve the optimization of the return trajectory using Differential Evolution through the use Taylor series integration compared to different integration methods. Could be combined with the next topic. Chapters 2, 4 to 6, 8 and 9 and Section 3.1*
- **"Martian ascent trajectory optimization using different integration methods"** *The same as the previous topic, but now for the ascent trajectory. Could be combined with the previous topic. Chapters 2, 4 to 6, 8 and 9 and Section 3.1*

Please note that the Taylor series integration was suggested by the TU Delft supervisors and has not been discussed in this report yet.

11.2. MARS EDL FINAL RESEARCH TOPICS

Because of the different possible EDL combinations available and the different technologies that have to be investigated, a few different topics were set-up. In Chapter 10 it was mentioned that this would be done for the MSL 2 mission, but it could be focused on other high mass missions or even human missions to Mars as well.

- "**Hypersonic decelerators optimization for high-mass Mars EDL**" This would involve the aerodynamic optimization of different entry options, using hypersonic IADs, ordinary heat shields and other possible options. Also, The performance of different IADs would be compared to find different optimal EDL strategies using a combination of both hypersonic and supersonic IADs Chapters 2 and 4 to 7 and Section 3.2
- "**New optimized EDL strategies to be able to land everywhere on Mars**" In this case, the descent trajectory would be optimized (using Differential Evolution) for, for instance the MSL 2 (or a different mission) in order to land at higher altitude areas on Mars (with high payload masses) and will involve the use of new technologies Could be combined with the next topic. Chapters 2 and 4 to 7 and Section 3.2
- "**High-thrust liquid supersonic retro-propulsion Mars descent trajectory optimization**" This topic would involve the Mars descent trajectory optimization (Differential Evolution) using supersonic retro-propulsion and a hypersonic decelerator, which kind will depend on the optimum solution Could be combined with the previous topic. Chapters 2 and 4 to 7 and Section 3.2

11.3. HAZARD AVOIDANCE FINAL RESEARCH TOPICS

It was decided based on personal preference that hazard avoidance would not be suggested as a thesis topic.

12

RECOMMENDED PROCEEDINGS

From the final topics given in Chapter 11, the topic that fits best within the current plans of JPL and the wishes of the TU Delft supervisors will have to be selected, given that personal preference is also very important. In order to be able to proceed from these final topics, a time table guide has been created showing what has to be done and when it is planned to be done:

- **Settling and choosing a final thesis topic** (21st of September till 30th of September 2015)
- **Detailed literature study on the chosen topic together with the subject Research Methodologies** (1st of October till the 30th of November 2015)
- **Final thesis proposal** (1st of December till the 7th of December 2015)
- **Thesis work** (8th of December 2015 till the 1st of August 2016 including holidays)

These proceedings are based on the required 2 month literature study and 7 month thesis. The thesis study officially begins from the moment that the thesis proposal is approved.

BIBLIOGRAPHY

- [1] C. A. Brooks and S. Prasad, *Apollo program summary report*, website (2011).
- [2] E. Ferard, *Apollo 17: Les plus belles images de la dernière mission lunaire*, website (2012), in French.
- [3] C. H. Lowry, *Apollo-the last few miles home*, presentation/website (2012).
- [4] D. Capdevila, *Annexe 15 les sondes eplorent la lune partie 2*, (2001), in French.
- [5] E. Grayzeck, *Stardust/next*, (2014).
- [6] Unknown, *Sample return missions*, (2015).
- [7] E. Grayzeck, *Genesis*, (2014).
- [8] M. Woo, *Snatching some sun*, website (2007).
- [9] E. Grayzeck, *Hayabusa*, (2014).
- [10] J. Grinstead, P. Jenniskens, A. Cassell, J. Albers, and M. Winter, *Airborne observation of the hayabusa sample return capsule re-entry*, in *42nd AIAA Thermophysics Conference* (2011).
- [11] E. Grayzeck, *Mars 3 lander*, (2014).
- [12] E. Grayzeck, *Viking 1 lander*, (2014).
- [13] Lunar and Planetary Institute, *Luna exploration timeline*, website (2015).
- [14] E. Grayzeck, *Beagle 2*, (2014).
- [15] E. Grayzeck, *Spirit*, (2014).
- [16] E. Grayzeck, *Phoenix mars lander*, (2014).
- [17] E. Grayzeck, *Mars science laboratory (msl)*, (2014).
- [18] J. N. Maki, D. Thiessen, A. Pourangi, P. Kobzeff, L. Scherr, T. Elliott, A. Dingizian, and B. St Ange, *The mars science laboratory (msl) hazard avoidance cameras (hazcams)*, in *43rd Lunar and Planetary Science Conference* (2012).
- [19] O. Montenbruck, *Numerical integration methods for orbital motion*, Celestial Mechanics and Dynamical Astronomy **53**, 59 (1992).
- [20] J. Mulder, W. van Staveren, J. van der Vaart, E. de Weerdt, A. in 't Veld, and E. Mooij, *Flight dynamics, lecture notes*, Reader (2013).
- [21] R. Frost, *In space travel, which way is up?* Forum/website (2014).
- [22] M. Akerboom, M. Deklerck, J. Hess, F. Paredis, S. Petrovic, A. Rijndorp, A. Schulz, M. Talboom, R. Wildvank, A. Cervone, O. Stroosma, and D. Dirkx, *Delffi delta & phi: Two nanosatellites for formation flying in low-earth orbit*, Bachelor Thesis Report, Delft University of Technology (2013).
- [23] D. Woods and F. O'Brien, *The apollo 8 flight journal*, Website (2009).
- [24] D. Woods, K. MacTaggart, and F. O'Brien, *The apollo 11 flight journal*, Website (2011).
- [25] E. Mooij, *Ae3202-week1-lecture1b-frames*, Lecture slides (2013), course: Flight Dynamics.
- [26] R. Noomen, *ae4-878.basics.v4-14*, Lecture slides (2013), course: Mission Geometry and Orbit Design.

- [27] B. Guilhaire, [atan2, tricks](#), Blogpost/website (2013).
- [28] O. E. Akcasu and I. Akcay, [Solar ttime using gps technology](#), Patent (2013), wO Patent App. PC-T/US2012/063,283.
- [29] The Crankshaft, [what-when-how mars](#), website.
- [30] D. Isbell and F. O'Donnell, [Mars pathfinder landing press kit](#), (1997), nASA.
- [31] R. Laufer, [Mars express](#), Website (2010), in German.
- [32] D. Brown, S. Cole, and G. W. W. Agle, [Mars science laboratory landing press kit](#), (2012), nASA.
- [33] M. Viotti, [Spacesspace: Aeroshell](#), Website.
- [34] E. Mooij, [Re-entry systems](#), Reader (2013), lecture Notes AE4870B.
- [35] D. W. Way, R. W. Powel, A. Chen, A. D. Steltzner, P. D. Burkhardt, G. F. Mendeck, *et al.*, [Mars science laboratory: Entry, descent, and landing system performance](#), in [Aerospace Conference, 2007 IEEE](#) (2007) pp. 1–19.
- [36] E. Ewing, H. Bixby, and T. Knacke, [Recovery systems design guide](#), Tech. Rep. (DTIC Document, 1978).
- [37] S. Lingard, [Supersonic parachutes](#), in [3rd International Planetary Probe Workshop](#) (2005).
- [38] E. Mooij, [Ae4-870b 9 planetary entry and descent](#), Presentation (2013), lecture slides of AE4870B Re-entry systems.
- [39] A. Witkowski and G. Brown, [Mars deployable decelerators capability roadmap summary](#), in [Aerospace Conference, 2006 IEEE](#) (IEEE, 2006).
- [40] W. D. Deveikis, J. W. Sawyer, L. Li, W. D. Deveikis, and J. W. Sawyer, [Static aerodynamic characteristics, pressure distributions, and ram-air inflation of attached inflatable decelerator models at mach 3.0](#), Citeseer (1970).
- [41] M. Trinidad, E. Zabrensky, and A. Sengupta, [Mars ascent vehicle system studies and baseline conceptual design](#), in [Aerospace Conference, 2012 IEEE](#) (2012) pp. 1–13.
- [42] G. Mungas, D. Fisher, J. Vozoff, and M. Villa, [Nofbx single stage to orbit mars ascent vehicle](#), in [Aerospace Conference, 2012 IEEE](#) (IEEE, 2012) pp. 1–11.
- [43] D. Stephenson, [Mars ascent vehicle - concept development](#), AIAA Paper **4318** (2002).
- [44] R. Braeunig, [Interplanetary flight](#), website (2013).
- [45] K. Wakker, [Astrodynamics-ii](#), Reader, Delft University of Technology (2010), course: Astrodynamics-II AE4874, part 2.
- [46] L. V. der Ham, [Interplanetary Trajectory Design using Dynamical Systems Theory](#), Master's thesis, Delft University of Technology (2012).
- [47] J. Wertz, [Orbit & Constellation Design & Management](#), 2nd ed. (California: Microcosm Press and Springer, 2009).
- [48] Jet Propulsion Laboratory, [All missions](#), Website (2015).
- [49] Mars Program Planning Group, [Summary of the final report](#), (2012).
- [50] Mission Evaluation Team, [Apollo 11 Mission Report](#), Tech. Rep. (NASA Manned Spacecraft Center, 1971).
- [51] R. Christy, [Luna - exploring the moon](#), .
- [52] Lunar and Planetary Institute, [Luna mission](#), (2015).
- [53] E. Grayzeck, [Luna 16](#), (2014).

- [54] Br73, *Luna 16*, (2000), in Italien.
- [55] E. Grayzeck, *Hayabusa 2*, (2014).
- [56] D. Lauretta, *Osiris-rex*, (2015).
- [57] P. Blau, *Chareport test mission*, Website (2011).
- [58] L. David, *Project 'red dragon': Mars sample-return mission could launch in 2020 with spacex capsule*, (2014).
- [59] E. Grayzeck, *Mars pathfinder*, (2014).
- [60] G. Webster, *'lost' 2003 mars lander found by mars reconnaissance orbiter*, (2015).
- [61] J. Matijevic, *Autonomous navigation and the sojourner microrover*, Science **280**, 454 (1998).
- [62] R. Scammell, *Mars exploration rover technical data*, website (2015).
- [63] E. Grayzeck, *Luna 21/lunakhod 2*, (2014).
- [64] H. Visser, *Aircraft performance optimization course ae4447*, Reader, Delft University of Technology (2014).
- [65] R. Noomen, *ae4-878.optimistion.v4-7*, Lecture slides (2013), course: Mission Geometry and Orbit Design.
- [66] P. Musegaas, *Optimization of Space Trajectories Including Multiple Gravity Assists and Deep Space Manoeuvres*, Master's thesis, Delft University of Technology (2012).
- [67] S. Boyd and L. Vandenberghe, *Convex Optimization* (Cambridge University Press, 2004).
- [68] M. Fenniak, *Latin hypercube sampling*, website (2015).
- [69] I. Sobol, *On quasi-monte carlo integrations*, in *Mathematics and Computers in Simulation*, Vol. 47 (Elsevier, 1998) 2nd ed., pp. 103–112.
- [70] W. E. Hart, *Interval methods*, (1997).
- [71] P. Boggs and J. Tolle, *Sequential quadratic programming*, in *Acta Numerica*, Vol. 4 (Cambridge University Press, 1995) pp. 1–51.
- [72] M. Iwamatsu and Y. Okabe, *Basin hopping with occasional jumping*, in *Chemical Physics Letters*, Vol. 339 (Elsevier, 2004) 4th ed., pp. 396–400.
- [73] S. Lee, P. von Ailmen, W. Fink, A. E. Petropoulos, and R. J. Terr, *Design and optimization of low-thrust orbit transfers*, in *Aerospace Conference, 2005 IEEE* (IEEE, 2005) pp. 855–869.
- [74] P. Gage, R. Braun, and I. Kroo, *Interplanetary trajectory optimization using a genetic algorithm*, Journal of the Astronautical Sciences **43**, 59 (1995).
- [75] Y. H. Kim and D. B. Spencer, *Optimal spacecraft rendezvous using genetic algorithms*, Journal of Spacecraft and Rockets **39**, 859 (2002).
- [76] G. A. Rauwolf and V. L. Coverstone-Carroll, *Near-optimal low-thrust orbit transfers generated by a genetic algorithm*, Journal of Spacecraft and Rockets **33**, 859 (1996).
- [77] D. Myatt, V. M. Becerra, S. J. Nasuto, and J. Bishop, *Advanced global optimisation for mission analysis and design*, Final Report. Ariadna id **3**, 4101 (2004).
- [78] O. Abdelkhalik and D. Mortari, *N-impulse orbit transfer using genetic algorithms*, Journal of Spacecraft and Rockets **44**, 456 (2007).
- [79] M. Vasile, E. Minisci, and M. Locatelli, *On testing global optimization algorithms for space trajectory design*, in *AIAA/AAS Astrodynamics Specialist Conference and Exhibit, Honolulu, Hawaii* (2008).

- [80] J. A. Garcia, J. L. Brown, D. J. Kinney, J. V. Bowles, L. C. Huynh, X. J. Jiang, E. Lau, and I. C. Dupzyk, *Co-optimization of mid lift to drag vehicle concepts for mars atmospheric entry*, AIAA Paper **5052** (2010).
- [81] S. Li and Y. Peng, *Mars entry trajectory optimization using doc and dcnlp*, Advances in Space Research **47**, 440 (2011).
- [82] B. Addis, A. Cassioli, M. Locatelli, and F. Schoen, *A global optimization method for the design of space trajectories*, Computational Optimization and Applications **48**, 635 (2011).
- [83] J. T. Betts, *Survey of numerical methods for trajectory optimization*, Journal of guidance, control, and dynamics **21**, 193 (1998).
- [84] E. Boudestijn, *Development of a low-thrust earth-centred transfer optimizer for the preliminary mission design phase*, Master's thesis, Delft University of Technology (2014).
- [85] F. Miranda, *Design Optimization of Ground and Air-Launched Hybrid Rockets*, Master's thesis, Delft University of Technology (2015).
- [86] R. Hofsteenge, *Computational Methods for the Long-Term Propagation of Space Debris Orbits*, Master's thesis, Delft University of Technology (2013).
- [87] R. Noomen, *ae4-878.integrators.v4-3*, Lecture slides (2013), course: Mission Geometry and Orbit Design.
- [88] A. Milani and A. M. Nobili, *Integration error over very long time spans*, Celestial mechanics **43**, 1 (1987).
- [89] P. Deuflhard, U. Nowak, and U. Poehle, *Program descriptions of elib*, Website .txt document (1994).
- [90] H. Ramos and J. Vigo-Aguiar, *Variable stepsize störmer-cowell methods*, Mathematical and Computer Modelling **42**, 837 (2005).
- [91] E. Fehlberg, *Low order classical Runge-Kutta formulas with stepwise control*, Tech. Rep. (Marschall Space Flight Center, NASA, 1969) nASA TR R-316.
- [92] E. Fehlberg, *Classical fifth-, sixth-, seventh-, and eighth-order Runge-Kutta formulas with stepsize control*, Tech. Rep. (Marschall Space Flight Center, NASA, 1968) nASA TR R-287.
- [93] M. M. Berry, *A variable-step double-integration multi-step integrator*, Ph.D. thesis, Virginia Polytechnic Institute and State University (2004).
- [94] J. Meijaard, *A comparison of numerical integration methods with a view to fast simulation of mechanical dynamical systems*, in *Real-Time Integration Methods for Mechanical System Simulation* (Springer, 1991) pp. 329–343.
- [95] J. Dormand, M. El-Mikkawy, and P. Prince, *Families of runge-kutta-nystrom formulae*, IMA Journal of Numerical Analysis **7**, 235 (1987).
- [96] T. R. Quinn, S. Tremaine, and M. Duncan, *A three million year integration of the earth's orbit*, The Astronomical Journal **101**, 2287 (1991).
- [97] P. J. van der Houwen, E. Messina, and J. J. de Swart, *Parallel stormer-cowell methods for high-precision orbit computations*, Report-Modelling, analysis and simulation , 1 (1998).
- [98] A. B. Gonzalez, P. Martin, and D. J. Lopez, *On the numerical integration of orbital problems with high order runge-kutta-nystrom methods*, Applied numerical mathematics **35**, 1 (2000).
- [99] D. Gondelach, *A hodographic-shaping method for low-thrust trajectory design*, Master's thesis, Delft University of Technology (2012).
- [100] E. Mooij, *Ae3202-week1-lecture2ab-eom*, Lecture slides (2013), course: Flight Dynamics.
- [101] C. R. H. Solorzano and A. F. B. d. A. Prado, *Third-body perturbation using a single averaged model: application in nonsingular variables*, Mathematical Problems in Engineering **2007** (2007).

- [102] M. Macdonald and V. Badescu, *The International Handbook of Space Technology* (Springer, 2014).
- [103] V. Perminov, *The difficult road to mars*, National Aeronautics and Space Administration Monographs in Aerospace History (1999).
- [104] R. D. Braun and R. M. Manning, *Mars exploration entry, descent and landing challenges*, in *Aerospace Conference, 2006 IEEE* (IEEE, 2006).
- [105] D. Williams, [Mars fact sheet](#), Website (2015).
- [106] A. Smith, G. PArnaby, A. Matthews, and T. Jones, *Aerothermodynamic environment of the beagle 2 entry capsule*, in *Fourth Symposium on Aero thermodynamics for Space Vehicles*, Vol. 487 (2002) p. 271.
- [107] A. Steltzner, D. Kipp, A. Chen, D. Burkhardt, C. Guernsey, G. Mendeck, R. Mitcheltree, R. Powell, T. Rivellini, M. S. Martin, *et al.*, *Mars science laboratory entry, descent, and landing system*, in *Aerospace Conference, 2006 IEEE* (IEEE, 2006).
- [108] P. Plotard, P. Watillon, and V. Labaste, *Entry system development for martian landers*, Space Technology-Abingdon **23**, 207 (2003).
- [109] P. Blau, [Msl - aeroshell and heat shield](#), Website (2011).
- [110] J.-M. Bouilly, L. Dariol, and F. Leleu, *Ablative thermal protections for atmospheric entry. an overview of past missions and needs for future programmes*, in *Thermal Protection Systems and Hot Structures*, Vol. 631 (2006) p. 26.
- [111] E. L. Strauss, *Superlight ablative systems for mars lander thermal protection*, Journal of Spacecraft and Rockets **4**, 1304 (1967).
- [112] The Martin Company, [Ablative heat shield materials](#), (1975(?)).
- [113] J. R. Cruz and J. S. Lingard, *Aerodynamic decelerators for planetary exploration: past, present, and future*, AIAA Paper **6792**, 21 (2006).
- [114] E. F II and R. Sinclair, *Design and development of the main parachute for the beagle 2 mars lander*, in *17 th AIAA Aerodynamic Decelerator Systems Technology Conference and Seminar* (2005) pp. 372–386.
- [115] J. M. Lafleur and C. J. Cerimele, *Mars entry bank profile design for terminal state optimization*, Journal of Spacecraft and Rockets **48**, 1012 (2011).
- [116] NasaFacts, [Low density supersonic decelerators](#), website (2013), nASA fact sheet.
- [117] W. B. Pepper, *Development of a composite structure hypersonic parachute*, Journal of Spacecraft and Rockets **6**, 495 (1968).
- [118] L. L. Galigher, *Aerodynamic Characteristics of Supersonic X Parachutes at Mach Numbers of 2.1 and 4.0*, Tech. Rep. (DTIC Document, 1969).
- [119] J. C. Gallon, I. G. Clark, T. P. Rivellini, D. S. Adams, and A. Witkowski, *Low density supersonic decelerator parachute decelerator system*, in *AIAA Aerodynamic Decelerator Systems (ADS) Conference* (2013).
- [120] R. Sostaric, *The challenge of mars edl (entry, descent, and landing)*, Presentation (2010), nASA.
- [121] I. G. Clark, A. L. Hutchings, C. L. Tanner, and R. D. Braun, *Supersonic inflatable aerodynamic decelarators for use on future robotic missions to mars*, Journal of Spacecraft and Rockets **46**, 340 (2009).
- [122] B. A. Steinfeldt, J. E. Theisinger, A. M. Korzun, I. G. Clark, M. J. Grant, and R. D. Braun, *High mass mars entry, descent, and landing architecture assessment*, AIAA Paper **6684** (2006).
- [123] Jet Propulsion Laboratory, [Mars pathfinder](#), website (1997), old Pathfinder website.
- [124] F. Bonnefond, P. Tran, J. Bertand, J. Bolz, E. Ferreira, and D. Wilde, *Soft-landing: the key building block for exploration*, 57th International Astronautical Congress (2006).

- [125] G. A. Soffen, *The viking project*, Journal of Geophysical Research **82**, 3959 (1977).
- [126] J. G. McAllister and C. Parish, *Phoenix landing propulsion system performance*, paper AIAA **5264**, 2 (2009).
- [127] J. Whitehead, *Mars ascent propulsion options for small sample return vehicles*, in *Paper nr 97-2950* (American Institute of Aeronautics and Astronautics, 1997).
- [128] C. S. Guernsey, *Mars ascent propulsion system (maps) technology program: Plans and progress*, AIAA Paper **3664** (1998).
- [129] P. Desai, R. Braun, W. Engelund, F. Cheatwood, and J. Kangas, *Mars ascent vehicle flight analysis*, AIAA Paper (1998).
- [130] C. Stone, *Rice mars*, presentation/website (1999).
- [131] J. C. Whitehead, *Trajectory analysis and staging trades for smaller mars ascent vehicles*, Journal of space-craft and rockets **42**, 1039 (2005).
- [132] D. D. Stephenson and H. J. Willenberg, *Mars ascent vehicle key elements of a mars sample return mission*, in *Aerospace Conference, 2006 IEEE* (IEEE, 2006).
- [133] A. Sengupta, A. Kennett, M. Pauken, M. Trinidad, and E. Zabrensky, *Systems engineering and technology considerations of a mars ascent vehicle*, (2012).
- [134] B. Natan and S. Rahimi, *The status of gel propellants in year 2000*, International journal of energetic materials and chemical propulsion **5** (2002).
- [135] J. Pearson, *The orbital tower: a spacecraft launcher using the earth's rotational energy*, Acta Astronautica **2**, 785 (1975).
- [136] K. Lofstrom, *The launch loop-a low cost earth-to-high orbit launch system*, AIAA Paper (1985).
- [137] R. H. Frisbee, *Advanced space propulsion for the 21st century*, Journal of Propulsion and Power **19**, 1129 (2003).
- [138] J. T. Kare, *Modular laser launch architecture: Analysis and beam module design*, Final Report USRA (2004).
- [139] J. Hunter, *Quicklaunch affordable space exploration*, website (2012).
- [140] Zero2infinity, *Zero2infinity will launch nanosatellites from the stratosphere*, website (2014), press Release.
- [141] R. Noomen, *ae4-878.orbit-design.v4-7*, Presentation (2013), course: Mission Geometry and Orbit Design.
- [142] P. Wercinski, *Mars sample return-a direct and minimum-risk design*, Journal of spacecraft and rockets **33**, 381 (1996).
- [143] M. R. Patel, J. M. Longuski, and J. A. Sims, *Mars free return trajectories*, Journal of Spacecraft and Rockets **35**, 350 (1998).
- [144] A. Miele and T. Wang, *Optimal trajectories and mirror properties for round-trip mars missions*, Acta Astronautica **45**, 655 (1999).
- [145] R. Mattingly, S. Matousek, and F. Jordan, *Mars sample return, updated to a groundbreaking approach*, (2003).
- [146] R. Mattingly, S. Matousek, and F. Jordan, *Continuing evolution of mars sample return*, in *Aerospace Conference, 2004. Proceedings. 2004 IEEE*, Vol. 1 (IEEE, 2004).
- [147] R. Mattingly and L. May, *Mars sample return as a campaign*, in *Aerospace Conference, 2011 IEEE* (IEEE, 2011) pp. 1–13.

- [148] T. Engelhardt, *Is there life on mars? a sample return mission concept*, Presentation/website (2012).
- [149] D. A. Tito, G. Anderson, J. P. Carrico, J. Clark, B. Finger, G. A. Lantz, M. E. Loucks, T. MacCallum, J. Poynter, T. H. Squire, *et al.*, *Feasibility analysis for a manned mars free-return mission in 2018*, in *Aerospace Conference, 2013 IEEE* (IEEE, 2013) pp. 1–18.